J of LDS TRANSACTIONS OF THE BAKU STATE UNIVERSITY

ISSN 2308-068X

JOURNAL OF LOW DIMENSIONAL SYSTEMS

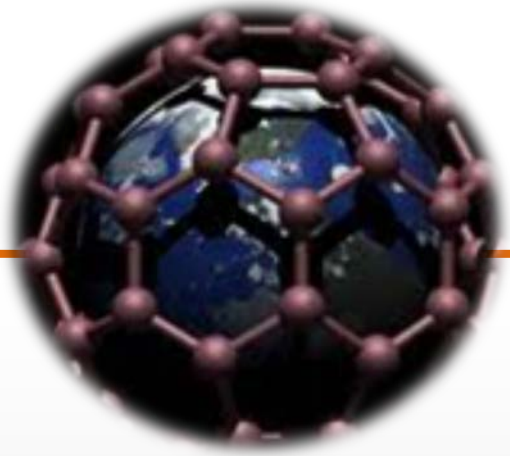

Physics, Chemistry and Biology of Low Dimensional Systems

May 2018

BSU JOURNALS

Aims and scope

The *Journal of Low Dimensional Systems* is co-edited by Baku State University.

It publishes papers and review articles on the fundamental and applied aspects of physics, chemistry and biology. General areas of interest are the electronic, spectroscopic and structural properties of low dimensional systems, including perfect and defect lattices, surfaces, two-dimensional electron systems, interfaces, thin films and multilayers, amorphous materials, micro- and nanostructures, and layered structures. Papers dealing with biomaterials for medical purposes are accepted.

Typical examples include the preparation and structural characterization of novel and advanced low dimensional materials, especially in relation to the measurement and interpretation of their electrical, magnetic, optical, thermal and mechanical properties, phase transitions, electronic structure and defect properties, and the application of appropriate experimental and theoretical techniques in these studies. Articles are encouraged in all the above areas, but especially those which emphasize fundamental aspects of materials science.

Address:

Az1148, Z.Khalilov str. 23,
Baku State University, BSU publication, Baku, Azerbaijan

E-mail: journal_lds@bsu.az

Journal of LDS

Published by the Baku State University and devoted to original papers in experimental and theoretical physics, chemistry and biology

Table of Contents

NANOSTRUCTURING BY SEVERE PLASTIC DEFORMATION. EXPERIMENTAL AND THEORETICAL ASPECTS

COSTICA BEJINARIU[1], ALIN M. CAZAC[1], MARICEL AGOP[2, 3, 4*], VLAD GHIZDOVAT[5, 6]

[1]"Gheorghe Asachi" Technical University, Materials Science Department,
59A Prof. dr. docent DimitrieMangeron Blvd., 700050, Iasi, Romania
[2]Physics Department, Faculty of Machine Manufacturing and Industrial Management,
"Gheorghe Asachi" Technical University, 59A Prof. dr. docent DimitrieMangeron Blvd., 700050, Iasi, Romania
[3]Lasers, Atoms and Molecules Physics Laboratory, University of Science and Technology,
Villeneuve d'Ascq, 59655, Lille, France
[4]Academy of Romanian Scientists, 54 SplaiulIndependentei, sector 5, 050094 Bucuresti, Romania
[5]Faculty of Physics, "AlexandruIoanCuza" University, No. 11 Carol I Blvd., Iaşi 700506, Romania
[6]"Grigore T. Popa" University of Medicine and Pharmacy, Faculty of Medicine,
Biophysics and Medical Physics Department, 16 University Str., Iaşi - 700115, Romania

The principle of nanostructuring by multiaxial forging is presented. A sample of Al 99,5% was subjected to severe plastic deformation, its structural characteristics being analyzed using SEM and TEM imaging. Fractal analysis conducted on our experimental data reveals that the behaviors of materials subjected to severe plastic deformation imply multi-scale type dynamics, so that, in this case, the classical models must be replaced with fractal ones.

PACS numbers: 81, 81.16.-c, 61.46.-w, 68.65.-k
Keywords: severe plastic deformation, nanostructures, multi-scale dynamics, fractals
E-mail:m.agop@yahoo.com*

1. INTRODUCTION

Multiaxial forging is a discontinuous deformation process made up of a series of deformation processes. The severe plastic deformation cycle creates a nanostructured deformed material, after a specific number of passes [1, 2].

The shape and dimensions of the blank and the workpiece obtained after one pass remain unchanged [3]. This is possible by correlating these parameters with the configuration and size of the deformation tools [4].

The principle of nanostructuring by multiaxial forging has been developed by Ghosh et al., and the schematic representation of this method and the device used are shown in Fig. 1 [5].

This paper presents the implementation of Gosh's nanostructuring principle by means of a device that uses blanks of regular quadrangular prism shape. The shape and dimensions of the blank are maintained after each pass. Also, some theoretical considerations on the multi-scale type behaviors of materials under severe plastic deformation are discussed.

2. RESULTS AND DISCUSSION

The structural characteristics of the studied material (Al 99,5%) have been analyzed using a high-resolution scanning electron microscope (SEM) with field emission - FEI Quanta FEG 450. Also, we used a Tecnai G^2 F30 S-TWIN transmission electron microscope (TEM) at 300 kV with field emission gun (FEG).

In Fig. 2a the SEM image of a sample which was not subjected to a severe plastic deformation is presented.

The SEM images of the Al sample for each passage (12 passages in total) are shown in Fig. 2, for the severe plastic deformation process. Also, in Fig. 3, the nanostructure of the Al sample (TEM image) is displayed.

Our experimental data, collected from the Al sample severe deformation process, was analyzed using the following procedure (fractal analysis):

i) transformation of SEM images into mathematical objects (binary images) using the "Image J" software – see Figs. 4a-d;

ii) fractal dimension and lacunarity calculus [6-8] for the binary images – see Figs. 5a, b.

In our opinion, in the case of severe plastic deformation, a material structure passes from a "mesoscopic phase" to a "mixt phase or interphase", and then finally to a "nanoscopic phase". The "mesoscopic phase" is characterized by low correlated "minimum relevant dimensions" (microns sized) grains, while the "nanoscopic phase" is characterized by high correlated "minimum relevant dimensions" (nanometers sized) grains.

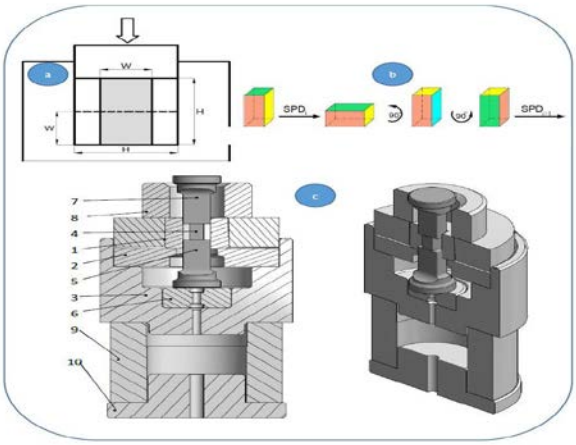

Fig.1. a) Ghosh type scheme for multiaxial forging (W is the side of the initial square section of the blank; H - initial height of the blank); b) Gosh type principle; c) The constructive functional scheme of the multiaxial forging device

Our results lead to the conclusion that, if a material is subjected to severe plastic deformations, a multi-scale behavior can be observed. Each scale can be correlated to a specific phase: the mesoscopic scale with the "mesoscopic phase", the mixt scale with the "interphase", and the nanoscopic scale with the "nanoscopic phase". This kind of behavior implies that, in order to describe such physical dynamics of structures under severe plastic deformation, but still remaining tributary to a differential hypothesis, it is necessary to introduce, in an explicit manner, the resolution scale in the expressions of the physical variables that describe these dynamics and, implicitly, in the fundamental equations of "evolution" (for example, density, momentum and energy equations etc.). This means that any dynamic variable, dependent, in a classical meaning, on both spatial coordinates and time [9, 10], becomes, in this new context, dependent also on the resolution scale. In other words, instead of working with a dynamic variable, described through a strictly non-differentiable mathematical function, we will just work with different approximations of that function, derived through its averaging at different resolution scales. Consequently, any dynamic variable acts as the limit of a functions family, the function being non-differentiable for a null resolution scale and differentiable for a non-zero resolution scale [6].

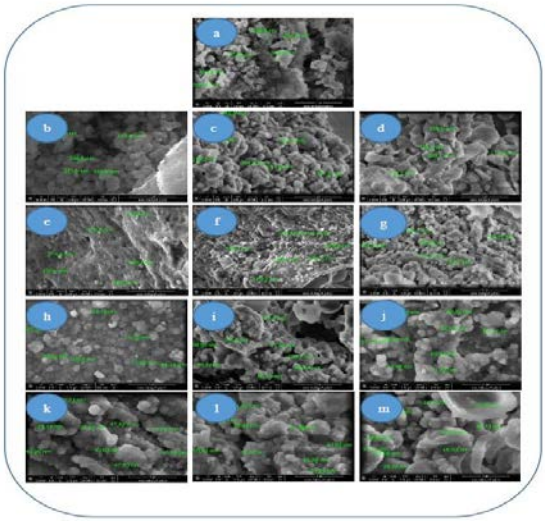

Fig.2. a) Initial state of the Al sample (SEM images); b)-e) Al sample subjected to severe plastic deformation – passages 1 to 4 (SEM images); f)-i) Al sample subjected to severe plastic deformation – passages 5 to 8 (SEM images); j)-m) Al sample subjected to severe plastic deformation – passages 9 to 12 (SEM images)

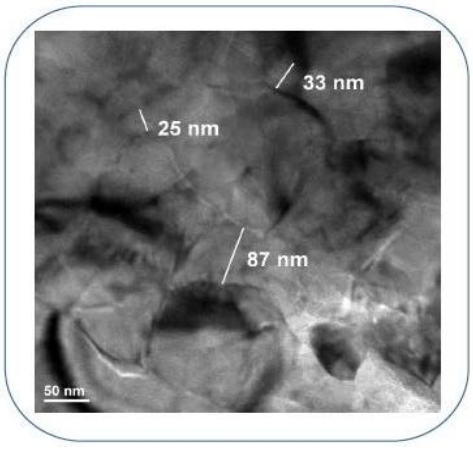

Fig. 3. Nanostructure of the Al sample (TEM image)

The "interphase" consists of grains mixtures (medium correlated grains of various "minimum relevant dimensions", between microns and

nanometers). These "phase transitions" are presented in Fig. 6.

This approach, well adapted for applications in the field of materials under stress, where any real determination is conducted at a finite resolution scale, clearly implies the development both of a new geometric structure and of a physical theory (applied to structures under severe plastic deformation) for which the motion laws, invariant to spatio-temporal coordinate transformations, are completed with scale laws, invariant at scale transformations. Such a theory that includes the geometric structure based on the above presented assumptions was developed in the Scale Relativity Theory [9] and more recently in the Scale Relativity Theory with an arbitrary constant fractal dimension [10]. Both theories define the "fractal physics models" class [11], i.e. the severe plastic deformation in a fractal space.

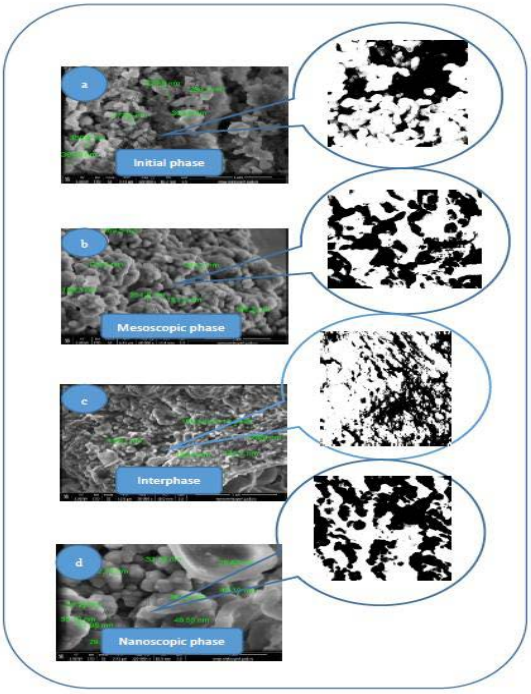

Fig. 4. The transformation of SEM images into mathematical objects (binary images) using the "Image J" software a) Initial state of the Al sample, b) Al sample subjected to severe plastic deformation – passage 3 (mesoscopic phase), c) Al sample subjected to severe plastic deformation – passage 5 (interphase), d) Al sample subjected to severe plastic deformation – passage 12 (nanoscopic phase)

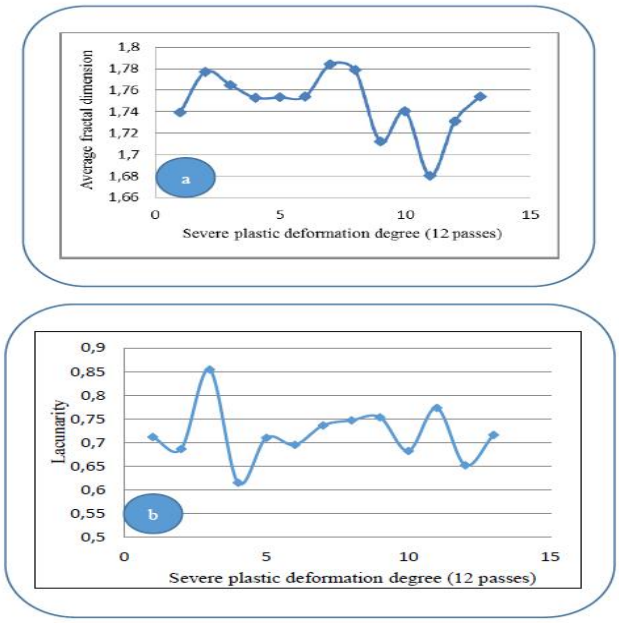

Figs. 5. a) The dependency of the average fractal dimension to the 12 steps severe plastic deformation degree; b) Lacunarity dependence on the 12 steps severe plastic deformation degree

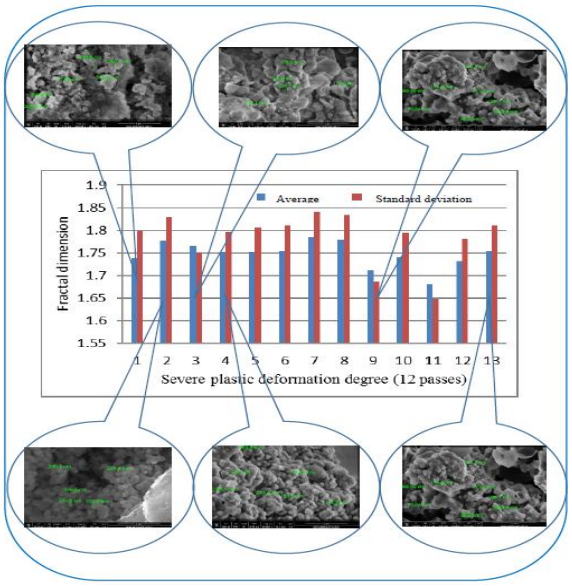

Fig. 6. Correlations between material structures under severe plastic deformation (SEM images) and their average fractal dimension and standard deviation of their fractal dimension, respectively

3. REFERENCES

1. Valiev R.Z., Islamgaliev R.K., Alexandrov I.V. / Progress in Materials Science, 2000, 45, p.103–189.

2. Rosochowski, A.,Olejnik, L.,Richert, M./ Steel GRIPS, v.2, 2004, p.35-44.
3. Comaneci R., Chelariu R., Zaharia L., Obtaining Nanostructured Materials by Severe Plastic Deformation; Performantica: Iasi, 2006 (in Romanian).
4. Cazac A.M., Bejinariu C., Baciu C., Toma S. L., Florea C.D. / Applied Mechanics and Materials 2014, 657, p.137-141.
5. Azushima A., Kopp R., Korhonen A., et all / CIRP Annals Manufacturing Technology, 2008, 57, p.716–735.
6. Mandelbrot B. B. The Fractal Geometry of Nature; W. H. Freeman: New York, 1983.
7. Federer J., Aharoner, A. Fractals in physics; North Holland: Amsterdam, 1990.
8. Badii R., Politi A. Complexity: Hierarchical Structures and Scaling in Physics; Cambridge University Press: Cambridge, 1999
9. Nottale L. Scale Relativity and Fractal Space-Time. A New Approach to Unifying Relativity and Quantum Mechanics; Imperial College Press: London, 2011
10. Merches I., Agop M. Differentiability and Fractality in Dynamics of Physical Systems; World Scientific: Singapore, 2016
11. Mitchell, M., Complexity: A Guided Tour; Oxford University Press: Oxford, 2009.

NEW APPROACHES TO DEVELOPMENT OF NEW NANOMATERIALS FOR MAGNETIC HYPERTHERMIA OF CANCER CELLS AND PROSPECTIVES OF COMBINED TREATMENT OF CANCER IN GEORGIA

A. CHIRAKADZE[1*], D. JISHIASHVILI[1,2], Z. BUACHIDZE[1], K. GORGADZE[1], Z. SHIOLASHVILI[1],A. JISHIASHVILI[1], N. MITAGVARIA[3], I. LAZRISHVILI[3]

[1] Georgian Technical University, 77 Kostava St., 0175, Tbilisi, Georgia.
[2] E. Andronikashvili Institute of Physics, I. Javakhishvili Tbilisi State University, 6 M.Tamarashvili St., 0177, Tbilisi, Georgia.

Paper deals with the development and testing of materials for magnetic hyperthermia of cancer utilizing of the microwave and hydrazine based new technologies for the growth of Ag-doped $LaMnO_3$ and/or Ni-Cu coated nanocomposites. Methods of testing toxicity (examining the negative effects these particles have on biological entities) of MNPs at the levels of impact far below the level of clearly revealed cytological changes are proposed and discussed. The proposed and utilized preliminary studies were focused on behavioral effects, which do not threaten the life and health of experimental animals and, most importantly, determine the toxicity at the levels far below of commonly registered by means of usually applied assays. Prospective of use of the developed nanocomposites as materials for effective combined methodology of cancer treatment including radiotherapy, chemotherapy, hormone therapy, magnetic hyperthermia and photodynamic therapy in several developed countries (Germany, UK, USA, Australia, Canada) and in Georgia are reviewed and discussed.

PACS numbers: 87.19.xj; 87.50.S-, 81.07Bc, 87.50.y
Key words: Magnetic hyperthermia, cancer, Curie Temperature, combined methodology, toxicity, behavioural.
*E-mail: achirakadze@gtu.ge

1. INTRODUCTION

Among the pressing problems of our time, a special place belongs to the problem of "combating" cancer. Disappointing is the fact that cancer is growing all over the world [1-8]. Today, powerful cancer control methods are applied, such as surgical treatment, chemotherapy and radiation therapy (radiotherapy). The latter two methods are characterized by high efficiency, but are aggressive with a number of side effects that negatively affect the normal functioning of the body, and the quality of life in general. Use of Hyperthermia as a treatment modality has been significantly increased in duration of last decades, especially in cancer clinics [9-15]. Hyperthermia is almost always used with other forms of cancer therapy, such as radiation therapy and chemotherapy. Hyper-thermal exposure can make some cancer cells more sensitive to radiation or harm other cancer cells that radiation cannot damage. Hyperthermia can also enhance the effects of certain anticancer drugs, which is mutually strengthening and makes healing more likely – the so-called synergistic effect of hyperthermia. It was revealed that cytostatic drugs (chemotherapy substances) clearly act more aggressively at temperatures over 40° C than within the range of normal body temperature. By many researchers Hyperthermia is considered as one of the promising methods of preventing and treating cancer. However, when the body is under thermal impact of different level and duration, this definitely will lead to appropriate metabolic and functional changes not just in tumor tissue, but in normal one also. In other words, we have to study not just clinical effects of Hyperthermia, but the mechanisms of its action as well. In the previous research Georgian and American scientists showed that besides an action of temperature factor by itself and changes of blood rheological properties, Hyperthermia triggers the action of so called "phenomenon of Hormesis" which can be one of the main (and, may be, even leading) mechanism for developing of both positive and negative effects of Hyperthermia. Hence, now we have to clarify maximally all possible effects of Hyperthermia, as well

as maximally concentrate its action just on tumor tissue [16-26]. From this point of view the Magnetic hyperthermia (MHT) looks like a most prospective method [27-29]. The main component of magnetic hyperthermia is the magnetic fluid [30], with concentration of magnetic nanoparticles for an order or two less than the concentration of drugs that are usually administered during chemotherapy, while their toxicity is significantly lower. Location of heating can be effectively controlled by the magnetic field, which allows him to be concentrated and retained at the site of the tumor [31-32]. Taking into account all above, we will focus on the development of materials of the self-regulated (Curie temperature limited) hyperthermia Magnetic nanoparticles play the role of heat inductors, which locally heat their surrounding medium (tumor) to the necessary temperature to provide the therapeutic effect. There is very important to select appropriate heating velocity and to know the doses of thermal exposure when the therapeutic effect is optimal, to ensure their uniformity and dispersity of nanoparticles and sure, their biocompatibility (nontoxicity) [33-38]. All these aspects must be taking into account when we are trying to develop new magnetic nanoparticles with improved properties. Magnetic hyperthermia (MHT) is a prospective method which can significantly increase the efficiency of chemotherapy and radiotherapy when used as adjuvant means and several times reduce the required amount of drugs and doses of radiation. Location of heating can be effectively controlled by a magnetic field, which allows him to be concentrated and retained at the site of the tumor. The efifficiency of MHT (especially when used in conjunction with other therapies) was proven in case of different kinds of cancer deseases – e.g. brain, prostate and pancreatic cancer [39-44]. Table 1 illustrates the efficiency of MHT tratment for curing glioblastoma, which was classified by WHO as extremely malignant and is associated with a very short survival period.

Although standard therapy includes the application of all classical treatment methods, from surgery to radiation and chemotherapy, the probability of the tumour's recurrence is very high. According to statistics, following an average survival rate of 32 - 36 weeks, glioblastoma recurrence is unavoidable (Recurring Glioblastoma Multiforme – article on medscape.com). Overall, the average survival rate is between 12 and 18 months, with a very reduced probability of survival of less than 10% after five years.

Table 1. Efficiency of MHT tratment for curing glioblastoma

Average survival	Treatment by radiation and Magnetic Hyperthermia (months)	Treatment by radiation alone (months)
Average survival after recurring glioblastoma	13.4	6.2
Average survival following primary diagnosis	23.2	14.6

The diagnosis of a malignant brain tumour is typically followed by the surgical removal of the affected tissue with subsequent radiation. In the user study conducted between 2005 and 2009 for the approval of NanoTherm® therapy in Europe, this was combined with standard treatment and statistically analysed. This not only included the verification of the safety profile but also led to improvements regarding the average survival rate after the determination of recurrence or following the primary diagnosis. In 2010, MagForce AG successfully completed a clinical study for "glioblastoma" and therefore attained European certification for NanoTherm® therapy [45]. A total of 66 patients (with 59 patients being recurrent suffering from the recurrence of glioblastoma) were included in a single-arm study at two treatment centres. For prostate cancer, the NanoTherm® therapy can not only be applied in the treatment of intermediary state cancer but also as a combination therapy in high-risk patients with recurring prostate cancer. The advantages of minimally invasive as well as low toxicity procedures during the application of the MagForce therapy also are presented here. However, as the prostatectomy is a major surgical intervention, it is frequently associated with numerous side effects. Apart from side effects directly related to the surgery, long-term effects may also include incontinence and impotence. With regard to radiation, the side effects (inflammation of the treated regions) are directly related to the treatment. NanoTherm® therapy is to be primarily applied on patients in a comparatively early stage of prostate cancer, with the aim of keeping the carcinoma in a non-aggressive stage. This permits the

extension of the treatment-free period and the prevention of associated side effects.

Pancreatic cancer remains one of the leading causes of cancer related death worldwide with an overall five-year survival of less than 5%. There is only marginal improvement in outcome of treating pancreatic cancer in the last two decades. It is time to open up and have a fresh look at complementary adjuvant treatment options. Hyperthermic intraperitoneal chemotherapy (HIPEC) predominantly as a intrasurgical procedure has already proved its justification. Non-invasive loco regional hyperthermia as complement to either chemo or radiation therapies has not yet reached a comparable status of evidence. However the potential to eventually grow into such evidence is already clearly observable. Hyperthermia has the potential to significantly prolong life expectancies while maintaining a satisfying quality of life. The Hyperthermia European Adjuvant Trial (HEAT) study [46]. compares adjuvant gemcitabine to adjuvant gemcitabine plus capecitabine plus regional hyperthermia treatment - a regime that has previously been utilized with low reported toxicity. It has been shown that heat can increase the cytotoxicity of certain chemotherapeutic agents including gemcitabine in vitro experiment with pancreatic cancer cell lines. One phase II the study combined gemcitabine with regional heat treatment of both metastatic and locally advanced disease. Median survival was 8 months in the entire study population, but extended to 17.7 months in those with localised disease. More recently, a retrospective analysis of 23 patients with gemcitabine refractory inoperable disease was published whereby patients received gemcitabine plus cisplatin alongside regional hyperthermia two-times weekly for four months. Though 21/23 patients suffered from metastatic disease at recruitment, a median overall survival of 12.9 months was achieved (95% Confidence Interval: 9.9-15.9). Thus, hyperthermia may be one of the most efficient adjuvant options.

Recently the interest towards hyperthermia has been significantly increased thanks to the thorough critical analysis of the results of previous experimental research and several randomized studies that demonstrated the considerable increase of treatment effectiveness after the incorporation of hyperthermia into the medical schedule [47-54], provided that there was sufficient temperature-exposure of tumor during the hyperthermia procedure. It is ascertained that hyperthermia alone has the anti-cancer effect only in 12-13% of cases while in combination with radiotherapy and/or chemotherapy the effectiveness of treatment substantially increases. But potentialities of hyperthermia are even broader. It is proved that hyperthermia is fatal not only towards the tumor cells, but also towards bacteria and viruses. The principal reason for inclusion of artificial hyperthermia into the multi-component treatment of oncologic patients is that it takes into account morphological and functional peculiarities of tumors that distinguish them from homologous normal tissues by number of rather important and correlated parameters: insufficiency of blood supply, especially on the level of microcirculation; degree of oxygenation; capacity of glycolysis; levels of pH. Through the application of strictly dosed regimen of hyperthermia, it becomes possible to manage above mentioned morpho-functional parameters of tumorous and normal tissues. This leads to the expansion of therapeutic range and, ultimately, to the practical realization of the concept of selective enhancement of tumor sensitivity towards radiation and medication. As a result of decreased volume blood flow (especially in hypoxic areas), tumors may overheat at least 1-2^{0}C higher than surrounding normal tissues; at that, their thermal damage and effect of consequent exposure to radiation are also amplified.

High effectiveness of hyperthermia, as adjuvant of radiotherapy, is also caused by following circumstances: 1. Hyperthermia has damaging action on cellular level and this effect depends on the temperature and duration of heating; thus, it follows that exposure to hyperthermia should be located in tumor area (as well as for the cases of application of ionizing radiation). In contrast to ionizing radiation, reduction of oxygen concentration in tissues during exposure to hyperthermia does not lead to weakening of damaging action. Therefore, hyperthermia allows overcoming radio resistance of hypoxic tumor cells; 2. During hyperthermia the damaging action's correlation with cell cycle stage is different from what is typical for the ionizing radiation. Thus, the highest resistance is typical for S-period, while during the heating the most sensitive is the period of DNA synthesis. That's why the hyperthermia comes forward as the "ideal" adjuvant, which is smoothening tumor cells' survival rate fluctuations subject to the cell cycle stage, in which exposure took place; 3. Usually, tumor

cells' thermo sensitivity is similar to that of cells in surrounding normal tissues, but because of number of physiological peculiarities, such as low blood flow, more acid medium as a whole, critically low pH in hypoxic areas and insufficient maintenance, they are damaged much heavier than normal ones; 4. Together with damaging action, hyperthermia is characterized by significant radio-sensitizing effect caused by the temporary disturbance of repair processes; this leads to substantial increase of cellular radiosensitivity, which is also in correlation with temperature, duration of heating and time interval between heating and radiation; 5. Apart from biological effects emerging on a cellular level, hyperthermia evokes change of the blood flow in heated area; this effect has dynamic character and correlates with heating in a complex way; 6. Depending on the level of temperature and duration of its action Hyperthermia may induce oxidative stress, activate the system of HSP (heat shock proteins) and stimulate one of the most powerful defence system in organism; 7. Exposure to hyperthermia evokes complex pathophysiological processes in tumor tissues: changes in blood flow, its rheology, oxygenation, metabolic and energy status. At that, human tumors are characterized by the apparent heterogeneity of blood flow, changes of which during heating are unpredictable and depend on spatial arrangement and time. In some cases, increase of the blood flow may result in the increased heat diffusion, thus stipulating unattainability of therapeutic temperature values.

Thus, the increase of temperature of tissue during heating is largely dependent on the influx of heat from the external heat source, and also on the efflux of heat through dissipation by the circulating blood . Therefore, preferential heating and damage of tumor can be expected only if heat is preferentially delivered to the tumor or if heat dissipation by blood flow is slower in the tumors than in surrounding normal tissues. So far, the most important area of hyperthermia method application is the treatment of oncologic diseases. The point is that heating of the organism to 43-43,5^{0}C has a direct effect on tumor cells; however, the mechanism of high temperature effect as such is not yet completely explained. It is supposed that several factors are simultaneously crucial for the final impact: thermal damage of cells, delay of their division and triggering of the apoptosis.

It turned out that tumor cells are heating up much stronger than healthy cells; therefore they die sooner. The main goal of hyperthermia treatment is affecting tumour tissue causing apoptosis or necrosis depending on the level of temperature and duration of hyper-thermal exposure. It turned out that in tumour tissue most pronounced apoptosis is observed at prolonged hyperthermia exposure. During the comparison of long-lasting (6 hours) low temperature (40^{0}C) hyperthermia in combination with chemotherapy, with short-term, high temperature hyperthermia, most pronounced apoptosis in tumour tissue has been revealed using the high temperature short term heating. At the same time it has been established, that an acidic environment (pH=6,6) enhanced the hyperthermia-induced apoptosis in HL-60 human promyelocytic leukemia cells as judged by the DNA fragmentation, flow cytometric analysis of DNA content, and cleavage of poly (ADP-ribose) polymerase. The clinical use of hyperthermia for cancer treatment was increasingly accepted during past decades and today there is well established fact that the hyperthermia pre-treatment at temperatures between 40-44^{0}C greatly enhances the therapeutic effect of radiotherapy or chemotherapy. Most biological tissues, with the exception of the central nervous tissue, are tolerant to hyperthermia treatment and can survive at a temperature of up to 44^{0}C. In regard to tissue of central nervous system, there are some discrepancies in published data concerning irreversible damages that were found after treatment: at 42-42.5^{0}C, at 43.1^{0}C, at 43.9^{0}C and greater. And, what is more important, there were shown no obvious irreversible changes in monkeys normal brain tissue at 44^{0}C and below in case of non-survival experiment, and just in survival experiment (animals were sacrificed 7 days after the treatment), showing that the safety limit for brain hyperthermia is close to 43^{0}C for 60 min. Analysis of experimental data received on dogs and cats (using different techniques for brain local hyperthermia allowed to conclude that maximum tolerable heat dose is 42-42,5^{0}C for 40-60 min or 43^{0}C for 10-30 min of exposure. Effects of hyperthermia were expressed immediately or within a few days after treatment. It turned out, that in tumor tissue most pronounced apoptosis is observed at prolonged hyperthermia exposure.

In the early experimental studies of local hyperthermia effects on rabbit's cerebral tissue,

microwave induced local hyperthermia caused remarkable changes in cerebral blood flow manifested by increase of blood flow intensity at the beginning of hyperthermia, and than its slump decreasing after raising the brain temperature upwards of 43^0C. In case of the same animal species (in conditions of whole body hyperthermia) doubling of cerebral blood flow intensity has been observed at the core body temperature 43^0C; 2.5 times increasing of cerebral blood flow at 44^0C and 3.5 times increasing at 45^0C. At the same time augmentation of tissue oxygen partial pressure and pH have been observed. However, it is very important to ascertain normal tissue safety and the absence of irreversible damage. From this point of view special attention has to be paid to the central nervous tissue because of its extremely high sensitivity to any exogenous exposure, including hyperthermia. One of the most significant reasons for extensive damage of nervous (or any other) tissue under hyper thermal exposure is the deterioration of blood rheological properties, formation of micro thrombi and occlusion of vessels. Stoppage of blood flow in the zone of vascular occlusion decreases of temperature clearance from the exposed area of the brain and that causes increase in temperature and aggravates the destructive action of hyperthermia. When this kind of processes are taking place in tumor tissue this is exactly what we are looking for, but not in normal tissue which must be maximally prevented from this kind of action. That creates the necessity of very precise and careful localized hyperthermic exposure on tumor tissue and should be considered when determining the optimal combination of temperature level and duration of its action in the clinical set up.

Importance of self regulated (Curie Temperature limited) hyperthermia. Magnetic nanoparticles play the role of heat inductors, which locally heat their surrounding medium (tumor) to the necessary temperature to provide the therapeutic effect. Parameters of the alternating magnetic field should be carefully selected to provide appropriate heating velocity [55-60]. According to the most popular opinion of scientists, optimum interval of the controlled heating temperature should be T ≈ (41-44)°C with appropriate dose of thermal exposure (when the therapeutic effect is optimal). In case when T exceeds 43-44°C it can damage the healthy tissues. On the other hand, if T is below 41°C or the exposure time is sufficiently short, conditions for effective therapeutic treatment will not be achieved. Moreover, in the latter case there is a veiled danger - the heating of cancer cells to 39°C, on the contrary, stimulates their rapid multiplication. That is why, providing a self-regulated process of heating with strictly fixed temperature range is highly important. The optimal way to perform this is the development of magnetic heating agents with controlled Curie temperature (Tc) near to 42°C, and avoiding surgical intervention and invading of special thermometers. But it must be always taken into account, that a considerable group of researchers widely use the temperature intervals T ≈ (39-40)°C or (45-47)°C and are sure that in different special casess these intervals must be used as optimal if using the appropriate exposure dose. Thus, developing and study of nanomaterials for self-regulated hyperthermia with T_C ≈ (39-46)°C should become the object of a special interest of the medical clinicians and researchers in the field of combined therapy of cancer.

Uniformity and dispersity of nanoparticles. Another important problem of MHT is the achievement of uniform heating of the cancer tumor directly which depends on how homogeneously distributed are the nanoparticles in the tissue [38] . In case of heterogeneous (uneven) distribution, the tumor will heat up in some areas more than in others, and there is a significant danger of overheating or underheating of different parts of irradiated tissues. The correct control of the temperature-doze regime and the achievement of a uniform distribution of nanoparticles in the tumor region ensure the efficacy of MHT and, crucially affects its safety for living organisms.

Biocompatibility (nontoxicity). One of the most important characteristics of the materials for medical use is their biocompatibility (non or very low toxicity) [61-63]. From our point of view, the neccesity of assessing and comparing the impacts far below the level of clearly revealed negative health effects is unanimous. That is why the preliminary toxicity tests proposed to be carried out are focused on behavioral effects, which do not threaten the life and health of experimental animals. It appears that the development of new nanomaterials and novel applications should not rely on the existing assumptions. So, the comparison of many toxicological data indicates that palladium, platinum, and gold compounds, often considered heavy and toxic, may in fact be not so dangerous, whereas complexes of nickel and copper,

typically assumed to be green and sustainable alternatives, may possess significant toxicities, which is also greatly affected by the solubility in water and biological fluids.

Choice of materials to be studied. Magnetic nanoparticles for hyperthermia must meet the number of strict criteria [31-38]. They should be non-toxic or low toxic; ensure a uniform strictly localized distribution in the tumor and prevent thrombogenesis; have approprieta dimensions for effective penetration into cells; provide effective heating in an alternating magnetic field with the amplitude and frequency limited by the medical restrictions (not exceeding 2 kA/m and 100 kHz respectively); allow to facilitate the "self regulated" heating and control of T_c in the required temperature range At the same time, volume production of the materials requires higher capacity and lower costs of the production process. Several groups of compounds can be proposed to be the object of the detailed research. However, the above requirements "narrow" the possible choice and reduce it to a small group of compounds, among which two materials attracted a special interst: Cu-Ni and $Ag_xLa_{1-x}MNO_3$. Ni-Cu nanoalloys with TC = 41-44^{0}C have been synthesized and tested as a material for self-regulating magnetic hyperthermia. Recently, the nanostructured $La_{1-x}Ag_xMnO_3$ has attracted great attention for magnetic hyperthermia applications as a nanomaterial with very specific properties as a basis for therapeutical heating agent with precisely regulated and controlled T_c. However, there are no available data on their toxicity under the conditions of relatively low exposure.

2. RESEARCH METHODOLOGY

2.1. Development and study of materials for the Curie Temperature limited magnetic hyperthermia.

Intensive research in the field of developing microwave enhanced and hydrazine and ammonium chloride utilizing technologies and corresponding installation for producing nanoparticles and nanostructures has been recently carried out in Georgia, and abroad [55-60]. The applied methods showed the following advantages compared with the methods utilizing conventional heating and chemicals: heating of samples is uniform and proceeds from "inside"; an extremely high heating rate of selective heating of the individual components in the mixture, low inertia of treatment, additional non-thermal excitation of precursor, etc. As a result, the synthesized nanomaterials show improved monodispersity, perfect crystal structure and uniform composition.

As mentioned above, during the last 5 years the main activities of a group of researchers were focused on the processing of manganese oxide compounds, manganese based alloys and multi-component master alloys, as well as synthesis of nanoparticles and nanomaterials using metal oxides and magnesium/aluminum reductants.

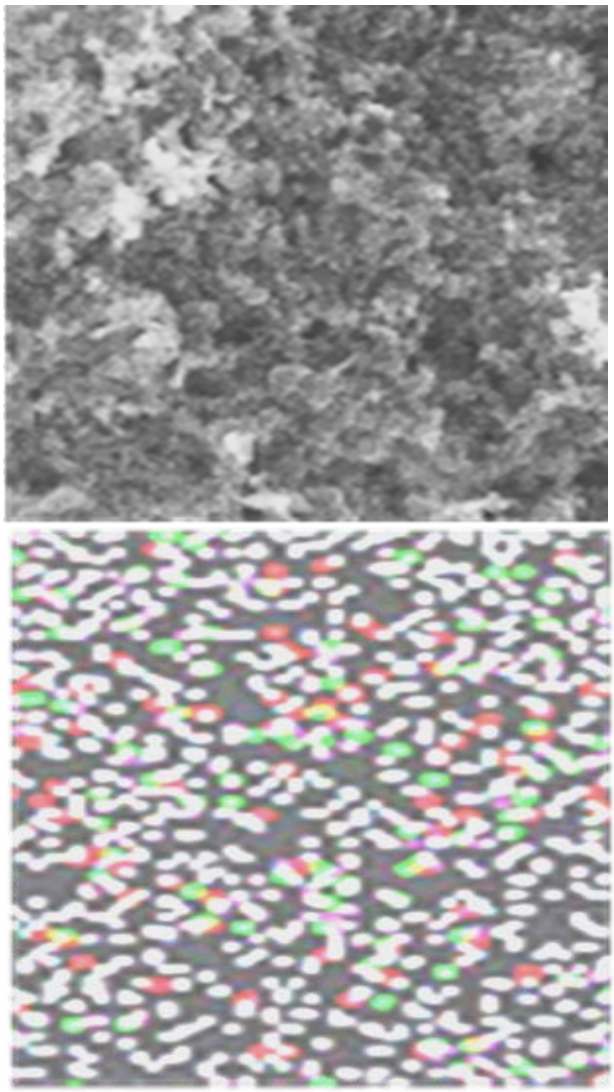

Figure. 1. TEM image of carbon-Ag doped lanthanum manganite hybrids and corresponding mapping of Ag, La, Mn and C

Another important area of research was the microwave enhanced "green" and SHS synthesis of Au, Ag, $Mn/MnO/MnO_2$ and $MnO_{1-x}Mg_x$ nanoparticles. A novel technology using manganese

oxides and hydrazine utilizing conventional and microwave enhanced methods can be also applied to obtain samples of nickel-copper compounds and silver doped lanthanum manganite.

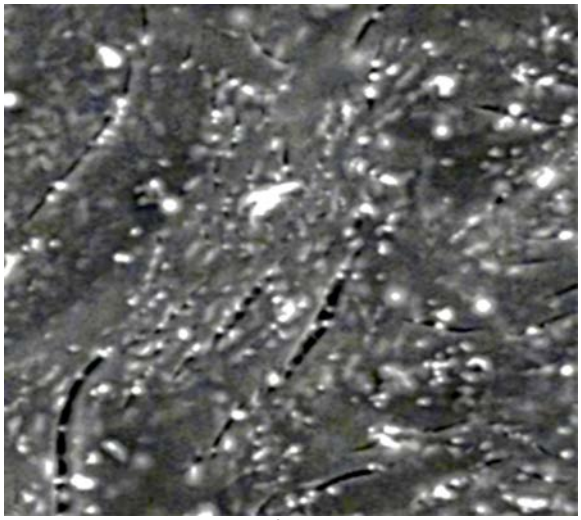

Figure 2. SEM image of a Ni 0.7Cu 0.3/C sample

The research also aimed at the microwave enhanced synthesis and study of La1-$_x$Ag$_x$MnO$_3$ particles was executed utiliazing SEM and TEM microscopy and high power-density (up to 10^3 kW/m3) microwave technique, as well as at the development installation for microwave enhanced "green synthesis", synthesis of Mn-MNPs and pyrolytic synthesis of core-shell nanomaterials using hydrazine vapor [64-70]. All this provided the possibility for obtaining the targeted materials – nickel-copper alloy nanoparticles and Ag doped lanthanum manganite nanoparticles – with the optimal content of Ni-Cu and Ag-LaMnO$_3$ for the required ranges of Tc (39-48) °C. Properly controlled size and monodispersity of nano-particles was the main goal of the research. A special issue of the research was the possibility of obtaining the La$_{1-x}$Ag$_x$MnO$_3$ nanoparticles using soluble salts of La, Ag, Mn and methods of two stage "green" synthesis (including CO_2 super-extraction and reducing of metals in "green" solvents). The TEM image of AgLaMnO$_3$/C and the corresponding mapping of the synthesized nanocomposites are given in Fig. 1. TEM images of Ni-Cu/C nanocomposites are given in Fig.2 and Fig.3.

As was mentioned above, the biological compatibility of the developed materials for magnetic hyperthermia is one of the most important characteristic and reduce of the toxicity to human organism is one of the main aim of the current research. One possible approach for minimizing the toxicity is to wrap the nanoparticle in a shell of a nontoxic material.

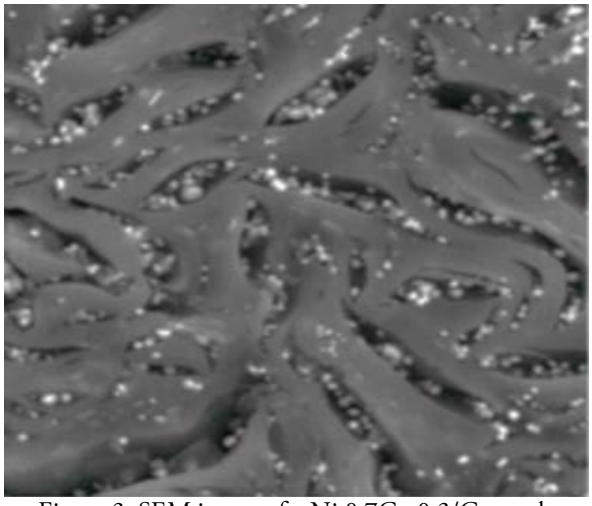

Figure 3. SEM image of a Ni 0.7Cu 0.3/C sample prepared at T ≈ 900°C, t ≈ 30 min

Our new technological approach is based on the application of a well-established nontoxic zinc phosphate shell for covering the magnetic nanoparticles. Previously, we have successfully tested this technology for producing $Zn_3(PO_4)_2$ core/shell nanowires. As a result, the synthesized nanomaterials showed improved mono-dispersity, crystal structure and uniformity, increased velocity of synthesis reaction. Coating and comparing the nanomaterials with $Zn_3(PO_4)_2$ and carbon shells should provide the choose of a better coating method for reducing toxicity and improving dispersity and specific absorption rate of the nanomaterials. For the farther improvement of the required properties of the efficient nontoxic heating nanomaterials for self-regulated magnetic hyperthermia the following works should be especially recommended: a more detailed comprehensive study of the current status of research and planning of the detailed approach for synthesis of nanomaterials and assessment of relative toxicity of investigated materials for magnetic hyperthermia; synthesis of Ni-Cu nanoalloys using conventional and microwave heating, preliminary study and comparative analysis of materials; synthesis of Ni-Cu nanoalloys using conventional and microwave heating, hydrazine and ammonium chloride as additional activating agents, preliminary study and comparative analysis of materials; synthesis of La$_{1-x}$Ag$_x$MnO$_3$ using microwave enhanced and conventional heating,

preliminary study and comparative analysis of materials; synthesis of $La_{1-x}Ag_xMnO_3$ using microwave enhanced and conventional heating, hydrazine and ammonium chloride as additional activating agents; coating of the developed nanoparticles with $Zn_3(PO_4)_2$ shells; study of magnetic properties, monodispersity, uniformity and "morphology' of developed nanoparticles, systematization of the results taking into account the material (Cu-Ni or $La_{1-x}Ag_xMnO_3$), composition, synthesis method, coating, dispersion and uniformity, capacity of methods; analyzis and systematization of the achieved results, selection and optimizing of the most prospective methods (conventional or microwave enhanced) for the synthesis of investigated nano-materials .

2.2. Toxicity Assessment.

Development and/or application of widely differing methods of testing toxicity (examining the negative effects these particles have on biological entities) of MNPs are especialy caused by the neccesity of assessing the impacts far below the level of clearly revealed cytological changes . That is why the preliminary toxicity tests should be focused on behavioral effects, which do not threaten the life and health of experimental animals and, most importantly, determine the toxicity at the levels far below of commonly register by means of usualy applied assays [61-63].Special attention should be paid to the methodologies of toxicity testing with regard to animal right activists around the world who are increasingly opposing the use of animals. Although it seemes impossible in the near future to ban the "involvment" of animals into bio-medical testing, the researchers have to find ways of decrease the number and suffering of animals used and also increase the humane care of animals. To fulfill this goal a number of new in vitro techniques have been devised which are called 'Alternatives' or 'Substitutes' for use of animals in research involving drugs. The proposed approach is aimed to implement the 4R principles in testing of toxocity of nanoparticles for medical use [71-75]. An advanced research for adequate testing of the toxicity of developed materials without and on the background of hyperthermia in the range of (38-48) ^{0}C is focused on the experiments on toxicity assessment on laboratory rats of both sexes. Prior to the injection of the test substances and the initiation of hyper-thermal exposure, experiments are conducted on control animals to reveal the initial state of learning and memory processes, the fear and anxiety levels. To assess the learning and memory processes, a multi-branch maze can be used, while assessment of the levels of anxiety and fear should also utilize the "Elevated Plus-maze" and testing of animals in the so-called "open field". To move on an optimum trajectory rodents are learning due to the "trial and error" method. Changes in quantity of errors (entry into the deadlock compartments of maze), and the time of maze passage are used for evaluation of the process of learning. To be adapted to experimental conditions, all groups of animals prior to the beginning of experiments for a few days have to be placed in a nest-box. At the beginning of the experiment an animal is placed on the start-platform and i it has to find out the correct way to the nest-box. Every subsequent movement on the platform brings the animal to a novel situation and it is a stimulus for a new movement ahead. Reaching of the target-box, therefore deliverance from non-ethological conditions is regarded as an essential reward and serves as a motivation for forward moving through the maze. Anxiety reduction in the plus-maze is indicated by an increase in the ratio of times spent in the light and darkened arms. The total number of entries into the both arms, sometimes are used as the measure of general activity.The general methodology is presented in [76-83]. Here we describe several particular methods which are the following:

Biological (bahavioral) methods. Utilization of various maze techniques in studies of behavioural responses, and learning and memory processes in animals was used at the beginning of the twentieth century and continues to be used up to the present. A variety of maze constructions are in use in experiments; those which are the most convenient and simple to use in experiments on rats, proved to be the maze consisting of platforms (multi-way maze) fixed on supports as high as 30 cm (Fig. 4). This kind of maze allows arbitrary and ready modification - creating more complex or simple tasks, and allowing observations on the animal's behaviour under various experimental conditions.

To move on an optimum trajectory rats are learning by a trial and error method. Changes in quantity of errors (entry into the deadlock compartments of maze), observed from trial to trial in searches of an optimum way to the nest-box (housing)

and full time, needed for complete passage of maze, are used for evaluation of the process of learning. For adaptation to experimental conditions, all groups of animals prior to the beginning of experiments for a few days have to be placed in a nest-box. This nest-box is located at the exit platform of maze. At the beginning of the experiments an animal is placed on the start-platform and it has to find the correct (shortest) way to the nest-box.

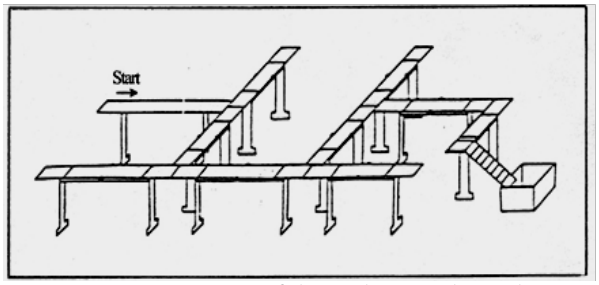

Figure 4. Construction of the multi-way elevated maze

The maze task will be presented to each animal 5 times a day up to the reaching the level of "automatic" behaviour (in normal cases it takes about 7-10 days of testing). The learning process is estimated by maze test performance (to reach the nest-box) - by the number of errors made during ambulation through the maze (enter into the deadlock sections) and by the time spent for maze passage. We believe that this approach is the most adequate for the tasks set out similar studies. By the way, thanks to this maze, the first clear behavioral manifestation of the phenomenon of a Hormesis in vertebrates (laboratory rats) has been achieved. Before, the behavioral manifestation of this phenomenon was described only on Drosophila flies. In order to evaluate of exploratory activity and anxiety-related behaviour of animals the Open Field and Elevated Plus-Maze tests are used. The Open Field is the broadly used test to assess exploratory behaviour and is valid for use in the measurement of anxiety-related behaviour. It is an circular chamber, 80 cm in diameter. The floor in the chamber is divided into 16 sectors. In the corners of the central squares deep 9 "burrows" are located. The rats are placed in the chamber just for 5 minute. In this period of time the following behavioral activities are registered: (1) The number of crossed lines (horizontal loco-motor activity); (2) The number of vertical standings (vertical loco-motor activity); (3) The number of entering in central sectors; (4) The number of explored burrows per minite; (5) The number of fecal boluses. The Elevated Plus-Maze consists of platforms elevated from the floor and has cross-like configuration. Two branches of the maze are open and the other two are surrounded by high walls. Open part allows to investigate the environment, while the protected branches provide safety of the animal. The level of anxiety is evaluated by comparison of the time intervals spent in the open and protected parts of the maze.

Analysis of Blood rheology: Determination of the erythrocytes aggregation index (EAI). Blood samples must be centrifuged and about 0.1 ml blood diluted 1:200 in own plasma in the Thoma pipettes preliminary rinsed with 5% sodium citrate solution, without addition of any other anticoagulants. Following standard mixture with the diluted blood must be placed into a glass chamber. The quantitative index of erythrocyte aggregation is assessed with a special program at the Texture Analysis System (TAS-plus, "Leitz, Germany), representing the relationship of the aggregated and disaggregated red cells.

Blood plasma viscosity: Blood plasma viscosity will be examined in the capillary viscometer. Diameter of the capillary is about 1.8 mm. Displacement of plasma samples is induced by the gravity force related to the difference of levels of the plasma under study (without application of an additional pressure) For evaluation of the plasma viscosity in centipoises (cp) we determin the calibration factor. Blood plasma viscosity is calculated by multiplying the time for plasma displacement through the capillary by the instrument calibration factor.

Evaluation of Systemic Hematocrit: Systemic hematocrit is assessed with centrifuging the blood sample in the standard hematocrit centrifuge, at 8000 rpm, for 10 min.

Statistical analysis: For evaluation of statistical significance of the obtained results and revealed differences between experimental conditions (time of maze passing, mistakes in maze tests and others), a standard one-way and two-way analysis of variance (ANOVA) should be used.

2.3. Evaluation of the prospective of combined treatment of cancer in Georgia.

Evaluation of the near prospective of combined treatment of cancer in several the developed countries (Germany, UK, USA, Australia, Canada) and in

Georgia were made based on the analysis and systematization of available statistical data, a number of scientific papers and the analysis of existing information on the joint state-private project of establishing a specialized centre for Hadron Therapy in Georgia. A three-component „strategy" of evaluation was chosen which utilized the following sources and instruments: cancer statistics; the market research and scientific/technical reports: development and efficiency of common and new methods and materials for cancer treatment, provided by the biggest world actor in the field of magnetic hyperthermia, the German/USA company MagForce AG; information on establishing of the Georgian Institute of Technology (Kutaisi, Georgia) and its scheduled cooperation with partners in Switzerland and Italy.

Cancer statistics. The preliminary analysis of statistics of morbidity and scientific forecast of the risks of contracting cancer was carried out based on the data of more than 100 scientific and statistical sources, papers, presentations and reports (see, for example [1-8, 84-97]. The analysis of data (e. g. the risk of contracting cancer in Germany by five different age categories for next ten years; forecast number of cancer diseases in North America and Europe; probability of contracting cancer in Australia, Canada, North America, Western and Northern Europe, and the world; forecast of the number of prostate cancer in the USA; pancreatic camcer incidence and mortality prediction in UK from 2020 to 2030; projected case numbers in Germany for the five most common cancers in both sexes by 2020 and 2030; projected cancer death numbers in Germany by 2020 and 2030; trends in cancer incidence from 1975 to 2013 and death rates from 1975 to 2014 in USA; trends in incidence rates for selected cancers in United States from 1975 to 2013; etc.) clearly shows, that despite the relative stabilization and even reduction in the projected morbidity and deaths (achieved on the background of increasing the effectiveness of treatment for most types of cancer), their total number is steadily (and in some cases super-linearly) and rapidly increasing. This, apparently, is caused by population growth and excessive pollution of the environment around the world. The sad truth is that, at least for the next several decades, the demand for drugs, equipment and materials and services for cancer treatment will also grow rapidly and steadily. Table 3 represents the statistics of new cases (in thousands) and death cases for different types of cancer in USA in 2017.

Market research and scientific/technical reports. The world leader in magnetic hyperthermia treatment - MagForce AG - operates and develops its activities in Germany and the United States together with its subsidiary MagForce USA Inc., and is a leading medical device company in the field of nanomedicine focused on oncology [98-99]. The Group's proprietary NanoTherm™ therapy enables the targeted treatment of solid tumors through the intra-tumoral generation of heat via activation of superparamagnetic nanoparticles.

Table 3. Estimation of new cases (in thousands) and death cases for different types of cancer in USA in 2017

Type of cancer	Estimated new cases	Male	Female	Estimated deaths, 2017	Male	Female
Breast	255.3	2.5	253.000	41.1	40.6	0.5
Lung and bronchus	222.5	117.0	105.5	155.9	84.6	71.3
Prostate	161.4	161.4	-	26.7	26.7	-
Colon and rectum	135.4	71.4	64..0	50.3	27.2	23.0
Melanoma of skin	87.1	52.2	34.9	9.7	6.4	3.3
Urinary bladder	79.0	61.55	18.5	16.9	12. 3	4.6
Non-hodgkin lymphoma	72.2	40.1	32.5	20.1	11.4	8.7
Kidney and renal pelvis	64.0	40.6	23.4	14.4	9.5	4.9
Leukemia	62.1	33.5	25.1	24.5		
Uterine corpus	61.4	-	61.4	10.9	-	10.9
Thyroid	56.9	14.4	42.5	2.0	0.9	1.1
Pancreas	53.7	28.0	25,7	43.1	22.3	20.8
Oral cavity and pharinx	49.7	35.7	14.0	9,7	7.0	2.7
Liver and inter-hepatic blue duct	40.7	29.2	11.5	28.9	19.6	9.3
Myeloma	30.3	17.5	12.8	12.6	6.7	5.9
Stomach	28.0	17.7	10.3	11.0	6.7	4.3
Brain and other nervous system	23.8	13.4	10.4	16.7	9.6	7.1
Ovary	22.4	-	22.4	14.1	-	14.1
Esophagus	16.9	13.4	3.5	15.7	12.7	3.0
Larynx	13.4	10.6	2.8	3.7	2.9	0.8
Cervix	12.8	-	12.8	4.2	-	4.2
Testis	8.9	8.9	-	0.4	0.4	-
Hodgkin lymphoma	8.3	4.7	3.6	1.1	0.6	0.5
Childhood and adolescent cancer	10.3			1.2		

Mithril Capital Management, a growth-stage technology fund, along with MagForce AG, are investors and strategic partners in MagForce USA, Inc. In November 2015 MagForce AG announced that MagForce USA, Inc., MagForce AG's US subsidiary, has successfully installed the first clinical NanoActivator® in the USA. This NanoActivator® is similar in design to the five NanoActivator® devices operating at University Hospitals in Germany applying NanoTherm™ Therapy for the treatment of

Brain Tumors. However, the USA NanoActivator® has been modified to apply NanoTherm™ Therapy for the treatment of Prostate Cancer in addition to the treatment of Brain Tumors.

There are currently six hospitals in Germany who offer NanoTherm® Therapy with the NanoActivator in Berlin, Kiel, Cologne, Munster, Gottingen, and Frankfurt. The USA NanoActivator® is located in Seattle, Washington, near the University of Washington Medical Center, and will be utilized during the Focal Thermal Ablation Registriation Study for Prostate Cancer for which the Company has established an Investigational Device Exemption (IDE) with The US Food and Drug Administration (FDA) in May 2015. The business policy of Mag Force (as well as our expectations) is based on the two main three factors: analysis of statistics of cancer and scientific forecast of the risks of contracting cancer, analysis of the sales/earns history and forecasts of the MagForce AG, and analysis of efficiency of the NanoTherm™ Therapy when utilized separately and in conjunction with other therapies (chemotherapy, radiotherapy, hormone therapy). Taking into account the recent achievements in development of basics of photodynamic treatment and our unpublished preliminary data on development of complex nano-liquids for combined radio-, chemo-, hormone-, photodynamic- and magnetic hyper-thermal an intensive extent of research in development of four-five component nanostructured materials research can be predicted [30, 100-103. Moreover, the recent preliminary research of the possibility of incorporating appropriate photosensitizers (phthalocyanines, photoditazine, e6 chlorine derivatives, etc.) into the outer shell of the developed nanocomposites for magnetic hyperthermia (carbon or $Zn_3(PO_4)_2$) shows that the developed materials can be used in the photodynamic therapy (PDT) and/or magnetic hyperthermia. In addition, in the case of a detailed study of the dependence of the absorption spectra and the radiation of photosensitizers (PS) on the temperature in the range 40-50 ° C, a technique for direct measurement and control of the heating temperature during magnetic hyperthermia and photodynamic therapy can be proposed. The existing data also show us, that the period after 2021 should be a very promising time for the sustainable commercial implementation of findings and achievements of the scientific research.

Establishing of the Georgian Institute of Technology (Kutaisi, Georgia). An especially important factor providing and enhancing the sustainability and successful commercialization of project results in Georgia and at the international level is the linked with establishing of the fifth largest Institutes of Technology (after Italy, Switzerland, Austria and Japan) which has begun in Georgia. The most important component of the project is the construction of a particle accelerator (collider) to conduct important studies, including the main component-research and practicle treatment using Hadron Therapy. The Government of Georgia has signed memoranda with some of the world's leading centers, including CERN (European Center for Nuclear Research), CNAO (National Center for Hadron Therapy), and INFN (Italian National Institute of Nuclear Physics) on cooperation in implementation of the project funded with the leading participation of the International Charity Fund "Cartu" with total amount of Euro 500,000,000. Adjuvant treatment options (combining hadron therapy, magnetic hyperthermia, and probably – chmeotherapy, hormone therapy and photodynamic) can be one of the important part of the research and practical activities of the Georgia Institute of Technology. In the nearest future researchers from the Georgian Technical University and Ivane Beritashvili Center for Biomedicine in cooperation with the foreign collaborators will work out a special program for investigation and implementation of combined treatment of brain, prostate and pancreas cancer utilizing the achievements in development of multi-component nano-liquids for cancer therapy.

3. CONCLUSIONS

Utilization of the microwave and hydrazine based new technologies for the growth of Ag-doped $LaMnO_3$ and/or NiCu coated nanocomposites for magnetic hyperthermia is a promising way for producing nanocomposites with the unique combination of properties as follows: very low or low toxicity, self-regulated ("self-controlled") heating in the required range of temperatures with precisely controlled temperature of heating agents by means of "tuning" of the Curie Temperature of developed nanomaterials, capability of performing hyper-thermal treatment

using the same material with different Curie points, low alternating magnetic field (AMF) power consumption, optimized size and monodispersity of nanoparticles (providing high efficiency and uniformity of heating).

Development and/or application of widely differing methods of testing toxicity (examining the negative effects these particles have on biological entities) of MNPs are especialy caused by the neccesity of assessing the impacts far below the level of clearly revealed cytological changes. Conclusions on applicability of behavioral (cognitive) assessment methods for toxicity testing of nanoparticles as alternatives and substitutes to usual "animal testing" practice can play certain role for more intensive implementation of 4R-proinciples in biomedical research.

The achieved results indicate the possibility of development of the new integrated nanocomposites for the magnetic hyperthetmia and photodynamic therapy of cancer, which can also be used for the indicating and control of the heating temperature. There is a great interest in developing of effective combined methodology of cancer treatment including radiotherapy, chemotherapy, hormone therapy, magnetic hyperthermia and photodynamic therapy.

4. ACKNOWLEDGMENTS

This work was financially supported by the Grant # 04/05-2016 of the Shota Rustaveli National Science Foundation and the Grant # 6204 of the Science and Tchnology Center in Ukraine.

5. REFERENCES

1. Rebecca L. Siegel, Kimberly D. Miller, Ahmedin Jemal./Cancer Statistics, CA: A Cancer Journal for linicians, 2017, 67, p.7-30.
2. Rebecca L. Siegel, Kimberly D. Miller, Ahmedin Jemal./ Cancer Statistics, CA: A Cancer Journal for Clinicians, 2015, 65, p.5-29.
3. Wingo PA, Cardinez CJ, Landis SH, et al. /Long-term trends in cancer mortality in the United States, 1930-1998. Cancer. 2003, 97(suppl 12), p.3133-3275.
4. Murphy SL, Kochanek KD, Xu J, Heron M./ Deaths: Final Data for 2012. National Vital Statistics Reports. v. 63. No. 9. Hyattsville, MD: National Center for Health Statistics; 2015.
5. Statistical Research and Applications Branch. DevCan: Probability of Developing or Dying of Cancer Software. Version 6.7.4. Bethesda, MD: Surveillance Research Program, Statistical Methodology and Applications, National Cancer Institute, 2012.
6. Howlader N, Noone AM, Krapcho M, et al./ SEER Cancer Statistics Review, 1975-2013. Bethesda, MD: National Cancer Institute, 2016.
7. Copeland G, Lake A, Firth R, et al./ Cancer in North America: 2009-2013. Vol 1. Combined Cancer Incidence for the United States, Canada and North America. Springfield, IL: North American Association of Central Cancer Registries Inc., 2016.
8. Steliarova-Foucher E, Stiller C, Lacour B, Kaatsch P./ International Classification of Childhood Cancer, Third Edition. Cancer. 2005,103, p.1457–1467.
9. Kerner T., Deja M., Ahlers O., Loffel J., Hildebrandt B., Wust P., Gerlah H., Riess H./ Intensive Care Med., 1999, v.25, 9, p.959-965.
10. Roesch,M. B.Mueller-Huebenthal/Indian J. Surg. Oncol., 2015, v.6, 1, p.75–81.
11. Jones O. P., J. D. Melling, P. Ghaneh./ World J. Gastroenterol., 2014, v.20, 40, p.14733–14746.
12. Neena Girish Shetake, Murali M.S Balla, Amit Kumar, Badri Narain Pandey./ Journal of Ratiation and Cancer Research, 2016, v.7, p. 13-17.
13. Kaur P, Hurwitz MD, Krishnan S, Asea A./ Cancers (Basel), 2011, v.3, p. 3799-823.
14. Alexandrov N., Savchenko N., Fradkin S./ Applying of Hypethermia to maligmnant tumours. Moscow: Medicine, 1980, p.598 (in Russian).
15. Selawry OS, Goldstein MN, McCormick T. / Cancer Res., 1957, v.17 (8), p.785-791.
16. Von Ardenne M, Kirsch R./Deutsche Gesundheitswesen, 1965, v. 20 (43), p.1935–1940.
17. Bicher, J., Hetzel F., Mitagvaria N./ Ann. N.Y. Acad. Sci., 1980, 335, p.236-237.
18. Bicher, J., Mitagvaria N./ Microvascular Research 1981, v.21, p.19-26.
19 Bicher, J., Vaupel P., O'Hara M., O'Brien T., Mitagvaria N./ Adv. Physiol. Scil, v. 25, Oxygen Transport to Tissue, Pergamon Press (Eds: A. Kovach, E. Dora, M. Kessler, I. Silver) 1981, p. 215-224.
20 Bicher, J., Mitagvaria N., Bruley D./ Changes in tumor tissue oxygenation during microwave

hyperthermia: Clinical relevance. In: Oxygen Transport to Tissue – VI, (EDS: D. 54. Bruley, H. Bicher, D. Reneau), Plenum Press, New York, 1984, p.861-879.
21 El-Sabban F., Fahim M.A./ Int. J. Biometeorol, 1995, v.38, 2, p.92-97.
22 Fahim M.A., El-Sabban F./ Anat. Rec., 1995, v.242, 1, p.77-82.
23 Fajardo L.F. / Cancer Res., 1984, v.44, p.4826-4835.
24 Fike J.R., Gobbel G.T., Satoh T., Stauffer P.R./ J. Int. J. Hyperthermia, 1991, v. 7, 5, p. 795-808.
25 Hall D.M., Baumgardner K.R., Oberley T.D., Gisolfi C.V./ Am. J. Physiol, 1999, v.276, 5, p.G1195-G1203.
26 Harris A.B., Erickson L., Kendig J.H., Mingrino S., Goldring S./ J. Neurosurg., 1962, v.19, p.514-521.
27 Bosort R./ Ferromagnetism, Moscow: IL, 1956, p. 195.
28 Lyons B.E., Britt R,H, Strohbehn J.W./ IEEE Trans. Biomed. Eng., 1984, v.31, p.53-62.
29 Madden A., Glaholm J., Leach M.O./ Br. J. Radiol., 1990, v.63, 746, p.120-124.
30 Urtizberea A., E. Natividad, A. Arizaga, M. Castro, A. Mediano./ J. Phys. Chem C, v.114, p.4916-4922.
31.Gupta, H., P. Paul, Kumar N./ Proc Mater Sci 2014, v.5, p.198–203.
32. Li, X. J. Wei, K. E. Aifantis, Y. Fan, Q. Feng, F. Cui, F. Watari./ Journal of Biomedical Materials Research A, 2016, v.104, 5, p.1285–1296.
33 Dutz S. and R. Hergt. / Nanotechnology, 2014, v.25, 45, p. 2001-2004 .
34 Deatsch A.E., B.A. Evans/ Journal of Magnetism and Magnetic Materials, 2014, v.354, p.163-167.
35 Shubitidze. F., K. Kekalo, R. Stigliano and I. Baker. / J. Appl. Phys., 2015, v.117, p.094302-07.
36 Chatterjee, J. M., Bettge Y., Haik, Ch.J. Chen. / J. Magn. Magn. Mater., 2005, v.293, p. 303-309.
37. Liu X.-M., S.-Y. Fu, C.J. Huang./ Mater. Lett., 2005, v.59, p.3791-3795.
38. Mehdaoui B., A. Meffre, J. Carrey, S. Lachaize, L. M. Lacroix, M. Gougeon, B. Chaudret, and M. Respaud./ Adv. Func. Mater., 2011, v.21, p.4573-4581.
39. Sminia P., Van der Zee J., Wondergem J./ Int. Hyperthermia, 1994, v.10, p.1-130.
40. Sminia P., Hulshof M. / Progress in Brain Research (H.S.Sharma and J. Westman (Eds)), 1998, v.115, p.337-350.
41. Toyota N., Strebel F. R., Stephens L. C., Rowe W., Matsuda H., Oshiro T., Jenkins G.N., Bull J.M./ Oncol. Rep., 1998, v.5, 5, p.1231-1236.
42. Samaras G.M., Salcman M., Cheung A.Y., Abdo H.S., Schepp R.S./ Natl. Cancer Inst. Monogr., 1982, v.61, p. 477-482.
43. Abhishek Srivastava, Laura M. Douglass, Victoria Chernyak, Kara L. Watts./ Current Urology Reports, 2017, v.18, 9, p. 156-160.
44. Qing Kay Li, Punit Shah, Yuan Tian, Yingwei Hu, Richard B. S. Roden, Hui Zhang, Daniel W. Chan/ Clinical Proteomics, 2017, v.14, p.1-7.
45. GBC AG Investment Research./ Research & investment analysen, 2015, v.19 (05), p.36-41.
46. Jones O., Melling J., Ghaneh P./World J Gastroenterol. 2014, v.20, 40, p. 4733–14746.
47. Silberman A.W., Morgan D.F., Storm F.K., Rand R.W., Bubbers J.E., Brown W.J., Morton D.L. / J. Surg. Oncol., 1982, v.20, p.174-178.
48. Ikeda N., Hayashida O., Kameda H., Ito H., Matsuda T./ Int. J. Hyperthermia, 1994, v.10, p.553-561.
49. Sneed P.K., Matsumoto K., Stauffer P.R., Fike J.R., Smith V., Guitin P.H./ Int. J. Radiat. Oncol. Biol. Phys., 1986, v.12, p.1887-1897.
50. Takahashi S., Tanaka R., Watanabe M., Takahashi H., Kakinuma K., Suda T., Yamada M., Takahashi H./ Int. J. Hyperthermia, 1999, v.15, 3, p.203-216.
51. Mitagvaria N., Bicher J./ Cerebral Blood Flow Regulation. Nova Science Publishers Inc, New York, 2009, p. 236.
52. Mitagvaria N., J. Bicher, M. Devdariani, L. Davlianidze, M. Nebieridze, N. Momtselidze/ Oncothermia Journal, 2013, v. 7, p. 62-68.
53. Torres-Lugo M., Rinaldi C./ Nanomedicine, 2013, v.8,10, p.1689-1707.
54. Ren Y. et al./ Int J Nanomedicine. 2012, v. 7, p.2261–2269
55. Gorbenko O., Melnikov O., Kaul A. , Balagurov A., Bushmeleva S., Koroleva L., Demin R../ Mater Sci Eng B., 2005, v. 116, p. 64-70.
56. Melnikov O.. Gorbenko Yu, Markelova M., Kaul A., Atsarkin V., Demidov V., Soto C.,. Roy E., Odintsov B./ Jornal of Biomedical Materials Research, 2009. DOI: 10.1002/jbm.a.32177.

57. Berberashvili T., Buachidze Z., Chirakadze A., Chakhvashvili1 L., Jishiashvili D., Kacharava G., Kervalishvili P., Khomeriki I., Aleqsanyan S., Gyulasaryan H., Manukyan A., Papoyan A., Sharoyan E., Sajti L./ Nano Studies, 2017, v.1, p.104-111.
58 Mirzakhanyan A., Manukyan A., Badalyan G, Khachatryan T., Maslova O., Yuzyuk L., Bugaev L., Sharoyan E./ Proc. SPIE, 2010, v.79981B-1–79981B-4.
59. Manukyan A., Mirzakhanyan A., Khachatyran T., Khachaturyan R., Badalyan G., Sharoyan E./ Armenian Journal of Physics, 2013, v.6, p.61-66,.
60. Kuznetsov A., Leontiev V., et al./ J. Magn. Magn. Mater., 2007, v.311, 197, p.204-207.
61. Soenen S, De Cuyper M./ Contrast Media Mol Imaging. 2011, v.6, 3, p.153-164.
62. Egorova K., Ananikov V./ Angewandte Chemie, 2016, v.55, 40, p.12150–12162.
63. Kalantzi I., Biskos G./ Toxics, 2014, v.2, p.79-91.
64. Bano S., Nazir S., Nazir A., Munir S., Mahmood T., Afzal M., Ansari F., Mazhar K./ Int. J Nanomedicine, 2016, v.11, p. 3833–3848.
65. Kahrilas G., L. M. Wally, S. J. Fredrick, M. Hiskey, A. L. Prieto, J. E. Owens/ ACS Sustainable Chem. Eng., 2014, v.2, 3, p.367–376.
66. Chirakadze A. et al./ Advenced materials and Technologies" Proceedings. Tbilisi, Georgia, 2015, p. 297-301.
67. Di Corato R., Bealle G., Kolosnjaj-Tabi E., Espinosa A., Clément O., Silva A., Ménager C., Wilhelm C./ *ACS Nano,* 2015, v.9, 3, p.2904–2916.
68. Kervalishvili P., A. Chirakadze, Z. Buachidze, D. Jishiashvili1, T. Bjalava, G. Kervalishvili, W. Toscano, V. Gvakharia, G. Sergeenko. Microwave in environmental technologies and synthesis of nano-materials: Georgian experience. Nuclear Radiation Sensors and Nanosensory Systems. Edited by Paata 1J. Kervalishvili (Physics Department of Georgia Technical University, Tbili, Georgia) and Panos H. Yannakopoulos (Department of Electronic Computer Systems Engineering, Piraeus University of Applied Sciences). Selected paper from the Advanced Research Workshop which was held in Tbilisi, March 6-9 2014. Springer, 2016, p.22-86.
69. Patzke G. R., R. Kontic, Z. Shiolashvili, N. Makhatadze, D. Jishiashvili./ Materials, 2013, v.6, p.85–100.
70. Jishiashvili D, V. Kapaklis, X. Devaux, C. Politis, E. Kutelia, N. Makhatadze, V. Gobronidze, and Z. Shiolashvili./ Advanced Science Letters, 2009, v. 2, p.40–44.
71 Arora.T, A. K. Mehta,1 V. Joshi, K. D. Mehta, N. Rathor, P. K. Mediratta, K. K. Sharma./ Indian J Pharm Sci., 2011, v.73, 1, p.1–6.
72 Moser, V.C., S.E. Bowen, A.A. Li, W.S/ Sette, and W.P. Weisenburger./ Cognitive evaluation: Is it needed in neurotoxicity screening? Symposium presented at the annual Behavioral Toxicology Society meeting. Neurotoxicol. Teratol., 1999, 22, 6, p.785-798.
73 Kakeyama M, A. Haijimai, T, Endo, C. Tohyamai./ Japanese Journal of Animal Psychology, 2011, v.61, 1, p.33-42,
74 Schechtman L. M../ Implementation of the 3Rs (refinement, reduction, and replacement): Validation and regulatory acceptance considerations for alternative toxicological test methods. ILAR J. 43 (Suppl.), 2002, p.85–94.
75 Mandal J. and S. Chandra Parija./ Tropical Parasitology 2013, v.3, 1, p.4–6.
76 Van der Zee J., Broelmeyer-Reurink M. P. VAN DEN Berg A.P. van Geel B.N., Jansen R.F., Kroon B.B., van Wijk J., Hagenbeek A./ Eur. J. Cancer. Clin. Oncol., 1989, v.25, 8, p.1157-1163.
77 Van der Zee./ Annals of Oncology, 2002, v. 13, p. 1173-1184.
78 Yamada N./ No to Shinkei, 1989, 41, 2, p.205-212.
79 Mitagvaria N., J (H) Bicher./ Hormetic Effect of Whole Body Hyperthermia (experimental study on rats). In: Thesis Collection of The 32nd Annual Conference of The International Clinical Hyperthermia Society (ICHS), Guangzhou, CHINA, 2013, p.107-116.
80. Mitagvaria N., Gumberidze L., Davlianidze L., Devdariani M., Kvachakidze I., Nebieridze M., Sikharulidze N./ Proceedings of Georgian National Academy of Sciences, Biomedical Series, 2013, v.39, 3-4, p.113-123.
81 Mitagvaria N., I. Lazrishvili, M.Devdariani, L. Davlianidze, M. Nebieridze, N. Saginadze, I.Kvachakidze, L. Gumberidze, N. Sikharulidze./

Journal of Biological Physics and Chemistry, 2015, v.15, p.187-193.
82. Mitagvaria N., M. Nebieridze, M.Devdariani, et al./ The possible Mechanisms of Local Hyperthermia-induced Morphological Changes in Cerebral Tissue. In: Systemic, Cellular and Molecular Mechanisms of Physiological Functions and Their Disorders (Proceedings of I. Beritashvili Center of Experimental Biomedicine – 2015) Ed.: Nodar Mitagvaria. Nova Science Publishers Inc., New York, 2016, p. 187-206.
83 Rossi S., Zanier E.R., Mauri I., Columbo A., Stacchetti N./ J. Neurol. Neurosurg. Psychiatry, 2001, v.71, p.448-454.
84 Sato E./ Japanese Journal of Radiological Technology, 2017, v.73, 5, p.423-427.
85. Bogani G. et all / Gynecologic Oncology, 2017, v.56, p.277-289.
86. Carioli G, et all/ Annals of Oncology, 2017, p 121-125.
87. Smith Robert A., et all / Cancer Journal for Clinicians, 2017, v.67, 2, p.100-105.
88. Warren C., W. Chan, Ali Khademhosseini, Wolfgang Parak, Paul S. Weiss./ Cancer: Nanoscience and Nanotechnology Approaches, ACS Nano, 2017, v.11, 5, p.43-75.
89. Nicole M. Niehoff, Alexandra J. White, Dale P. Sandler./ Breast Cancer Research and Treatment, 2017, v.164, 3, p.697-703.
90. Michele M. Gage, Matthew T. Hueman./ Current Colorectal Cancer Reports, 2017, v.13, 4, p.316-320.
91. Jiaquan Xu, M.D.; Sherry L. Murphy, B.S.; Kenneth D. Kochanek, M.A, Brigham A. Bastian, B.S. National Vital Statistics Reports. Deaths: Final Data for 2013, v.64, 2, 2016, p.1-118.
92. Kenneth D. Kochanek, M.A., Sherry L. Murphy, B.S., Jiaquan Xu, M.D., Betzaida Tejada-Vera, M.S./ National Vital Statistics Reports. Deaths: Final Data for 2014, v.65, 4, 2017, p.1-116.
93. Statistical Research and Applications Branch. DevCan: Probability of Developing or Dying of Cancer Software. Version 6.7.4. Bethesda, MD: Surveillance Research Program, Statistical Methodology and Applications, National Cancer Institute; 2012.
94. Copeland G, Lake A, Firth R, et al./ Cancer in North America: 2009-2013. Vol 1. Combined Cancer Incidence for the United States, Canada and North America. Springfield, IL: North American Association of Central Cancer Registries Inc; 2016.
95. Rebecca Siegel, Jiemin Ma, Zhaohui Zou, Ahmedin Jemal./ CA: A Cancer Journal for Clinicians, 2014, v.64, p.9-29.
96. Jiang, Z., Z. Qiu, and J. Hatcher/ Joinpoint Trend Analysis of Cancer Incidence and Mortality using Alberta Data. Available at www.cancerview.ca/idc/groups/public/ documents/ webcontent/csen_cproj_fy0910q3 joinpoint.pdf (accessed on March 19, 2018).
97. Cancer in Germany 2011/2012. 2015. Association of Population-based Cancer Registries in Germany (GEKID). Robert Koch Institute (RKI), Berlin.
98. MagForce AG./ The Nanomedicine Company. Commercialisation and approval fully financed, important financing milestone achieved, increase in treatment figures expected, approval in the USA planned. Research Report (Anno). Completed and published: August 24, 2017, p. 20.
99. MagForce AG./ The Nanomedicine Company Regional Expantion with a Defined Strategy. Anual financial report 2016. Completed and published: June 30, 2017, p 78.
100. Uzdensky. A.B./ The biophysical aspects of photodynamic therapy. Biophysics, 2016, v.61,3, p.461-469.
101. Eun Ji Hong, Dae Gun Choi, Min Suk Shim./ Acta Pharmaceutica Sinica B, 2016, v. 6, 4, p.297-307.
102. Uzdensky A. B., O.Y. Dergacheva, A. A. Zhavoronkova, A. V. Reshetnikov, G. V. Ponomarev./ Life Sciences, 2004, v.74, p.2185-2197.
103. Rao W, Deng ZS, Liu J./ Crit Rev Biomed Eng 2010, v.38, p.101-116.

GROWTH OF InP BASED COMPOSITE NANOWIRES

D. JISHIASHVILI[12*], A. CHIRAKADZE[1], Z. SHIOLASHVILI[1], N. MAKHATADZE[1], A. JISHIASHVILI[1], D. KANCHAVELI[1], D. SUKHANOV[1], V. GOBRONIDZE[1]

[1] Georgian Technical University, 77 Kostava St., 0175, Tbilisi, Georgia.
[2] E. Andronikashvili Institute of Physics, I. Javakhishvili Tbilisi State University, 6 M.Tamarashvili St., 0177, Tbilisi, Georgia.

The core-shell nanowires comprising crystalline InP core and amorphous Zn3(PO4)2 shell were produced due to the spontaneous segregation of phases during the pyrolytic synthesis in hydrazine vapor. The nanowires were grown on Si substrate after sublimation of volatile species formed at the surfaces of Zn+InP or ZnO+InP source materials. It was established, that InP cores have a wurtzite structure, while the shells remained amorphous in the whole range of growth temperatures (420-460□C). The shell thickness was doubled when ZnO source was used instead of Zn. This was explained by an increase of oxygen content in the reactor, which led to the enhancement of Zn3(PO4)2 synthesis.

PACS numbers: 81.07.Gf, 61.46.Km
Keywords: InP, nanowire, zinc phosphate, core-shell, hydrazine.
***E-mail:** d_jishiashvili@gtu.ge

1. INTRODUCTION

The bulk Indium phosphide is a popular semiconductor, which has been well studied and applied in different devices. InP nanomaterials, particularly InP nanowires, also attracted great interest owing to their unique properties that arise due to the low dimensionality and subsequent increase of quantum mechanical and surface related features, ability to accommodate more strain than the planar structure etc. [1-4]. The core-shell nanostructures represent another rapidly developing class of nanowires. Their optical, mechanical and electrical properties can be precisely tuned by selecting a proper pair of core and shell materials [5-11].

In most core-shell nanowires the shell comprises crystalline material. However, in some cases the amorphous structure of a shell is more desirable, due to its homogeneous nature and anisotropy of physical properties. One such example is the gate-all-around nanowire transistor. The growth of amorphous 1D nanomaterials is problematic and needs the application of templates and special technological approaches [12-15].

The purpose of this work was to investigate the composition and structure of composite core-shell nanowires grown on Si substrate by annealing of Zn, In and phosphorus-containing solid sources in the vapor, formed after pyrolytic decomposition of hydrazine.

2. EXPERIMENTAL

Previously we have developed the simple pyrolytic technology for the growth of nanowires and the technological details can be found elsewhere [16]. The growth process of nanowires implies the annealing of solid sources up to 750°C in the vapor of hydrazine (N_2H_4) containing 3-5 mol.% H_2O. After interaction of sources with hydrazine decomposition products, the volatile species are formed, which then reach the substrate located in the cold zone of the vertical reactor, thus enabling the mass transfer and synthesis of nanowires. Some details of the developed technology will be discussed in the next section.

The morphology, composition and structure of NWs were studied using following instruments: TESCAN Vega 3 LMU Scanning Electron Microscope (SEM) equipped with Energy-dispersive X-ray spectrometer (EDS), Philips CM200 FEG Transmission Electron Microscope (TEM), and Fourier-transform IR spectrometer Shimadzu IRAffinity-1S Spectrometer.

3. RESULTS AND DISCUSSION

Two types of sources were used for the growth of nanowires: solid InP with metallic Zn and InP with ZnO powder. Zn easily evaporates because it has a low melting point and sufficiently high saturated pressure even at low temperatures (e.g. 10^{-4} Torr at 250°C [17]). As for ZnO, it has a high melting point ((1975°C) and dissociation temperature [18,19], which exceeds the temperatures used in our experiments. One way to overcome the problem is the application of reducing precursors that may transform ZnO to pure Zn, which will then readily sublimate. In our previous works it was established that the pyrolytic decomposition of hydrazine results in the formation of such active reducing radicals as NH and NH_2, together with the appearance of atomic and molecular hydrogen [16].

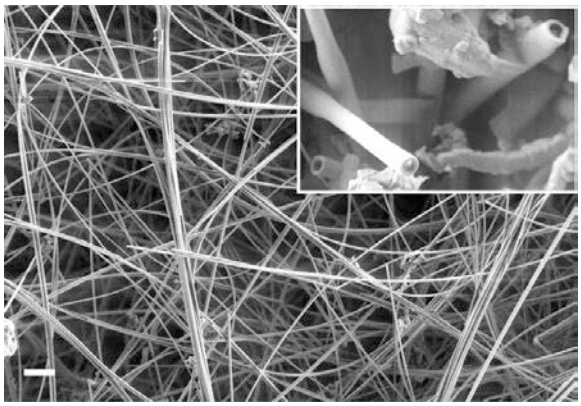

Figure 1. SEM image of nanowires synthesized at 440°C from InP+Zn source. Inset shows the cross-section of nanowires. The bar length equals to 1 mcm.

The dissociation of InP at elevated temperatures and subsequent formation of phosphorus vapor is another important issue, which deserves special attention. It has been reported that the atomic hydrogen, which in our technology can be generated via hydrazine decomposition, may reduce the InP decomposition temperature by 230°C, thereby promoting the formation of P, P_2, P_4 and PH_3 species with a pressure up to10^{-5} Torr [20,21]. The phosphorus vapor formed after dissociation of InP was successfully used for the synthesis of pure Zn_3P_2 nanowires, that were not containing even any traces of indium [22]. Besides the formation of phosphorus vapor, the decomposition of InP caused also the appearance of In droplets and the formation of volatile In_2O molecules after interacting with water molecules presented in hydrazine [16].

Fig. 1 represents SEM images of nanowires formed from the InP+Zn source on the Si substrate heated up to 440°C. The nanowires have uniform diameters ranging from 200 to tens of nanometers. The absence of ball-shaped catalyst tips at the ends of nanowires indicates that they were growing by the Vapor-Solid mechanism. The inset in Fig. 1 clearly demonstrates the formation of core-shell one dimensional nanostructures.

The same was confirmed by TEM data. Fig. 2a,b presents the TEM images of nanowires produced from InP+Zn (a) and InP+ZnO (b) sources. It was found that, in contrast to bulk InP, the crystalline core of nanowire comprises indium phosphide with a wurtzite structure, growing along [0001] direction. The inset in Fig.2a shows the Fast Fourier Transform (FFT) of a core material taken along $[\bar{2}1\bar{1}0]$ axis. The wurtzite (WZ) structure is frequently observed in InP NWs, because they have the increased surface to volume ratio. This forces the growing NW to adopt the WZ structure that has a lower surface energy in comparison with Zinc Blende nanowire [23,24]. The polytypism, which is usually observed in III-V nanowires [25], together with twins and stacking faults in InP cause the striation in FFT image.

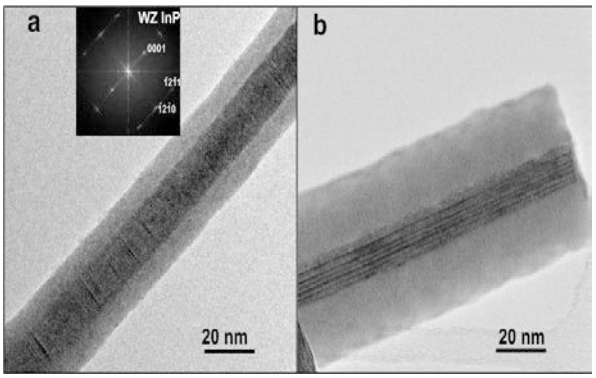

Figure 2. TEM images of core-shell nanowires grown from InP+Zn (a) and InP+ZnO (b) sources. The inset presents the FFT of the TEM image.

The composition of an amorphous shell was determined by two methods: EDS and IR spectroscopy. Two EDS spectrum that were taken from the core region and core+shell area are shown in Fig. 3a,b. As can be seen, In, P, Zn and Oxygen are the main constituents of grown core-shell nanostructures. Comparison of this two spectrum

reveals that the core contains higher amount of In and P, because it consists of a crystalline InP. This was also confirmed by EDS elemental maps shown in Fig. 4, which proved the deficiency of Zn in the core material (Fig. 4,b) and the excess of In in the same region (Fig. 4,d).

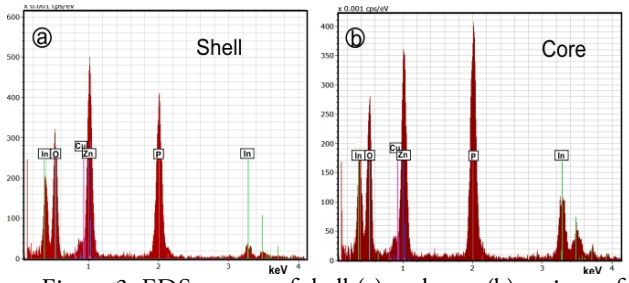

Figure 3. EDS spectra of shell (a) and core (b) regions of core-shell nanowire.

To determine the exact composition of core material the nanowires were scrapped off from the Si substrate, mixed with KBr powder, pressed in the form of a pellet and analyzed by IR spectroscopy (Fig. 5). The observed broad peaks at ~1000 and~ 550 cm-1can be assigned to the complex stretching and bending vibration bands of PO43- groups in amorphous zinc phosphate Zn3(PO4)2 [26-28]. These results clearly show that the complex nanowires consist of amorphous zinc phosphate shells and crystalline InP cores.

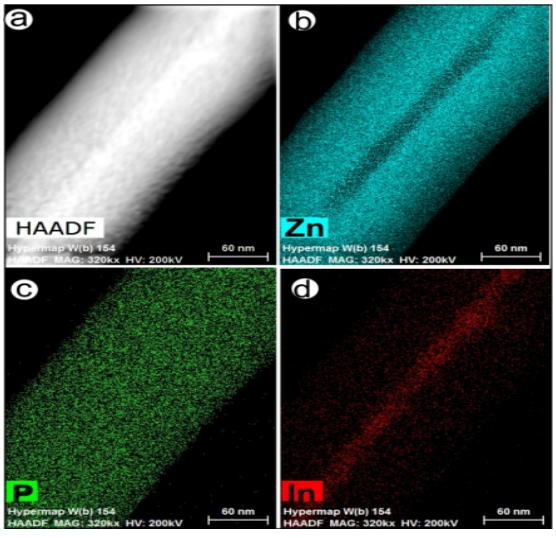

Figure 4. High Angle Anular Dark Field TEM image of core-shell nanowire (a) and elemental maps which represent the distribution of Zn (b), phosphorus (c) and indium (d) in the same nanowire.

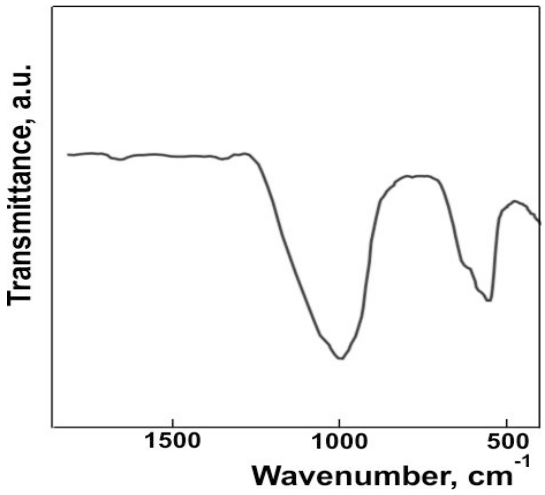

Figure 5. IR spectrum of core-shell nanowires pressed in pellet together with KBr powder.

Comparing TEM images of nanowires grown from Zn+InP and ZnO+InP sources it becomes obvious that, in spite of similar diameters of InP cores (~14 nm) the thickness of shell for nanowire grown from ZnO source is almost twice larger. Besides Zn and P, which have high vapor pressure at nanowire growth temperatures, the formation of $Zn_3(PO_4)_2$ shell needs also the presence of oxygen. When Zn+InP source was used, the 3 mol.% of water diluted in hydrazine was the only source of oxygen. However, when ZnO+InP was used, more oxygen arrived in the reactor due to the reduction of ZnO to pure Zn and formation of water molecules. This promoted the formation of larger amounts of zinc phosphate, thus increasing the thickness of a shell layer.

It should be emphasized, that the core and shell materials were formed simultaneously, during a one-step process, due to the spontaneous segregation of InP and $Zn_3(PO_4)_2$ phases. The preliminary study of thermochemical reactions that may have a place in our growth technology revealed that such a segregation of phases has a sound thermodynamic base. The segregation reactions have higher negative values of Gibbs free energy as compared to the synthesis of other compounds. Two examples of these reactions, which have highest free energies, are presented below:

$$3Zn + 8In_2O(g) + 18PH_3(g) = Zn_3(PO_4)_2 + 16InP + 27H_2(g) \quad \Delta G=-2724 \text{ kJ/mol} \quad (1)$$

$$3Zn + 8In_2O(g) + 18P(g) = Zn_3(PO_4)_2 + 16InP \quad \Delta G=-6447 \text{kJ/mol} \quad (2)$$

It should be note that the melting point of $Zn_3(PO_4)_2$ is sufficiently high (T_m=900°C), and accordingly the crystallization temperature is also high. The maximum growth temperature in our technology was 460°C. This temperature is sufficiently high for the crystallization of InP core, but it's still low for $Zn_3(PO_4)_2$ to form the crystalline shell. The formation of $Zn_3(PO_4)_2$ shell is of special importance for biomedical application of nanomaterials, because zinc phosphate has long been proved to be the non-toxic material, which is used as a basis for dental cement since 19th century [4].

Our initial evaluation of thermochemical reactions reveal that in the presence of NH and NH_2 radicals, produced after pyrolytic decomposition of N_2H_4, the amorphous $Zn_3(PO_4)_2$ can be further transformed into Zn_3P_2, which has a low melting point of 420°C, but relatively high boiling point (1100°C) to form the stable shell around InP core, which may solidify after cooling down.

4. CONCLUSIONS

The composite nanowires consisting of crystalline InP cores and amorphous $Zn_3(PO_4)_2$ shells were synthesized by annealing Zn+InP and ZnO+InP sources in the vapor of hydrazine containing 3 mol.% H_2O. The nanowires were produced on the Si substrate heated up to 420°C and located at 2 cm above the sources. Following volatile species served for the mass transfer to substrate: sublimated Zn atoms and molecules, NH and NH_2 radicals, In_2O suboxides, P, P_2 and PH_3 gaseous species.

The growth temperature was sufficient for the crystallization of InP core, but low for producing crystalline indium phosphide shell. InP cores have the wurtzite structure, in contrast to bulk indium phosphide. The spontaneous segregation of InP and $Zn_3(PO_4)_2$ phases, which led to the formation of a core-shell nanostructure, was driven by a high negative value of Gibbs free energies of corresponding thermochemical reactions.

5. ACCNOWLEDGMENTS

This work was financially supported by the Shota Rustaveli National Science Foundation Grant N04/05-2016 and by Grant #6204 of the Science and Tchnology Center in Ukraine.

6. REFERENCES

1. Goto H., Nosaki K., et al. / Appl. Phys. Express, 2009, v.2, p.035004-08.
2. Zanolli Z., Wacaser B.A., et al. / J. Phys.: Condens. Matter, 2007, v.19, p.295218-23.
3. Dupont D., Tessier M.D., et al. / Adv. Mater., 2017, v.29, p.1700686-90.
4. Wagh A.S. Chemically Bonded Phosphate Ceramics: Twenty-First Century Materials with Diverse Applications.: Elsevier, 2004, 304 p.
5. Zhang Y.,Wu J., et al. / J. Phys. D: Appl. Phys. 2015, v.48, p.463001-06.
6. Fang M., Han N., et al. / J. Nanomater., 2014 , v.2014 , p..702859-62.
7. Zhang A., Zheng G., et al., Nanowires: Building Blocks for Nanoscience and Nanotechnology: Springer, 2016, p. 322-325.
8. Royo M., De Luca M., et al. / J. Phys. D: Appl. Phys., 2017, v.50, p.143001-07.
9. Xia X., Tu J., / ACS Nano, 2012, v. 6 , p.5531-5538.
10. Dong Y. Tian B., et al. / Nano Lett. 2009, v.9 , p.2183–2187.
11. Li Ch., Wright J. B., et al. / Nano Lett., 2017, v. 17, p.1049–1055.
12. Huczko A. / Appl. Phys. A, 2000, v. 70, p.365–376.
13. Xie Y., Kocaefe D., et al. / Journal of Nanomaterials, 2016, v. 2016, p. 2302595-98.
14. Mao LB., Xue L., et al. / Nano Res., 2016, v. 9, p. 1334–1345 .
15. Nai J., Kang J., et al. / Sci. China Mater., 2015, v. 58, p.44–59.
16. Jishiashvili A., Shiolashvili Z., et al. / Orient. J. Chem., 2017, v.33, p.1103-1110.
17. Klimova A. M., Ananichev V. A., et al. / Glass Phys. Chem., 2005, v.31, p.760-762.
18. Schunk L.O., Steinfeld A. / AlChE Journal, 2009, v.55, p.1497-1503.
19. Chambon M., Abanades S., et al. / AlChE Journal, 2011, v.57, p.2264-2273.
20. Gorbenko V. I., Gorban A. N. / Radiophysics, 2012, v.1, p. 7-10.
21. Gorbenko V. I., Shvets J. A., et al. / Proceedings of Int. Symp.:III–Nitride Based Semiconductor Electronics and Optical Devices and Thirty-Fourth State-of-the-Art Program on Compound Semiconductors: Technol. & Eng., 2001, p.218.

22. Chen D., Liu Zh., et al. / Cryst. Eng. Comm., 2011, v.13, p. 7305–7310.
23. Algra R.E.,Verheijen M.A., et al. / Nature, 2008, v.456, p. 369–372.
24. Moewe M., Chuang L. C., et al. / J. Appl. Phys., 2008, v.104, p.044313-17.
25. Caroff P., Bollinsson J., et al. / IEEE J. of Sel. Top. Quant. Elec., 2011, v.17, p. 829-846.
26. Bach S., Celinski V.R., et al. / J. Am. Chem. Soc. 2015, v.137, p.2285–2294.
27. Jung S.H., Oh E., et al. / Bull. Korean Chem. Soc., 2009, v.30, p.2280-2282.
28. Frost R. L. / Spctrochim. Acta, 2004, v.60, p.1439-1445.

EFFECT OF COMPOSITION AND HEAT TREATMENT REGIMES ON THE ELECTRICAL PARAMETERS OF $Cd_{1-x}Zn_xO$ FILMS

H.M.MAMEDOV[1*], K.KORDAS[2], V.U.MAMEDOV[1], V.J.MAMEDOVA[1], KH.M.AHMEDOVA[1], E.A.KHANMAMEDOVA[1]

[1]Faculty of Physics, Baku State University, Az1148, Z.Khalilov str., 23, Baku, Azerbaijan,
[2]Microelectronics Research Unit, University of Oulu, P.O.Box4500,90570, Oulu, Finland

In this paper, the electrical properties of films $Cd_{1-x}Zn_xO$ (x=0.2÷0.9) deposited by electrochemical way, are investigated, depending on the film composition (x) and heat treatment (HT) regime in an oxygen atmosphere. It is established that the nonmonotonic dependence of the dark resistivity (ρ_d) on x and HT regime is due to changes in the ratio of donor and acceptor concentrations, depending on the film composition. The results are explained on the basis of the energy model for polycrystalline semiconductor films.

PACS numbers: 54.72.Hj; 34.34. Mn; 42.30. Ht
Keywords: electrochemical deposition, thin film, electrical conductance
***E-mail:** mhhuseyng@bsu.edu.az

1. INTRODUCTION

Oxide semiconductors receive considerable attention due to their low cost of fabrication, chemical robustness, high transmittance coefficient and high thermal conductance. *Films of* $Cd_{1-x}Zn_xO$ have received much attention because of their wide applications in the field of optoelectronic and photovoltaic devices. [1-5]. A variety of methods have been reported for the preparation of CdO–ZnO alloy films such as molecular beam epitaxy [6], sol–gel process [7] and spray pyrolysis [8]. Among these methods, electrodeposition is an attractive method to obtain these kinds of films [9], which is well known for its simplicity, reproducibility and possibility of producing cheap large-area films [10-12]. Although pure ZnO and CdO films have been studied by many research groups, a compound semiconductor of ZnO and CdO, that is to say, $Cd_{1-x}Zn_xO$ has seldom been studied.

In this work, we present electrical properties of $Cd_{1-x}Zn_xO$ (with x=0.1÷ 0.9) films depending on the films x and HT regime in oxygen atmosphere

2. EXPERIMENT

The electrochemical deposition of $Cd_{1-x}Zn_xO$ films has been performed with a three electrode configuration: graphite electrode as anode, $Ag/AgCl_3$ electrode as reference electrode and *glass*/SnO_2 substrates as cathode [1]. Total area of working electrodes (cathode) was 1×1 cm^2. The *glass*/SnO_2 substrates were cleaned with ethanol, acetone and deionized water and then dried in flowing N_2. At electrodeposition we used aqueous solutions of $Zn(NO_3)_2$ and $Cd(NO_3)_2$ salts (99.5% purities) with different molar fraction in solution (Table 1). The solution were kept on continuous stirring for 1 hour then filtered by filter paper. The solution was homogeneous, clear, transparent and stable at room temperature. The reaction temperature was kept at 80°C. In order to investigate the electrochemistry in the deposition process of $Cd_{1-x}Zn_xO$, cyclic voltammetry study was performed in the potential range of -1.6 to +1.6 V. $Cd_{1-x}Zn_xO$ formation potentials region were registered from cyclic voltammetry curves, and are summarized in Table 1.

The thickness of $Cd_{1-x}Zn_xO$ films were about 1 μm, depending on the deposition duration. All the films showed n-type conductivity. Hall Effect measurements showed that at room temperature the resistivity of films was 1100 – 80 Ω·cm and the free electron concentration was n=6.5×10^{17} - 8×10^{14} cm^{-3}, depending on the Zn content. EDS data were recorded to determine the composition of Cd and Zn in deposited layers.

The dark resistivity of films were was measured by using the two-probe method in the temperature range 300–450K by defining an area of 1.0 cm^2 on the film and silver paste was used for good ohmic contacts. Thus, the contact resistance can be negligible. The dark *I–V* measurements were made using dc multimeter.

Table 1. Mole fraction of salts, deposition current and potential for the $Cd_{1-x}Zn_xO$ films.

x	Mole fraction of salts (mM)		Deposition current and potential	
	$Zn(NO_3)_2$	$Cd(NO_3)_2$	J, mA/cm^2	U_c (V)
0.2	1.22	4.88	5.6	-0.96 – -1.21
0.4	4.13	6.21	5.1	-0.96 – -1.24
0.5	4.91	4.94	4.2	-0.93 – -1.26
0.6	5.92	3.95	3.4	-0.88 – -1.37
0.7	6.34	2.73	3.2	-0.89 – -1.38
0.8	6.5	1.63	2.7	-0.9 – -1.37
0.9	6.85	0.76	2.4	-0.91– -1.38

3. RESULTS AND DISCUSSION

The temperature dependence of dark resistivity, were conducted in films $Cd_{1-x}Zn_xO$ just after deposition with different composition. It was found that an increase of zinc concentration up to x=0.6 results to sharp increase of ρ_d. An insignificant change in the dark resistivity is observed, with further increase of x from 0.6 to 0.9. Such dependence of ρ_d on x is most likely indicative of nonmonotonic change in the ratio of N_d/N_a (where N_d and N_a are the concentrations of donors and acceptors, respectively) in films. Note that, the ratio of the photoconductivity to dark conductivity (integral photosensitivity at illumination 100 mW/cm^2) of films at room temperature is about 5-9 (depending on x).

Dark resistivity of all investigated films just after deposition and after the HT (at 600°C for 15 min) is exponentially dependent on temperature: $\rho_d(T) = \rho_0 exp(E/kT)$ (Fig. 1).

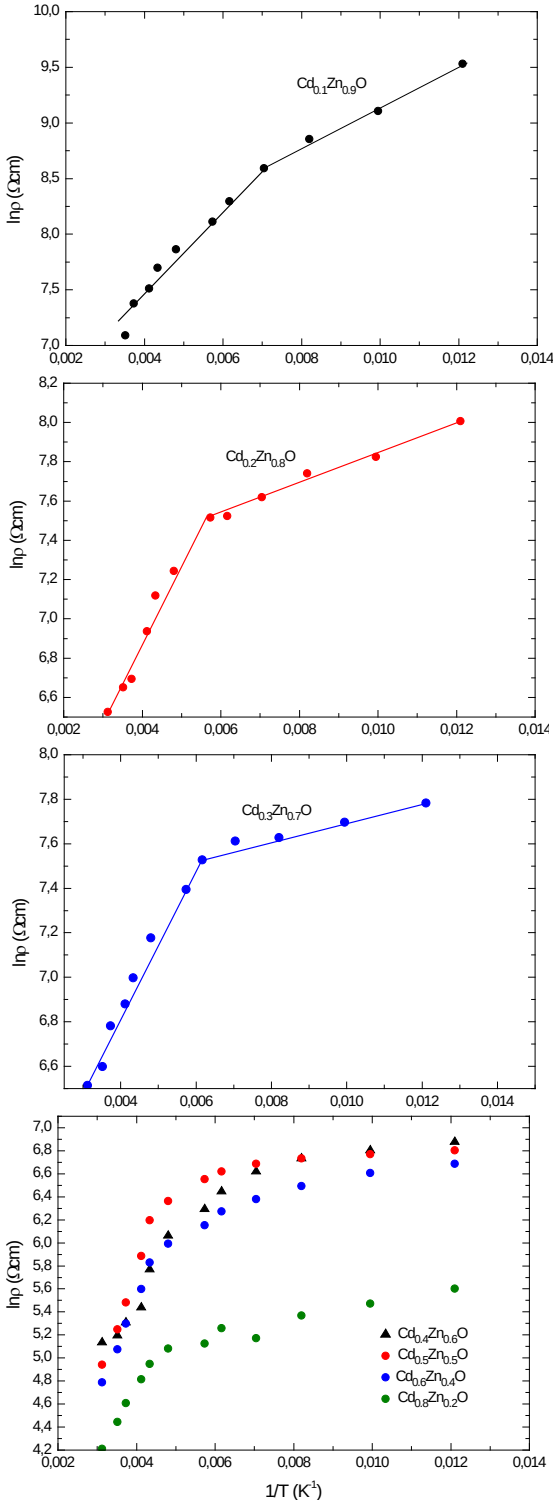

Fig. 1. Temperature dependence of dark resistivity of the $Cd_{1-x}Zn_xO$ films just after deposition.

The obtained value of the activation energy (E) of the dark resistivity for films just after deposition was 28-31 eV, which corresponds to the activation energy of desorption of oxygen [11, 12]. It is established that the value of E increases with HT temperature and, at

600°C for 15 minutes, was about 0.34 eV. This energy value, most likely, corresponds to the activation energy of cadmium and zinc vacancies or centers of more complex nature.

It is established that the current-voltage (*I-V*) characteristics of the just deposited films has a complex (nonlinear) form, which depends on the *x*. Thus, at x≤0.6, the *I-V* characteristics of films obeys an exponential (at U < 4 V), and then (at relatively high values of the applied voltage) power law (sublinear region of $I \sim U^m$, with m<1). As is the shown in Fig. 2, the sublinear region of the *I-V* characteristics replaced by quadratic region, with an increase of *x*. Further, for films with x≥0.6, a region with an exponential dependence gradually disappears, and value of *m* decreases to *m*=1.

It has been established that the behavior of dark *I-V* characteristics is not monotonically dependent on the HT temperature and duration (Fig. 3). At low HT temperatures (at 300-400^{0}C for 15 min), the nonlinear section on the *I-V* characteristics becomes linear. After HT at 600^{0}C for 15 min in oxygen atmosphere, only linear dependence is observed on the *I-V* characteristics. After that, at higher HT temperatures (>600^{0}C), despite a sharp decrease in the dark current, the linear nature of *I-V* characteristics is preserved.

The obtained results are explained on the basis of the energy model for polycrystalline semiconductor films, which can qualitatively explain the main features of various electronic processes in them. It should be noted that the features of the structure of such films determine the mechanisms of current transmission and photosensitivity, which differ from the properties of single crystals. First, because of the rather large value of the ratio of the surface area to the volume, in these films, surface effects play a dominant role. Secondly, after the removal of films from chemical solution to atmosphere, the adsorbed oxygen, due to the presence of intercrystalline pores, forms deep traps (capture levels) for electrons on the surface of individual crystallites.

As a result, potential barriers form at the boundaries of neighboring crystallites. The energy bands of films can be schematically depicted as a set of microcrystallites with potential barriers at the interface with neighboring and various types of local levels (trapping and trapping centers sensitizing, recombination, scattering). This is entirely permissible and is caused by the complex chemical compositions of the initial materials, the nature of the deposition process, and so on. According to this model, the film resistance as a whole consists of the sum of the resistances of individual crystallites and barriers.

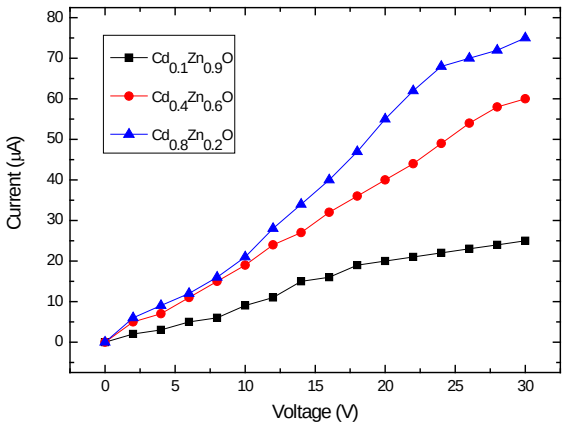

Fig. 2. *I-V* characteristics of $Cd_{1-x}Zn_xO$ films just after deposition.

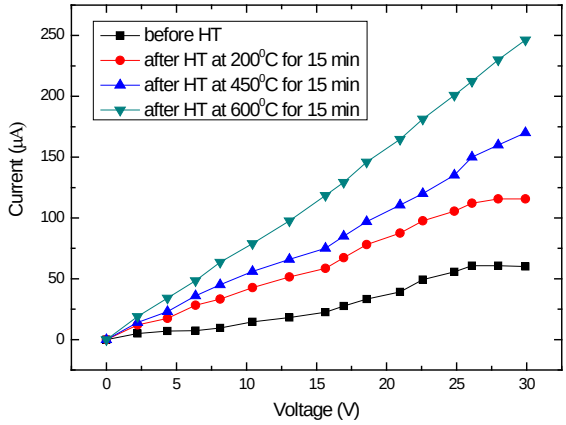

Fig. 3. *I-V* characteristics of $Cd_{0.4}Zn_{0.6}O$ after the HT.

Therefore, changes in conductivity under the influence of any action (for example, changes in film composition, temperature, HT regime, light, injection, etc.) in addition to the change in the concentration of free carriers can also be caused by a change in their effective mobility, due to the modulation of the height and width of potential barriers . Naturally, both of these, under certain conditions, can provide a transfer of carriers between the crystallites. In this case, an important role is played also by the small thickness of the films. It should be taken into account that in polycrystalline films the crystallite sizes are usually small (30-200 nm) in comparison with the diffusion displacement length. According to SEM studies, as already noted, the crystallite sizes after HT significantly (almost 20-50 times) increase. Naturally, change in the composition

and HT regime of the films can purposefully vary the main parameters of adhesion levels and microcrystallites, as well as interlayers and potential barriers between them. Within the framework of this model, a decrease of σ_d after HT, in comparison with the values in non-heat-treated films, can be explained directly by a change in the number of adsorbed oxygen molecules. The concentration of oxygen molecules adsorbed on the surface decreases with increasing annealing temperature. However, this decrease occurs not only due to desorption of oxygen molecules. If some part of this decrease in the concentration of oxygen molecules is associated with desorption, the other part is due to their decay into atoms, which play the role of capture centers for minority carriers (holes). In the general case, a decrease in the concentration of oxygen molecules after HT leads, first, to a decrease in the height of the barriers; secondly, to an increase in the ratio of the concentration of centers of various types; thirdly, to an increase in the density of capture centers of minority carriers. The capture of minority carriers by oxygen atoms leads to a decrease of σ_d with respect to the initial value. However, the rate of recombination of the main carriers also decreases. Therefore, after that, the photoconductivity increases with respect to the initial one.

4. CONCLUSION

Thin films of $Cd_{1-x}Zn_xO$ (x=0.2÷0.9) were deposited by electrochemical way. It has been established that regulating composition and HT regime can be specifically control the electrical parameters of $Cd_{1-x}Zn_xO$ films. The results are explained on the basis of the energy model for polycrystalline semiconductor films.

5. REFERENCES

1. Mamedov H.M., Shah S.I., Chirakadze A., Mammadov V.U., Mammadova V.J., Ahmedova Kh.M. / Photonics Letters of Poland, 2018, v.10, p.26-28.
2. Mamedov H.M., Mammadov V.U., Mammadova V.J., Ahmedova Kh.M. / Journal of Optoelectronics and Advanced Materials, 2015, v.17, p.67-70.
3. Kasumova R. J., Kerimova N.V., Mamedova V.J./ Journal of Nonlinear Optical Physics & Materials, 2017, v. 26, 1750019 (2017).
4. Caglar Y., Caglar M., Ilican S. and Ates A./ J. Phys. D: Appl. Phys., 2009, v. 42,p.065421-26.
5. Wang F., Ye Z., Ma D., Zhu L. and Zhuge F./ J. Cryst. Growth, 2005, v.283, p.373-377.
6. Sadofev S., Blumstengel S., Cui J., Puls J., Rogaschewski S., Schafer P. and Henneberger F./Appl. Phys. Lett., 2006, v. 89, p.201907-11 .
7. Torres-Delgado G., Zuniga-Romero C.I., Jimenez-Sandoval O., Castanedo-Perez R., Chao B. and Jimenez-Sandoval S./ Adv. Funct. Mater., 2002, v.12, p.129-132.
8. Tabet-Derraz H., Benramdane N., Nacer D., Bouzidi A. and Medles M./ Sol. Energy Mater. Sol. Cells, 2002, v.73, p.249-252.
9. Tortosa M., Mollar M. and Marı B./ J. Cryst. Growth, 2007, v.304, p.97-102.
10. Mamedov H., Konya Z., Muradov M., Kukovecz A., Kordas K., Hashim D., Mamedov V./J. Solar Energy Engineering, 2014, v.136, p.044503-07.
11. *Abdinov A.*, Mamedov H., and Amirova S./ Thin Solid Films, 2006, v.511-512, p.140-142.
12. Abdinov A., Mamedov H., Amirova S./ Jpn. J. Appl. Phys., 2007, v.46, p.7359-7362.

ACTIVATION PARAMETERS FOR ELECTRICAL CONDUCTIVITY OF Li^+, Na^+, K^+, Rb^+ AND Cs^+ IONS IN WATER SOLUTIONS

E.A. MASIMOV[1], B.G. PASHAYEV[1*], H.SH. HASANOV[1]

[1]Faculty of Physics, Baku State University, Az1148, Z.Khalilov str., 23, Baku, Azerbaijan

The paper presents limit values of molar electrical conductivity of Li^+, Na^+, K^+, Rb^+ AND Cs^+ ions in water solutions which were determined in temperature range of 283.15-333.15 K. For each type of ions an additive principle was applied to determine the temperature dependance of electrical conductivity and these measurements were discussed in terms of the Gibbs free energy, enthalpy and entropy of activation for this transport process of ions in electrolytic solutions. The different values of activation parameters were consistently explained by various level of hydration of ions.

PACS numbers: 82.20.Kh, 34.10.+x, 52.20.Hv
Key words: alkali metal ions, activation parameters.
***E-mail:** p.bakhtiyar@yahoo.com

1.INTRODUCTION

Inorganic substances (alkalis, salts, strong acids etc) when melting in water are easily dissociate into positively charged cation and negatively charged anions. As concentration of these ions sufficiently exceeds the concentration of water ions H^+ and OH^-, electrical conductivity of pure water can be ignored. When solution is under an electric field, e.a. potential difference is created between electrodes placed in solution, then ions migrating through water molecules start flowing out to the same direction and thus produce an electric current. It is necessary to note that in solutions ions and water molecules are bound to sulfonate groups in the membrane at low hydration levels. It means that during the transport process an interaction occurs between water molecules, directly "tied-up" with ions and other free water molecules. Such processes are usually associated by changes in enthalpy ($\Delta H_\eta^{\neq}$) and entropy ($\Delta S_\lambda^{\neq}$) and Gibbs free energy ($\Delta G_\lambda^{\neq}$).In this work, it was set out to create simulations that examined the impact of hydration and temperature on alkali metal ions in water solutions and to understand the dynamics of changes in limit values of electrical conductivity, Gibbs energy, enthalpy and entropy.

2. EXPERIMENTAL METHODS

The electrical conductivity of alkali metal ions in water solutions has been measured over the water mole fraction range 0.001-0.01 mol/l and over temperature ranges 283,15-333,15 K. By using the Kolraush law the limit values of electrical conductivity on concentration have been obtained (see Table 1). From the additivity law of and given that cations and anions mobility can be calculated by using the following expression [1,2]

$$\Lambda_m^0 = \lambda_+^0 + \lambda_-^0$$

(λ_+^0 and λ_-^0 are limit values of electrical conductivity of cations and anions). The temperature dependence of limit values of electrical conductivity of ions have been measured (see Table 2). Based on the results of experiment and using the Eyring theory for electrical conductivity of ions in electrolytic solutions [3], the activation parameters for each type of ion pairs have been found at the given temperature range.

3. CALCULATION METHODS

Having established correlation between the ions migration in water solutions under an applied electric field and motion of gas molecules during chemical reactions, Eyring has defined the temperature

dependence of limit values of conductivity ($\lambda_{\pm}^{0}$) by the following expression

$$\lambda_{\pm}^{0} = \lambda_0 \exp\left(-\frac{\Delta G_{\lambda}^{\neq}}{RT}\right) \quad (1)$$

Here $\Delta G_{\lambda}^{\neq}$-1 mol is a change of Gibbs energy during ion's migration, R-universal qas constant and T-absolute temperature. According to Eyring theory [3]

$$\lambda_0 = \frac{|z_{\pm}|eF}{6h} L^2 \quad (2)$$

Here $|z_{\pm}|$ is valency of an ion, e-elektron charge, F-Faraday's numbe, h-Planck constant, L- distance between two quasistationary conditions of an ion. It needs to be noted that $\Delta G_{\lambda}^{\neq}$ and L can be considered as kinetic parameters of process ion conducting process. These parameters depend on structure of solvent and for very liquid solutions may reach their peak values. To calculate the values of L, the assumptions are made that it equials to cubic root of a solvent molecule volume [4, 5]:

$$L = \sqrt[3]{\frac{V_m}{N_A}} \quad (3)$$

Here V_m-molecular volume of solvent, N_A-Avoqadro's number. Solvent moleculerr volume can be found by formula

$$V_m = \frac{M}{\rho} \quad (4)$$

Here ρ- solvent density, M-solvent molecular weight. From (2), (3) and (4) :

$$\lambda_0 = \frac{|z_{\pm}|eF}{6h}^2 \left(\frac{M}{\rho N_A}\right)^{\frac{2}{3}} \quad (5)$$

From formula (1) it's clear (1) that limit values of conductivity ($\lambda_{\pm}^{0}$) is a function of $\Delta G_{\lambda}^{\neq}$. Then we receive:

$$\Delta G_{\lambda}^{\neq} = RT \ln \frac{\lambda_{\pm}^{0}}{\lambda_0} \quad (6)$$

Having experimentally measured $\lambda_{\pm}^{0}$ at various temperatures and calculated λ_0-ı from formula (5) we then can determine by applying formula (6) the temperature dependence of Gibbs energy ($\Delta G_{\lambda}^{\neq}$) at migration of ions in electrolytic solutions.

Using relationships between $\Delta G_{\lambda}^{\neq}$, $\Delta H_{\eta}^{\neq}$ and $\Delta S_{\lambda}^{\neq}$ [4]

$$\Delta G_{\lambda}^{\neq} = \Delta H_{\lambda}^{\neq} - T\Delta S_{\lambda}^{\neq} \quad (7)$$

the equation (1) can be written as following:

$$\lambda_{\pm}^{0} = \lambda_0 \exp\left(\frac{\Delta S_{\lambda}^{\neq}}{R} - \frac{\Delta H_{\lambda}^{\neq}}{RT}\right) \quad (8)$$

Table 1 Limit values of molar electrical conductivity of hydroxids of alakali metals at various temperatures

$\Lambda_m^0 \cdot 10^3, Om^{-1}m^2mol^{-1}$					
T, K	*LiOH*	*NaOH*	*KOH*	*RbOH*	*CsOH*
283,15	17,054	17,897	19,728	20,103	20,096
288,15	19,329	20,262	22,266	22,653	22,642
293,15	21,490	22,518	24,702	25,118	25,081
298,15	23,636	24,774	27,115	27,540	27,504
303,15	25,924	27,164	29,684	30,106	30,064
308,15	28,100	29,454	32,121	32,572	32,510
313,15	30,378	31,835	34,689	35,129	35,051
318,15	32,524	34,093	37,069	37,533	37,459
323,15	34,838	36,494	39,679	40,131	40,032
328,15	37,022	38,778	42,060	42,581	42,461
333,15	39,288	41,182	44,660	45,101	44,978

Taking the logarithm from both sides of (8) we receive the folowing:

$$\ln \frac{\lambda_{\pm}^{0}}{\lambda_0} = \frac{\Delta S_{\lambda}^{\neq}}{R} - \frac{\Delta H_{\lambda}^{\neq}}{RT} \quad (9)$$

It follows from (9) the ion migration activation

enthalpy ($\Delta H_\eta^{\neq}$) $\ln\frac{\lambda_\pm^0}{\lambda_0} = f(\frac{1}{T})$ is a value of an tangent at any point of given function graph.

Then the activation enthalpy ($\Delta H_\eta^{\neq}$) can be expressed through the limit values of molar elecrical conductivity as following:

Table 2 Limit values of molar ion electrical conductivity of alkali metal ions at various tempretures

$\lambda_+ \cdot 10^3, \left(Om^{-1}m^2mol^{-1}\right)$					
T, K	Li^+	Na^+	K^+	Rb^+	Cs^+
283,15	2,642	3,485	5,316	5,691	5,684
288,15	3,039	3,972	5,976	6,363	6,352
293,15	3,451	4,479	6,663	7,079	7,042
298,15	3,876	5,014	7,355	7,780	7,744
303,15	4,327	5,567	8,087	8,509	8,467
308,15	4,800	6,154	8,821	9,272	9,210
313,15	5,292	6,749	9,603	10,043	9,965
318,15	5,804	7,373	10,349	10,813	10,739
323,15	6,333	7,989	11,174	11,626	11,527
328,15	6,882	8,638	11,920	12,441	12,321
333,15	7,432	9,326	12,804	13,245	13,122

$$\Delta H_\lambda^{\neq} = R\frac{d\ln\frac{\lambda_\pm^0}{\lambda_0}}{d(\frac{1}{T})} \qquad (10)$$

For this reason the temperature dependence graph for $\ln\frac{\lambda_\pm^0}{\lambda_0}$ - has been built and aligned with each line. The equation well defining this dependence has been determined:

$$\ln\frac{\lambda_\pm^0}{\lambda_0} = a_0 + a_1\left(\frac{1}{T}\right) + a_2\left(\frac{1}{T}\right)^2 + a_3\left(\frac{1}{T}\right)^3 \qquad (11)$$

Here a_0, a_1, a_2 and a_3 are parameters independent on temperature which were found mathematical by optimization techniques. Given (11) and (10), we can find for $\Delta H_\eta^{\neq}$

$$\Delta H_\lambda^{\neq} = R\left(a_1 + 2a_2\left(\frac{1}{T}\right) + 3a_3\left(\frac{1}{T}\right)^2\right) \qquad (12)$$

Hence, using $\Delta G_\lambda^{\neq}$ (6), the $\Delta H_\lambda^{\neq}$ can be calculated in (12). Through obtaining the $\Delta G_\lambda^{\neq}$ and $\Delta H_\lambda^{\neq}$ at various temperatures and applying the formula (7) the temperature dependance of activation entropy ($\Delta S_\lambda^{\neq}$) during migration of ions in electrolytic solutions can be measured.

4. RESULTS AND DISCUSSION

Fig. 1 show the temperature dependence of Gibbs energy during migration of Li^+, Na^+, K^+, Rb^+ and Cs^+ ions in eletrolytic solutions.

As is shown in Fig. 1, at the given temperature range for each ion $\Delta G_\lambda^{\neq}$ decreases with a temperature increase. It is well-known that as temperature increases water molecules migration is also accelerated It promotes reduction in number of molecules creating hydration shell around ions and simplifies movement of ions. Thus, as temperature increases, the water molecules become free and form a network along which ions can pop This leads to a dramatic increase in ions migration and conductivity which subsequently results in $\Delta G_\lambda^{\neq}$ decrease. As it's shown fron Fiq. 1, at given temperature range

$$\Delta G_\lambda^{\neq}\left(Li^+\right) > \Delta G_\lambda^{\neq}\left(Na^+\right) > \Delta G_\lambda^{\neq}\left(K^+\right) > \\ > \Delta G_\lambda^{\neq}\left(Rb^+\right) \approx \Delta G_\lambda^{\neq}\left(Cs^+\right).$$

This can be explained by different level of hydration of ions. Li^+, Na^+, K^+, Rb^+ and Cs^+ have got the same electrcal charge, crystalloic radius of ions are compared as following $R\left(Li^+\right) < R\left(Na^+\right) < R\left(K^+\right) < R\left(Rb^+\right) < R\left(Cs^+\right)$ [3]. Therefore, Li^+, compared with Na^+, Na^+, compared with K^+ have higher degree of hydration. For this reason, in solvents, the effective radius of ions relates as

$$R_{ef.}\left(Li^{+}\right) > R_{ef.}\left(Na^{+}\right) > R_{ef.}\left(K^{+}\right) > > R_{ef.}\left(Rb^{+}\right) > R_{ef.}\left(Cs^{+}\right).$$

Fig. 2 show the temperature dependence of activation enthalpy of the following ions Li^{+}, Na^{+}, K^{+}, Rb^{+} and Cs^{+} during migration in electrolytes. For the energy characteristics of conductivity process

in electrolyts, it is necessary to study $\Delta H_{\eta}^{\neq}$. $\Delta H_{\eta}^{\neq}$ is a change (carry-over) of ion energy from one condition to another. As it's shown in Fig. 2, at the given temperature range for each ion the value of $\Delta H_{\eta}^{\neq}$ is positive and tends to decrease when temperature goes up

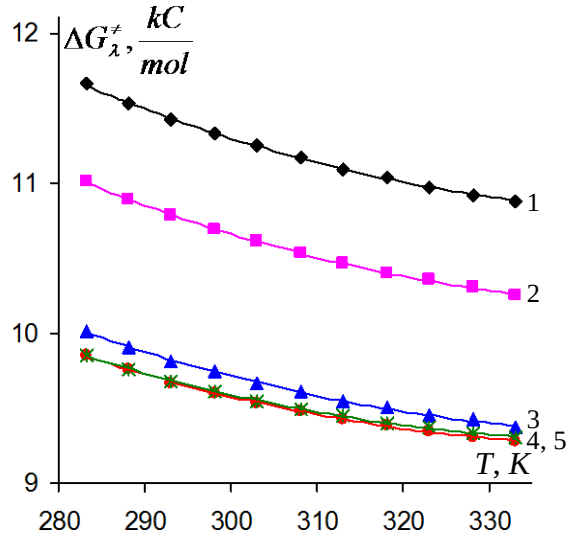

Fig. 1. Temperature dependance of ions Gibbs energy.

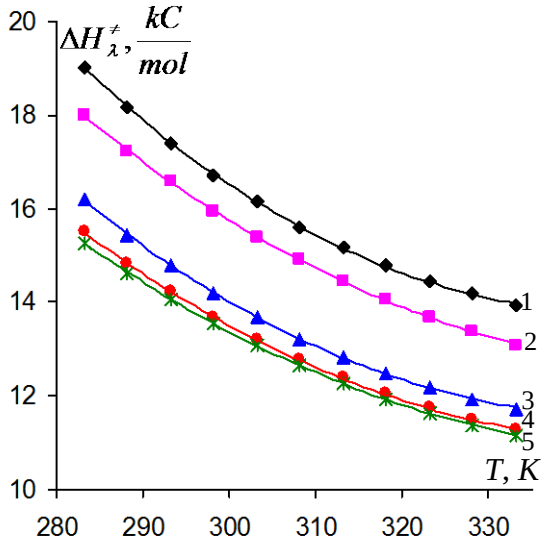

Fig. 2. Temperature dependance of ions enthalpy.

1- Li^{+}, **2-** Na^{+}, **3-** K^{+}, **4-** Rb^{+}, **5-** Cs^{+}

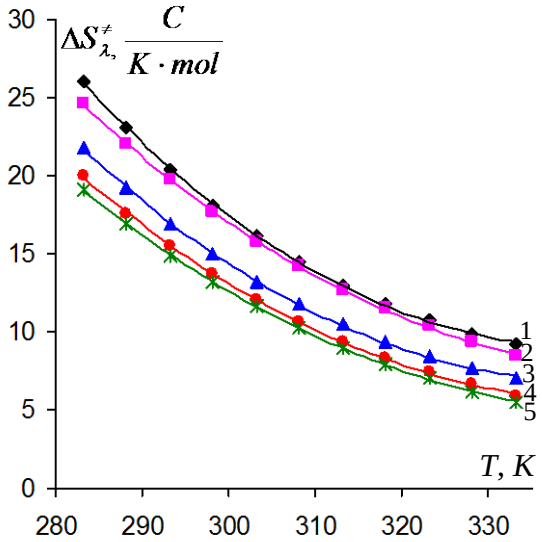

Fig. 3. Temperature dependance of ions entropy

1- Li^{+}, **2-** Na^{+}, **3-** K^{+}, **4-** Rb^{+}, **5-** Cs^{+}

$$\Delta H_{\lambda}^{\neq}\left(Li^{+}\right) > \Delta H_{\lambda}^{\neq}\left(Na^{+}\right) > \Delta H_{\lambda}^{\neq}\left(K^{+}\right) > \\ > \Delta H_{\lambda}^{\neq}\left(Rb^{+}\right) > \Delta H_{\lambda}^{\neq}\left(Cs^{+}\right).$$

This fact proves that, the higher ion's hydration is the more energy is required to change ions' original condition.

Fig. 3 show the temperature dependence of activation entropy of ions Li^{+}, Na^{+}, K^{+}, Rb^{+} and Cs^{+} during migration in electrolytes. In strong solvents, for example in water, activation entropy is always positive. Migration of molecules in active condition promotes destruction of structure of solvent at some dregree and consequently increase the activation entropy. Dissolving of alkali metals in water would destroy structure of water. In this case the entropy of water solution may be considered as a sum of entropy of water itself and etntropy of ions (cations and anions): $S_{sol.} = S_{water} + S_{kation} + S_{anion}$. Associating this with ions' (cations and anions) migration in water solutions then we can show ($S_{sol.}^{\neq} = S_{water}^{\neq} + S_{ion}^{\neq}$ ($S_{sol.}^{\neq} = S_{water}^{\neq} + S_{kation}^{\neq}$ or $S_{sol.} = S_{water} + S_{anion}$). Therefore, in electrolytic solutions the entropy changhe for arbitrary ion's migration will be

$$\Delta S_{\lambda}^{\neq} = \Delta S_{water}^{\neq} + \Delta S_{ion}^{\neq} \qquad (13)$$

As mentioned above, the temperature dependence of the activation entropy of water is positive. Fig. 3 show, at the given temperature range for the studied ions (Li^{+}, Na^{+}, K^{+}, Rb^{+} and Cs^{+}) $\Delta S_{\lambda}^{\neq}$ is positive, but $\Delta S_{\lambda}^{\neq}$ decrease with increasing of temperature. The redusing of $\Delta S_{\lambda}^{\neq}$ is possibly associated with the formula (13).

5. CONCLUSION

Electrical conductivity of alkali metal ions in water solutions determined in temperature range of 283.15-333.15 K, show the different values of activation parameters explained by various level of hydration of ions.

6. REFERENCES

1. Atkins P., De Paula J. Physical chemistry. Oxford University Press. 2006. 1067 p.
2. Eremin V. V, Kargov S.I., Uspenskaja I.A., Kuzmenko N. E, Lunin V.V. "Examination" Moscow 2005, 479p. (in Russion).
3. Glesston S, Lejdler C, Eyring G.Theory of absolute speeds. M: Foreign Lit., 1948. 600p. (in Russion).
4. Fialkov J., Zhitomir A.N. High schools. Chemistry and chemical technology. 1983. v. 26. №9. p.1086. (in Russion).
5. Zhitomir A.N. Physical Chemistry. 1987. v. 61. №7. p.1748. (in Russion).

BSU Publication | Journal of Low Dimensional Systems, v. 2 (1), 2018

SYNTHESIS AND X-RAY INVESTIGATION OF NITRO, DICHLORINE DERIVATIVES OF 1- (2,2-DICHLORO-1-PHENYLVINYL) -2-PHENYLDIAZENE BY CATALYTIC OLEFINATION REACTION

A.M.MAHARRAMOV[1], G.T.SULEYMANOVA[1], G.V.BABAYEVA[1], A.A.NIYAZOVA[1] , I.G.MAMEDOV[1], U.A.HASANOVA[1], N.G.SHIKHALIEV[1*], V.G.NENAJDENKO[2].

[1]Baku State University, Z.Khalilov 23 Str., Baku, Azerbaijan
[2]Lomonosov Moscow State University,Leninskiye Gory, Moscow, 119899

The introduction of functional groups into aromatic rings of dichlorodiazabutadiene derivatives synthesized by catalytic olefination reaction,endow the products of the reaction withnew physical, chemical and physiological properties. The parameters of non-covalent interactions(O···HC (2.58Å) , O···NH(2.377Å), O···Cl (3.164Å), O···O(3.000Å), (Cl···Cl (3.404Å)) and their role in crystal design have been studied by X-ray analysis method. Different crystalline structures have been observed due to different displacement of nitro groups and chlorine atoms in the benzene ring, and as consequence their non-covalent interactions. According to this the crystalline cage can be modified by changing the position of NO_2 group in benzoic aldehyde and Cl atoms in phenylhydrazine. X-ray diffraction studies were conducted to investigate non-covalent interactions that may arise in synthesized phenylhydrazon chloride obtained by catalytic olefination reactions. Cl-Cl bonds have not been observed in the crystals despite the presence of chlorine atoms in the phenylhydrazones. This was due to the maximal distance betweenCl atoms during the crystal packing due to the formation of strong intermolecular hydrogen bond.

PACS numbers: 61.66.hq, 61.05.c
Keywords: Catalytic olefination reaction, phenylhydrazon, diazabutadiene, non-covalent bond
***E-mail:** namiqst@gmail.com

1. INTRODUCTION

In our previous studies [1-6], were investigated the synthesis of 4,4-dichloro-1,2-diazabuta-1,3-diene obtained in one stage catalytic olefination reaction of N-substituted hydrazones and different aldehydes in the presence of CuCI catalyst.

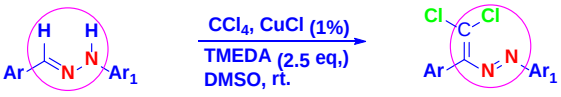

Scheme 1.Catalytic olefination reaction

Has been found that the presence of electrondonor methyl groups in 3-5 positions ofphenylhydrazine had a significant influence on the yield of the reaction product of some benzaldehyde derivatives [4-F, 4-N (CH_3) 2,2-NO_2,] with 3,5-dimethylphenylhydrazine and in the case of 4-F derivative led to the change in crystal design .It is interesting that, in contrast to the compounds of this type with 4,4-dichloro-1,2-diazabuta-1,3-diene structure, synthesi-zed in previous studies, as well as 4- (2,2-dichloro-1- ((3,5-dimethylphenyl) diazenil (vinyl) -N, N-dimethylaniline (A) and (E) -1- (2,2-dichloro-1- (2-nitrophenyl) vinyl) -2- (3,5-dimethylphenyl) diazene (B) (Figure 1 (b)) in the compound (E) -1- (2,2-dichloro-1- (4-fluorophenyl) vinyl) -2- (3,5-dimethyl-phenyl) diazene (Figure 1 (a)) Cl···CI interactions had not been observed. As it is evident from the structure, the crystalline packing occurs with the principle of "head to tail"[7-12] (1) since$\pi \cdots \pi$interaction between the fluorinated benzene ring and the aminated benzene ring and as a result, the Cl atoms were at a maximum distance from each other. In contrast to previous compounds, the interactions between theH atoms of CH_3 groupwith chlorine atoms of the neighboring moleculecreate new Cl···H hydrogen

bondsthat are a key factor in the design of the crystal structure of reaction product. It can be concluded from this that it is possible to manage the crystal design of compounds with 4,4-dichloro-1,2-diazabuta-1,3-diene frag-ments synthesized by changing the functional groups in the benzene ring.

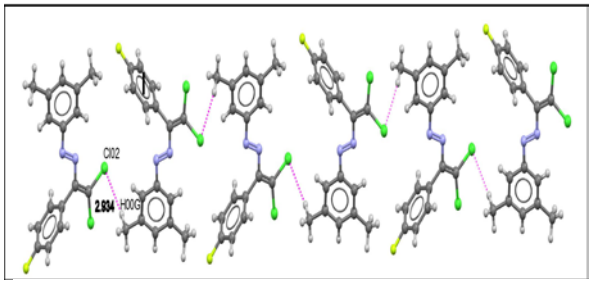

Figure 1. (a). The molecular structure of (E) -1- (2,2-dichloro-1- (4-fluorophenyl) vinyl) -2- (3,5-dimethylphenyl) diazene

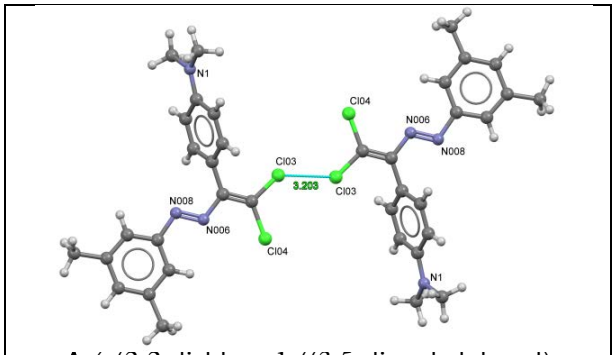

A.4-(2,2-dichloro-1-((3,5-dimethylphenyl) diazenil (vinyl) -N, N-dimethylaniline

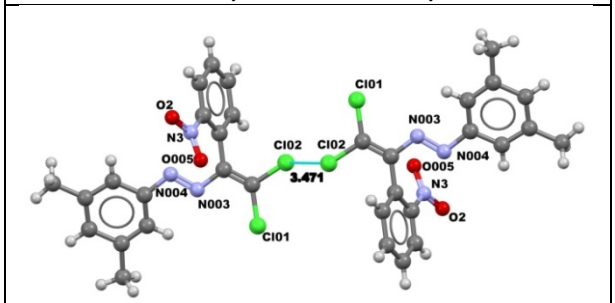

B. (E) -1- (2,2-dichloro-1- (2-nitrophenyl) vinyl) -2- (3,5-dimethylphenyl) diazene

Figure 1 (b). Cl···Cl interactions in A and B compounds are given in dotted lines.

2. EXPERIMENTAL

The X-ray analysis of the compounds 1,2,5,10,11 and 12 were carried out using of Bruker APEX II CCDdiffractometer (T = 273 K, λMoKα-radiation, graphite monochromator, φ- and ω-scanned). TheNMR ^{1}H and ^{13}C spectra were obtained by the Bruker Avance 300 (working frequency 300 and 75 MHz, solvents $CDCl_3$ and $DMSOd_6$).TMS were used as an standard, and TLC was carried out on the Silufol on UB-254, for visualization of the spots was used the $KMnO_4$ solution and UB lamp. Column chromatography was carried out using silica gel (Merck 63-200).

The general method of synthesis of hydrazones:

Ethanol (20-50 ml) and 0.820 g of CH_3COONa (10 mmol) are added to phenylhydrazine (5 mmol) in the tripodic tubular flack. Then 5mmol of aldehyde dropwise added and reaction mixture was stirred and heated. When the temperature reaches 78 ° C, the mixture is boiled for 5-10 minutes. Then, the reaction mixture is cooled to room temperature, 50 ml of distilled water is added to reaction mixture. Temperature reaches 60 ° C at intensive stirring. The cooled to room temperature reaction mixture is filtered. If necessary, the residue of the product is washed with distilled water. The resulting hydrazoneis dried at ambient temperature (15-20 hours). The NMR 1H and 13C spectra are compatible with the literature date.

Substance 1.1- (2,4-dichlorophenyl) -2- (2-nitrobenzilidene) hydrazine. Was obtained by the reaction of 2-nitrobenzaldehyde with 2.4-dichlorophenylhydrazine. The yield is 88%, bright orange solid substance. T_{melt} = 178°C, ^{1}H NMR (300 MHz, DMSO-d_6) δ 10.61 (s, 1H), 8.69 (s, 1H), 8.15 (d, J = 9.4 Hz, 1H), 7.98 (d, J = 9.4 Hz, 1H), 7.73 (t, J = 7.6 Hz, 1H), 7.61 – 7.44 (m, 3H), 7.32 (d, J = 11.3 Hz, 1H).^{13}C NMR (75 MHz, DMSO) δ 147.90, 140.55, 135.69, 133.61, 129.61, 129.57, 129.21, 128.57, 127.80, 124.87, 123.66, 117.61, 115.87.

Substance 2. (E)-1-(2,6-dichlorophenyl)-2-(2-nitrobenzylidene) hydrazine. Was obtained by the reaction of 2-nitrobenzaldehyde with 2,6-dichlorophenylhydrazine. The yield is 90%, yellow solid substance, T_{melt} = 120°C,^{1}H NMR (300 MHz, DMSO-d_6) δ 10.20 (s, 1H), 8.41 (s, 1H), 8.08 (d, J = 8.0 Hz, 1H), 7.98 (d, J = 8.2 Hz, 1H), 7.69 (t, J = 7.6 Hz, 1H), 7.57 – 7.44 (m, 3H), 7.13 (t, J = 8.0 Hz, 1H). ^{13}C NMR (75 MHz, DMSO) δ 147.47, 137.80, 133.76, 133.32, 130.17, 129.85, 129.16, 128.00, 127.08, 125.86, 124.96

Substance 3. (E)-1-(3,4-dichlorophenyl)-2-(2-nitrobenzylidene) hydrazine. Was obtained by the reaction of 2-nitrobenzaldehyde with 3,4-dichlorophenyl-hydrazine. The yield is 90%, dark red

solid substance, T_{melt}= 244-245°C,^{1}H NMR (300 MHz, DMSO-d_6) 11.12 (s, 1H), 8.28 (s, 1H), 8.17 (d, J=9.0 Hz, 1H), 7.79 (d, J=9.0 Hz,1H), 7.73 (t, J=8 Hz), 7.56-7.37 (m, 2H), 7.29 (d, J=3 Hz, 1H), 7.01 (dd, J=3 Hz, 1H). ^{13}C NMR (75 MHz, DMSO) δ 147.48, 145.10, 133.71, 133.63, 132.21, 131.48, 129.73, 129.30, 127.87, 124.99, 120.98, 113.74, 113.15

Substance 4. (E)-1-(2,4-dichlorophenyl)-2-(3-nitrobenzylidene) hydrazine. Was obtained by the reaction of 3-nitrobenzaldehyde with 2,4-dichlorophenyl-hydrazine. The yield is 95%, yellow solid substance, T_{melt} = 196°C, ^{1}H NMR (300 MHz,DMSO-d_6) δ10.20 (s, 1H), 8.43 (s, 1H), 8.14-8.16(d, 1H, J=6Hz), 8.08-8.10 (d, 1H, J=6Hz),7.70-7.73 (t, 1H, J=9Hz), 7.65(s, 1H), 7.52(s, 1H), 7.38-7.40 (d, 1H, J=6Hz), 7.20-7.21 (d, 1H, J=3Hz),^{13}C NMR (75 MHz, DMSO-d_6) δ 146.40, 142.48, 138.00, 136.43, 132.59, 129.39, 129.09, 128.00, 124.45, 124.13, 122.31, 121.65, 117.86.

Substance 5. (E)-1-(2,6-dichlorophenyl)-2-(3-nitrobenzylidene)hydrazine. Was obtained by the reaction of 3-nitrobenzaldehyde with 2,6-dichlorophenyl-hydrazine. The yield is 72%, yellow solid substance, T_{melt} = 150°C, ^{1}H NMR (300 MHz, DMSO-d_6)δ 11.13(s, 1H), 8.43 (s, 1H), 8.14-8.16(d, 1H, J=6Hz), 8.08-8.10 (d,1H,J=6Hz),7.69-7.73(m, 2H), 7.35-7.36 (d, 1H, J=3Hz), 6.99-7.02(t,1h, J-9Hz),^{13}C NMR (75 MHz, DMSO)δ 146.40, 142.54, 138.41, 136.43, 132.59, 129.39, 128.95, 128.17, 124.48, 124.13, 121.65.

Substance 6. (E)-1-(3,4-dichlorophenyl)-2-(3-nitrobenzylidene) hydrazine. Was obtained by the reaction of 3-nitrobenzaldehyde with 3,4-dichlorophenyl-hydrazine. The yield is 81%, yellow solid substance, T_{melt} = 177°C, ^{1}H NMR (300 MHz, DMSO-d_6)δ10.75 (s, 1H), 8.43(s, 1H), 8.08-8.16 (m, 2H), 7.64-7.73 (m, 3H), 7.32-7.33 (d, 1H, J=3Hz), 6.93-6.95 (d, 1H, J=6Hz),^{13}C NMR (75 MHz, DMSO)δ 146.40, 142.81, 142.73, 136.43, 132.59, 131.98, 129.39, 129.32, 126.10, 124.13, 121.65, 119.58, 116.73.

Substance 7. (E)-1-(2,4-dichlorophenyl)-2-(4-nitrobenzylidene)hydrazine. Was obtained by the reaction of 4-nitrobenzaldehyde with 2,4-dichlorophenyl-hydrazine. The yield is 87%, yellow solid substance, T_{melt} = 190°C, ^{1}H NMR (300 MHz, DMSO-d_6) 10.13 (s, 1H).δ 8.30 – 8.24 (m, 2H), 7.90 – 7.84 (m, 2H), 7.66 (d, J = 1.4 Hz, 1H), 7.52 (d, J = 2.1 Hz, 1H), 7.39 (dd, J = 7.4, 1.9 Hz, 1H), 7.17 (d, J = 7.5 Hz, 1H), , ^{13}C NMR (75 MHz, DMSO)δ 148.56, 141.60, 141.44, 138.00, 129.09, 128.00, 125.92, 125.58, 124.45, 122.31, 117.86.

Substance 8. (E)-1-(2,6-dichlorophenyl)-2-(4-nitrobenzylidene)hydrazine. Was obtained by the reaction of 4-nitrobenzaldehyde with 2,6-dichlorophenyl-hydrazine. The yield is 92%, orange solid substance, T_{melt}= 150°C, ^{1}H NMR (300 MHz, DMSO-d_6) ,δ, 10.13 (s, 1H), 8.19-8.21(d,2H, J=6Hz),8.00 (s,1H), 7.77-7.80 (d, 2H, J=9Hz), 7.47-7.50 (d, 2H, J=9Hz), 7.12-7.17 (t, 1H, J=15Hz), ^{13}C NMR (75 MHz, DMSO-d_6) δ 146.86 , 142.62 , 137.51 , 135.95 , 129.88 , 128.31 , 126.61 , 126.20 , 124.51 .

Substance 9. (E)-1-(3,4-dichlorophenyl)-2-(4-nitrobenzylidene)hydrazine. Was obtained by the reaction of 4-nitrobenzaldehyde with 3,4-dichlorophenyl-hydrazine. The yield is 90%, red solid substance, T_{melt} = 185°C,^{1}H NMR (300 MHz, DMSO-d_6)δ 10.15 (s, 1H),8.30 – 8.24 (m, 2H), 7.90 – 7.84 (m, 2H), 7.69 – 7.62 (m, 2H), 7.29 (d, J = 2.0 Hz, 1H), 6.94 (dd, J = 7.5, 2.0 Hz, 1H),, ^{13}C NMR (75 MHz, DMSO)δ 148.56, 145.66, 142.73, 140.72, 131.98, 129.32, 126.10, 125.92, 125.58, 119.58, 116.73.

The general preparation method of ((2,2-dichloro-1-phenylvinyl) diazenyl) phenyl) methanes

1 mmol of starting (E) - (2,2-dichloro-1-phenylvinyl) diazenyl) phenyl) methanes is added to the flack, then 10-12 ml of DMSO, and then (290 mg; 1.25 mol / eq) TMEDAandcatalyst CuCl (6 mg; 3 mol%) were added. Finally was added CCl4 (4-5 mol / eq., 1.5 g. The reaction mixture was stirred. Typically, the reaction goes in 1.5-3 hours. At the end of reaction 50-60 ml of water was added.Then the product ofreaction is extracted with methylene chloride (3 * 15 ml). After washing with water (3 * 50 ml) organic phase washed once with saturated NaCl solution (1 * 50 ml). Dried on Na_2SO_4 ($MgSO_4$), filtered and dichloromethane was removed by rotor evaporation in the vacuum. The residue (eluent is dichloromethane / hexane 1: 1) is purificated by column chromatography method. Fractions containing the main reaction product identified by TLC.

Substance 10. 1-(2,2-dichloro-1-(2-nitrophenyl) vinyl)-2-(2,4-dichlorophenyl) diazene. Was obtained by the reaction of 1-(2,4-dichlorophenyl)-2-

(2 nitrobenzylidene)hydrazine with CCI_4. The yield is 55%, red crystal, T_{melt} =115 °C, ^{1}H NMR (300 MHz, $CDCl_3$) δ, 7.87-7.89 (d,1H, J=6Hz), 7.67-7.69 (d, 1H, J=6Hz), 7.56-7.63(m, 2H), 7.44-7.46 (d,1H, J=6Hz), 7.33- 7.37 (m, 2H),^{13}C NMR (75 MHz, $CDCl_3$) δ 149.53, 147.96, 143.54, 137.25, 136.19, 133.89, 132.53, 129.69, 129.59, 129.50, 128.05, 123.97, 123.72.

Substance 11. 1-(2,2-dichloro-1-(2-nitrophenyl) vinyl)-2-(2,6-dichlorophenyl) diazene. Was obtained by the reaction of (E)-1-(2,6-dichlorophenyl)-2-(2-nitrobenzylide-ne)hydrazine with CCI_4. The yield is 40%, red crystal, T_{melt}=98 °C, ^{1}H NMR (300 MHz, $CDCl_3$) δ 8.32- 8.29 (d, 1H, J=9 Hz), 7.79-7.74 (t, 1H, J=9Hz), 7.67-7.62 (t, 1H, J= 6Hz), 7.39-7.33 (m, 3H),7.18- 7.13 (t, 1H, J=9Hz), ^{13}C NMR (75 MHz, $CDCl_3$) δ 175.25, 162.33, 142.72, 139.76, 134.02, 132.11, 130.52, 129.17, 129.10, 124.88, 118.28, 110.51

Substance 12. 1-(2,2-dichloro-1-(2-nitrophenyl) vinyl)-2-(3,4-dichlorophenyl) diazene. Was obtained by the reaction of (E)1-(3,4-dichlorophenyl)-2-(2-nitrobenzyli-dene)hydrazine with CCI_4. The yield is 45%, yellow crystal, T_{melt}=58°C, ^{1}H NMR (300 MHz, $CDCl_3$) ^{1}H NMR δ, 7.84-7.86 (d, 1H,J=6Hz), 7.73 (s, 1H), 7.64-7.66 (d, 1H, J=6Hz), 7.50-7.59 (m, 3H), 7.33-7.37 (t, 1H, J=12Hz),.^{13}C NMR (75 MHz, Common NMR Solvents) δ 149.53, 148.98, 143.54, 136.19, 133.89, 132.53, 132.08, 131.43, 130.28, 129.88, 129.69, 123.72, 122.41.

Substance 13. 1-(2,2-dichloro-1-(3-nitrophenyl) vinyl)-2-(2,4-dichlorophenyl) diazene. Was obtained by the reaction of (E)-1-(2,4-dichlorophenyl)-2-(3-nitrobenzylide-ne)hydrazine with CCI_4. The yield is 30%, red crystal, T_{melt}=147 °C, ^{1}H NMR (300 MHz, $CDCl_3$)8.33-8.34 (t, 1H, J=3), 8.18-8.20 (m, 1H), 7.64-7.66 (m, 2H), 7.45-7.52 (m, 2H), 7.32-7.33 (d, 1H, J=3Hz),^{13}C NMR (75 MHz, $CDCl_3$) δ 147.69, 147.58, 138.29, 137.25, 135.51, 133.98, 133.48, 130.37, 129.59, 129.50, 128.05, 127.37, 126.40, 123.97.

Substance 14. 1-(2,2-dichloro-1-(3-nitrophenyl) vinyl)-2-(2,6-dichlorophenyl) diazene. Was obtained by the reaction of (E)1-(2,6-dichlorophenyl)-2-(3-nitrobenzyli-dene)hydrazine with CCI_4. The yield is 30%, red crystal, T_{melt} =128°C, ^{1}H NMR (300 MHz, $CDCl_3$)8.37 (s, 1H), 8.17-8.20 (m, 1H), 7.63-7.65 (m, 1H), 7.49-7.52 (t, 1H, J=9Hz), 7.38-7.43(m, 3H),^{13}C NMR (75 MHz, $CDCl_3$) δ 147.58, 147.34, 138.29, 135.51, 133.98, 133.48, 130.37, 127.76, 127.70, 127.37, 127.29, 126.40.

Substance 15. 1-(2,2-dichloro-1-(3-nitrophenyl) vinyl)-2-(3,4-dichlorophenyl) diazene. Was obtained by the reaction of (E)-1-(3,4-dichlorophenyl)-2-(3-nitrobenzylide-ne)hydrazine with CCI_4. The yield is 35%, red crystal, T_{melt} =177°C, ^{1}H NMR (300 MHz, $CDCl_3$) δ 8.32-8.30 (d,1H, J=6Hz), 8.08 (s, 1H), 7.87(s, 1H),7.68-7.50 (m, 4H), ^{13}C NMR (75 MHz, $CDCl_3$) δ 151.33, 150.29, 148.17, 141.60, 138.66, 136.20, 136.09, 133.71, 130.98, 129.37, 125.27, 124.54, 123.92, 122.89

Substance 16. 1-(2,2-dichloro-1-(4-nitrophenyl) vinyl)-2-(2,4-dichlorophenyl) diazene. Was obtained by the reaction of (E)-1-(2,4-dichlorophenyl)-2-(4-nitrobenzylide-ne)hydrazine with CCI_4. The yield is 50%, red crystal, T_{melt}=168°C, ^{1}H NMR (300 MHz, $CDCl_3$)δ8.12-8.15 (m, 2H), 7.65-7.66 (d, 1H, J=3Hz), 7.45-7.48 (d, 3H, J=9Hz), 7.33 (s, 1H).^{13}C NMR (75 MHz, $CDCl_3$) δ 148.26, 147.96, 147.75, 137.76, 137.25, 134.98, 129.71, 129.59, 129.50, 128.05, 125.98, 123.97.

Substance 17. 1-(2,2-dichloro-1-(4-nitrophenyl) vinyl)-2-(2,6-dichlorophenyl) diazene. Was obtained by the reaction of (E)-1-(2,6-dichlorophenyl)-2-(4-nitrobenzylide-ne)hydrazine with CCI_4. The yield is 45%, red crystal, T_{melt} =80 °C, ^{1}H NMR (300 MHz, $CDCl_3$)δ, 8.12-8.14 (m, 4H), 7.47-7.49 (d, 2H, J=6Hz), 7.41-7.43 (t, 1H, J=9Hz).^{13}C NMR (75 MHz, $CDCl_3$) δ 148.26, 147.76, 145.55, 137.76, 134.98, 129.71, 127.76, 127.70, 127.29, 125.98.

Substance 18. 1-(2,2-dichloro-1-(4-nitrophenyl) vinyl)-2-(3,4-dichlorophenyl) diazene. Was obtained by the reaction of (E)-1-(3,4-dichlorophenyl)-2-(4-nitrobenzylide-ne)hydrazine with CCI_4. The yield is 35%, red crystal, T_{melt} =160 °C, ^{1}H NMR (300 MHz, $CDCl_3$) δ 8.35-8.30 (dd, 2H, J=6Hz), 7.89 (s, 1H), 7.65-7.53 (m, 2H), 7.40-7.35 (m,2H), ^{13}C NMR (75 MHz, $CDCl_3$) δ 151.35, 150.59, 148.05, 138.97, 138.28, 136.13, 135.41, 133.69, 131.20, 131.00, 124.47, 123.51, 122.88, 29.72.

3. RESULTSAND DISCUSSION

Have been synthesized the 2,4-dichloro-, 2,6-dichloro-, 3,4-dichloro-phenylhydrazones of o-, m- and p-nitrobenzaldehydes for clarifying the effects of

functional groups on the reaction yield, the design of the crystal cage, and the CI···CI non-covalent interactions [13-17] parameters.

The hydrazones derived from aldehyde and ketones, belong to the class of organic compounds having non-substituted $R_1R_2C=NNH_2$ and substituted $R_1R_2C=NNHR$ [18] structures. The nitrogen atoms of the hydrazones have nucleophilic properties and the carbon atom has both electrophilic and nucleophilic nature. [19]. The functionalization of hydrazones with different functional groups brings to obtaining compounds with unique physical and chemical properties and structure. Hydrazones have different biological and pharmacological properties as antibacterial, pain-resistant, antiplatelet, heart-protective, anti-aging, antidepressant, antiinflammation, antifungus, antituber-culosis, antiswollen, antivirus, anticancer, antimalaria, and etc. According to their biological and pharmacological properties, they are very important compounds for the synthesis of heterocyclic compounds. [20]. Hydrasons are used in the preparation of new medicines. There are a lot of researches devoted to the synthesis of hydrazones and investigation of their biological activity. [21-22]. In the present paperwe report of X-ray investigations of synthesized phenylhyd-razones andrevealing the dependence of antimicrobial properties from their structure. (Scheme 2)

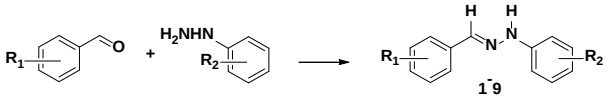

R_1=o, m, p-NO_2-, R_2= 2,4-dichloro-, 2,6-dichloro-, 3,4-dichloro-.

Scheme 2.Synthesize of phenylhydrazone

It is apparent from the structure 1 that the oxygen atomof the nitro group created two hydrogen bonds (O···HC (2.620), O···HN(2.407)] with the azomethine group (-HN = N-CH-). In the structure 2 along with hydrogen bonds [O···HC (2.58), O···HN (2.621)] the O···O non-covalent interaction between two oxygen atoms [O···O (3,000Å)] was observed, due to NO2 groups in the structure 2 are disposed under the $113^0 13'$that in turn led to approximate of NO_2 groups in the space, while the O···O interaction was not observed in structure 1. On the Figure 3 we can see that in addition to strong hydrogen bond [O···HN (2,377Å)], in the structure 5 appeared non-covalent interactions between the oxygen and Cl atoms [O···Cl (3.286Å)]. This interactionsoccure due to the fact that the nitro group is in a meta position.At the same time the angle between the O···HN atoms is 48.69, and it allows the formation of this interaction.

Table 1. Crystallographic and structural data of compounds 1, 2 and 5

	1	2	5
X-ray structure	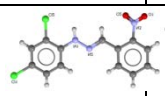	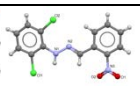	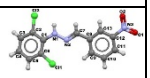
Substance name	1-(2,4-dichlo-rophenyl)-2-(2-nitrobenzy-lidene) hydra-zine	E-1-(2,6-dichlorophenyl)-2-(2-nitro-benzylidene) hydrazine	E-1-(2,6-dichloro-phenyl)-2-(3-nitro-benzylidene) hydrazine
Formula	C_{13} H_9 Cl_2 N_3 O_2	C_{13} H_9 Cl_2 N_3 O_2	C_{13} H_9 Cl_2 N_3 O_2
Mr	310.13	310.13	310.13
Crystal cage	Triclinic	Monoclinic	Monoclinic
Spacial group	P_1	$P2_1/c$	$P2_1$
a, (Å)	7.6115(11)	4.0673(5)Å	7.1169 (15)
b, (Å)	11.5961(17) Å	25.200(3) Å	12.689 (3)
c, (Å)	37.959(5) Å	12.9655(16)	7.6890 (17)
α,^{0}	84.661(4)°.	90°	-
β, ^{0}	88.681(4)°	97.662(5)°	105.978 (8)
γ, ^{0}	85.477(4)°	90°	-
V, ($Å^3$)	3325.1(8)	1317.0(3)	667.6 (3)
ρ(calc.),g/cm^3	1.326	1.564	0.49
Z	8	4	2

Thusit is possible to tune and design the crystalline structure of the prepared compounds by means of different dispositions of nitro groups and chlorine atoms in the benzene ring. So, it can be concluded that the crystalline cage can be designed by changing the position of nitro group in benzaldehyde and Cl atoms in the phenylhydrazine.

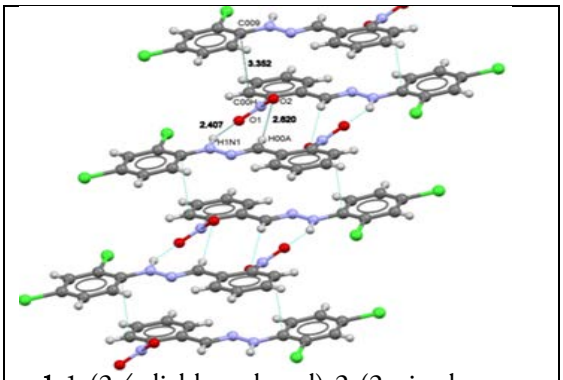

1.1-(2,4-dichlorophenyl)-2-(2-nitrobenzy-lidene)hydrazine

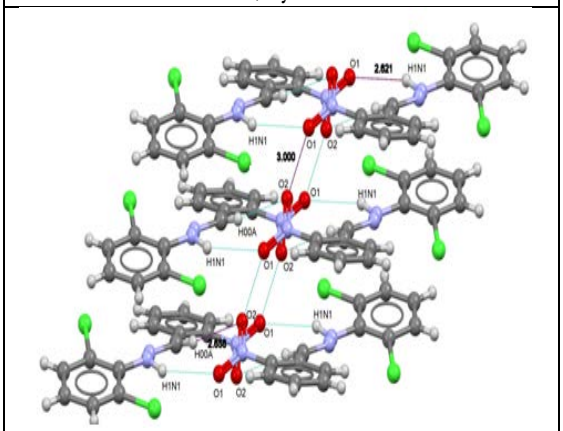

2.1-(2,6-dichlorophenyl)-2-(2-nitrobenzy-lidene)hydrazine

Figure 2. Intermolecular non-covalent interactions in compounds 1 and 2 shown by dotted lines.

Note that, despite the presence of two chlorine atoms in the hydrazine derrivaties, there is no Cl···Cl interactions in these molecules, unlike compounds synthesized in our previous studies. This was due to the formation of strong hydrogen bonds between molecules, with the maximal distance of Cl atoms to each other in the crystal packaging, in other words, the location according to the "head-tail" principle.

Then, the catalytic olefination reaction of the hydrazones we synthesized was performed (Scheme 3)

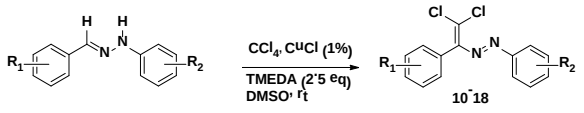

R_1=o, m, p-NO_2-, R_2= 2,4-dichloro-, 2,6-dichloro-, 3,4-dichloro-.

Scheme 3.Synthesise of derivatives of dichloorodiazobutadienes from phenyl-hydrazones

The structure of the compounds obtained has been fully confirmed by the X-ray and NMR methods. As previously mentioned, Cl···Cl (3.203-3.471Å) non-covalent interaction observed in compounds A and B (Figure 1 (b)) was also observed in compound 12 (Cl···Cl (3.404Å) (Fig. 4).

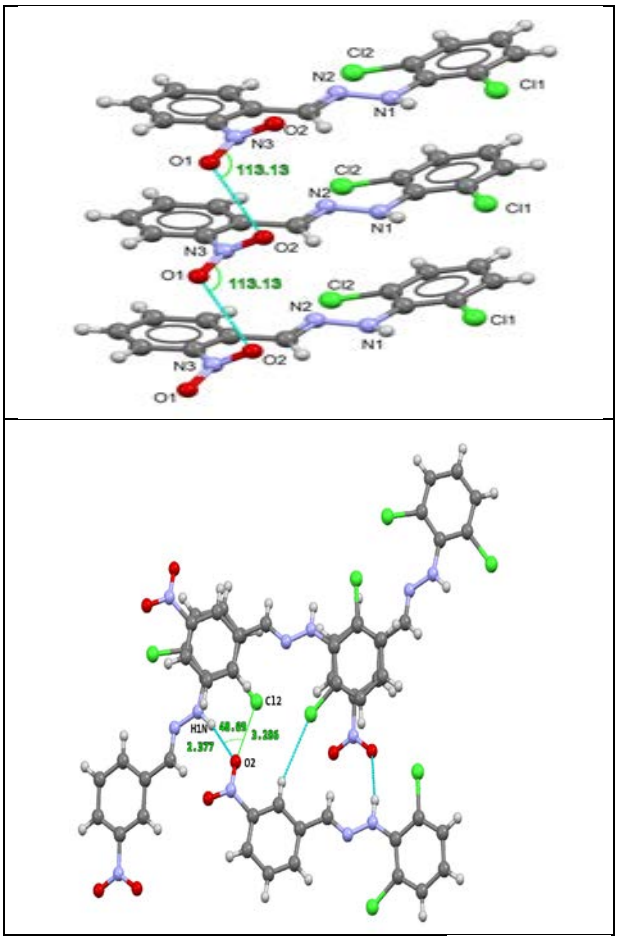

Figure 3. Intermolecular non-covalent interactions in compounds 2 and 5 shown by dotted lines.

Table 2. Structural parameters of compounds 10,11 and 12

	1	2	5
X-ray structure	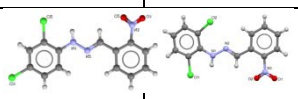		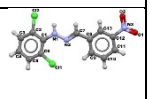
Substance name	1-(2,4-dichlo-rophenyl)-2-(2-nitrobenzy-lidene) hydra-zine	E-1-(2,6-dichlorophenyl)-2-(2-nitro-benzylidene) hydrazine	E-1-(2,6-dichlorophenyl)-2-(3-nitro-benzylidene) hydrazine
Formula	C_{13} H_9 Cl_2 N_3 O_2	C_{13} H_9 Cl_2 N_3 O_2	C_{13} H_9 Cl_2 N_3 O_2
Mr	310.13	310.13	310.13

Crystal cage	Triclinic	Monoclinic	Monoclinic
Spacial group	P_1	$P2_1/c$	$P2_1$
a, (Å)	7.6115(11)	4.0673(5)Å	7.1169 (15)
b, (Å)	11.5961(17) Å	25.200(3) Å	12.689 (3)
c, (Å)	37.959(5) Å	12.9655(16)	7.6890 (17)
α,^{0}	84.661(4)°.	90°	-
β, ^{0}	88.681(4)°	97.662(5)°	105.978 (8)
γ, ^{0}	85.477(4)°	90°	-
V, (Å^3)	3325.1(8)	1317.0(3)	667.6 (3)
ρ(calc.) ,g/cm^3	1.326	1.564	0.49
Z	8	4	2

In the sturucture ofcompound 12 (figure 4), we can see that the presence of the NO_2 group led to the Cl···O interaction (3.164Å) in contrast to the compounds A and B.

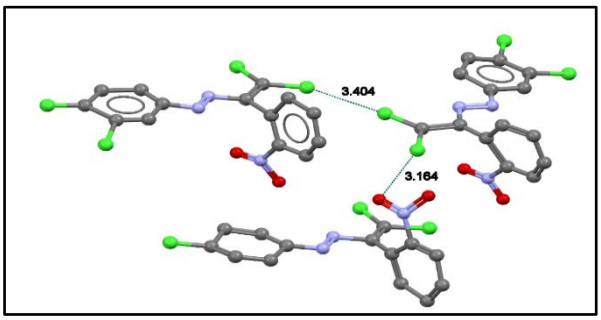

Figure 4.Intermolecular non-covalent interactions in compound 12 shown by dashed lines.

4. CONCLUSION

Thus, the introduction of functional groups into benzene rings in dichlordiazabutadiene derivatives synthesized by catalytic olefination reaction has resultedthe product with new physical, chemical and physiological properties. The parameters of non-covalent interactions (O···HC (2.58Å), O···NH(2.377Å), O···Cl (3.164Å), O···O(3.000Å), (Cl···Cl (3.404Å)) and their role in crystal design was studied by the X-ray method.

5. REFERENCES

1. Nenajdenko V.G., ShastinA., GorbachevV., ShorunovS., MuzalevskiyV.M., LukianovaA., DorovatovskiiP.V., and KhrustalevV./ ACS Catal, 2017, v. 104, 3, p.1-6 – 672
2. ShikhalievN.Q., AhmadovaN.E. Gurbanov A.V., Maharramov,A.M., MammadovaG.Z., NenajdenkoV.G., ZubkovF.I., MahmudovK.T.,/ Dyes and Pigments, 2018, v.150, p. 377–381.
3. Shikhaliev,N.G., et all/ News of Baku University, 2016, №1, p.40-49.
4. Shikhaliev N.G., et all // News of Baku University, 2016, №3, p.5-12
5. Israyilova,A. et all / International Journal of Innovative Research in Science. Engineering and Technology. 2017, v.6, 8, p.1111-1115.
6. Maharramov A.M., et all/ Journal of Low Dimensional Systems, 2017, v 1, 1, p.4-7.
7. Calvo S., Navarrete H, Lopez J. T. Journal of Physical Chemistry A, 2000, v. 104, №3, p. 661 – 672
8. Ericson, D.P., et all /Crystal Growth and Design, 2015, v. 15, p. 5744 - 5748
9. Higuchi, H. et all/ Bulletin of the Chemical Society of Japan, 2001, v. 74, p. 2467 – 2468
10. Hu, Xian-Lei; Zhao, Zhong; Liu, Xiang-Hua; Zhang, Qing-Chun-Kang /Iron and Steel (Peking),2007, v. 42, № 4, p. 50 – 52
11. Angiolini, L., et all / Synthetic Metals,2015, v. 202, p. 169 – 176.
12. Molecular statics simulations of head to head and tailtotailnanodomains of rhombohedral barium titanate, Endres; Steinmann-Computational Materials Science, 2014, vol. 97, p. 20 – 25
13. Maharramov A.M., K.T. Mahmudov, M. N. Kopylovich and A. J. L.PomberioNon-Covalent Interactions in the Synthesis and Design of new Compounds, ,Willey pub,2016
14. Maharramov A.M., K.T. Mahmudov , M.N, Kopylovich, M.Fatima C. Activation of covalent bonds through non-covalent interactions, Guedes da S.J. Pomberio and A.J. Pomberio/Non-Covalent Interactions in the Synthesis and Design of new Compounds, Willey pub, 2016, p 3-21
15. Maharramov A.M., N. Q. Shixaliyev, A. V. Gurbanov, K.T. Mahmudov, V.G.Nenajdenko, Armando J.L.Pombeiro and M.N. Kopylovich, Halogen Bonding in the sythesis and design of

coordination and organometallic compaunds , Non-Covalent Interactions in the Synthesis and Design of new Compounds, Willey pub,2016, p 146-162

16. Shixaliyev N. Q., A. V. Gurbanov, A.M. Maharramov, K.T. Mahmudov , Maximilian N. Kopylovich, L. M. D. R. S. Martins ,V.G.Nenajdenko, A.J.L.Pombeiro, /New J. Chem. 2014, v.38, p.48807-11.
17. Selective Moleculyar binding and nanosupramolecular Assembly of p-sulfonatocalix [n] arenes, Non-Covalent Interactions in the Synthesis and Design of new Compounds, Willey pub, 2016, p 261-281
18. Uppal G, Bala S, Kamboj S, Saini M. /Der Pharma Chem 2011, v. 3, 250, p.68-71.
19. Corey EJ, Enders D / Tetrahedron Lett 1976, v. 17, p.11-4.
20. Xavier AJ, Thakur M, Marie JM. /J Chem Pharm Res, 2012, v.4, p.986-90.
21. Verma G., A.Marella, M. Shaquiquzzaman, M. Akhtar, M.R. Ali, M. M.Alam/ Journal of Pharmacy and Bioallied Sciences, 2014, v. 6 2, p.69-80.
22. Asif M. / International Journal of Advanced Chemistry, 2014, v.2, p.85-103

BSU Publication | Journal of Low Dimensional Systems, v. 2 (1), 2018

THE STUDY OF ANTIMICROBIAL ACTIVITY OF 2-AMINO-1-METHYL-6-(METHYLTHIO)-5-NITRO-4-ARYL-1,4-DIHYDROPYRIDINE-3-CARBONITRILES

A.M.MAHARRAMOV[1], A.I.ISMIEV[1], K.E.HAJIYEVA[1*]

[1]Baku State University, Z.Khalilov 23 Str., Baku, Azerbaijan

The biological activity of a series of polyfunctionalizednitroethenamine analogues bearing 1,4-dihydropyridine structure, synthesized by multicomponent condensation reaction, has been investigated and found to exert a suppressive effect on bacteria such as St. Aureus, Ps. Aeruginoza, E. coli and Cand. Albicans.

PACS numbers: 82.39.-k, 87.68.+z
Keywords: 1,4-dihydropyridine, biological activity, nitroethenamine derivatives
***E-mail:** kushvar.hajiyeva@gmail.com

1. INTRODUCTION

Multicomponent reactions (MCRs) have found increasing application for the synthesis of complex pharmacologically important structures [1-6]. They provide a powerful tool for the one-pot synthesis of diverse compounds of medicinal interest. The diversity, efficiency and rapid access to small and highly functionalized organic molecules makes this approach of central current interest in the construction of combinatorial libraries and optimization in drug discovery process. Among them, 1,4-dihydropyridines have received much attention because of their wide range of pharmaceutical and biological properties such as bronchodilator, antibacterial, antiviral and anticancer effects [7-9].1,4-Dihydropyridine derivatives also exhibit biological proper-ties such as antihypertensive, antiinflam-matory and antiischemic activities and act as calcium channel modulators of the nifedipine type. Several methods have been described for the synthesis of 1,4-dihydropyridine [10–12]. Recently, some new 3,5-substituted 1,4-dihydropyridine derivatives were synthesized which exhibit pharmacological activities[13–16].

As a part of our ongoing investigations aimed the study of aforementioned bioactive compounds and in continuing of our previous research [17] on the one-pot synthesis of 2-ami-no-1-methyl-6-(me-thylthio)-5-nitro-4-aryl-1,4-dihydropyridine-3-car-bonitriles we have discussed here their antimic-robial properties.

2. EXPERIMENTAL

As was mentioned, a series of polyfunctionalized2-amino-1-methyl-6-(methylthio)-5-nitro-4-aryl-1,4-dihyd-ropyridine-3-carbonitriles were synthesized by one-pot multicomponent reaction of aldehydes, N-methyl-1-(methylthio)-2-nitroethenamine and malononitrile in the presence of Et_3N (Scheme 1).

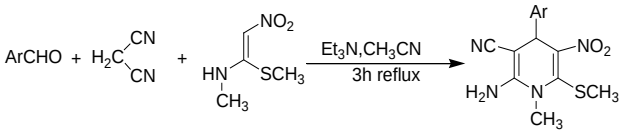

Scheme 1. Reaction between aldehydes, N-methyl-1-(mehylthio)-2-nitroethenamine and malononitrile

Antimicrobial and fungicidal properties of 2-amino-4-(4-fluorophenyl)-1-methyl-6-(methylthio)-5-nitro-1,4-di-hydropyridine-3-carbonitrile (compound 1), 2-amino-1-methyl-6-(methylthio)-5-nitro-4-phenyl-1,4-dihydropyri-dine-3-carbonitrile (compound 2), 2-amino-4-(4-cyano-phenyl)-1-methyl-6-(methylthio)-5-nitro-1,4-dihydropyri-dine-3-carbonitrile (compound 3), 2-amino-4-(4-met-hoxyphenyl)-1-methyl-6-(methylthio)-5-nitro-1,4-dihyd-ropyri-dine-3-carbonitrile (compound 4) and 2-amino-1-methyl-6-(methylthio)-5-nitro-4-(p-tolyl)-1,4-dihydropy-ridine-3-carbonitrile (compound 5) were studied.

Biological activity of these compounds have studied by a series of dilution. For this purpose, four sterile test tubes were taken. To the first and second test tubes 1 ml of substance to be tested are added (1% of substance was dissolved in ethanol), starting from

second one 1 ml of sterile distilled water was added to each test tube. Then, from second test tube, 1 ml of mixture were taken and added to the third test tube, from third one to the fourth one and at the end, 1 ml of mixture was taken from fourth test tube and thrown away. Thus, new compounds to be tested, dosed in 1: 100 (1), 1: 200 (2), 1: 400 (3), 1: 800 (4) proportions in the test tubes. After dilution for each test tube, one drop of emulsion added, containing 500ml of microbial particles per 1ml, and inoculation carried out every 10-20 minutes for 1 hour. After 10-minutes, 20 minutes, 40 and 60 minutes of exposure, from each test tube the nutrient-filled environment in Petri cups were grown. Bacteria inoculation were carried out under the conditions of a thermostat, for 24 hours at a temperature of plus 37° C, and for fungi for 48 hours at a temperature of 28° C.

3. RESULTS AND DISCUSSION

The antimicrobial properties of the synthesized compounds have shown in Table 1, and the control compounds in Table 2.

Table 1. Antimicrobial activity of the synthesized compounds

Test culture	Exposure time (min)	Synthesized compounds															
		1				2				3				4			
		1	2	3	4	1	2	3	4	1	2	3	4	1	2	3	4
St. Aureus	10	-	-	+	+	-	-	+	+	-	+	+	+	-	+	+	+
	20	-	-	+	+	-	-	+	+	-	-	+	+	-	-	+	+
	40	-	-	+	+	-	-	+	+	-	-	+	+	-	-	+	+
	60	-	-	+	+	-	-	+	+	-	-	+	+	-	-	+	+
E.Coli	10	-	-	+	+	-	-	+	+	+	+	+	+	-	-	+	+
	20	-	-	+	+	-	-	+	+	-	+	+	+	-	-	+	+
	40	-	-	+	+	-	-	+	+	-	+	+	+	-	-	+	+
	60	-	-	+	+	-	-	+	+	-	+	+	+	-	-	+	+
Ps.Aeruginoza	10	-	-	+	+	-	+	+	+	-	+	+	+	-	+	+	+
	20	-	-	+	+	-	-	+	+	-	+	+	+	-	-	+	+
	40	-	-	+	+	-	-	+	+	-	+	+	+	-	-	+	+
	60	-	-	+	+	-	-	+	+	-	-	+	+	-	-	+	+
Candida Albicans	10	-	-	+	+	-	-	+	+	-	-	+	+	-	-	+	+
	20	-	-	+	+	-	-	+	+	-	-	+	+	-	-	+	+
	40	-	-	+	+	-	-	+	+	-	-	+	+	-	-	+	+
	60	-	-	+	+	-	-	+	+	-	-	+	+	-	-	+	+

Note:1,2,3,4 – shows 1:100, 1:200, 1:400, 1:800 ratios ; “+” shows completion; “-” shows there is no completion

According to the analysis of the data in Table 1, the synthesized compounds has a strong antimicrobial effect on the investigated microorganisms, unlike control substances, compounds 1, 2 and 4 destroyed microorganisms in 10 minutes, while in 20 minutes at the same ratio only compound 2 on coliforms and compound 4 on stafilococes, had a negative effect. Compound 3 had a relatively weaker antibacterial effect than others had, as it did not affect in 1:200 ratio on coliforms and had a lethal effect on Pseudomonas Aeruginosa in 1 hour at the same ratio, but in 1: 200 ratio, it stopped the growth of Candida fungus for 10 minutes, staphylococcus for 20 minutes. By its antibacterial effect compound 5 is very similar to compound 1 and compound 2, totally these bacteria were destroyed in 10 minutes in 1: 200 ratio, but remains relative to fungicidal effects (against the fungus), as it stops the growth of Candida in 1:200 ration for 40 minutes.

Table 2. Antimicrobial activity of control sub-stances

Test culture	Exposure time (min)	Control substances															
		Ethanol				Rivanol				Furasilin				Nitrofunqin			
		1	2	3	4	1	2	3	4	1	2	3	4	1	2	3	4
St. Aureus	10	-	+	+	+	+	+	+	+	-	-	+	+				
	20	-	+	+	+	+	+	+	+	-	-	+	+				
	40	-	+	+	+	+	+	+	+	-	-	+	+				
	60	-	+	+	+	+	+	+	+	-	-	+	+				
Ps.Aeruginoza	10	+	+	+	+	+	+	+	+	+	+	+	+				
	20	-	+	+	+	+	+	+	+	+	+	+	+				
	40	-	+	+	+	+	+	+	+	+	+	+	+				
	60	-	+	+	+	-	+	+	+	+	+	+	+				
E.Coli	10	+	+	+	+	-	-	+	+	-	+	+	+				
	20	-	+	+	+	-	-	+	+	-	+	+	+				
	40	-	+	+	+	-	-	+	+	-	+	+	+				
	60	-	+	+	+	-	-	+	+	-	+	+	+				

4. CONCLUSION

Antimicrobial effects of a number of substances used for comparison also was study in the same manner and showed in the table. Only rivanol (1: 200 ratio) is similar by the effects on coliforms (E. coli), and the rest are weaker than these substances. Given these, almost all of the substances studied can be considered antimicrobial, especially 2-amino-4-(4-fluoro phenyl)-1-methyl-6-(me-thylthio)-5-nitro-1,4-dihydropyridine-3-carbonitrile,2-amino-1-met-hyl-6-(methylthio)-5-nitro-4-phenyl-1,4-dihydropyridine-3-carbonitrile and 2-amino-4-(4-met-hoxyphenyl)-1-methyl-6-(methylthio)-5-nitro-1,4-dihyd-ropyridine-3-carbonitrile.

5. REFERENCES

1. Dömling A., Wang W., Wang K /Chem Rev., 2012, №112, p.3083-3135.
2. D’Souza D.M., Muller T.J/ J. ChemSoc Rev., 2007, №36, p.1095-1120.
3. Allen E. E., Zhu C., Panek J. S et al. / Organic Letters, 2017, v.19, №7,p.1878-1881.
4. Eckert H / Molecules, 2012, v.17, №9, p.1074-

11025.
5. Ganem B / Acc. Chem. Res, 2009, v.42, №3, p.463-472.
6. Suresh T., Swamy S. K., Reddy V.M / Indian J Chem, 2007, №46B, p.115-221.
7. Amini M., Navidpour L., Shafiee A / Daru, 2008, №16, p.9-12.
8. Stout D.M., Meyers A.I / Chem Rev., 1982, №82, p.223-243.
9. Ji S.J., Jiang Z.Q., Lu J, Loh T.P / Synlett, 2004, №5, p.831-835.
10. Suarez M., Ochoa E., Verdecia Y/ Tetrahed-ron, 1999, №55, p.875-884.
11. Tu S., Wei Q., Ma H / Synth Commun, 2001, №31, p.2657-2661.
12. Pattan S.R., Rasal V.B., Venkatramana N, Khade A.B., Butle S.R., Jadhav S.G et al/ Indian J Chem. 2007, 46B, p. 698–701.
13. Schnell B., Krenn W., Faber K., Kappe C.O / J Chem Soc Perkin Trans 1, 2000, №24 p.4382-4389.
14. Bhavik D., Sureja D., Naliapara Y., Shah A., Saxena A.K / Bioorg Med Chem., 2001, №9, p.1993- 1998.
15. Sabitha G., Reddy G.S., Reddy C.S / Tetrahedron Lett., 2003, №44, p.4129-4131.
16. Hajiyeva K., Ismiev A., Franz M., Schmidtmann M, Martens J.,Maharramov A / Synthetic Communications, 2017, № 47, p.2031-2035.

THE SYNTHESIS OF THE NANOENSEMBLE ON THE BASIS OF DIAZACROWN ETHER WITH MAGNETITE NANOPARTICLES AND THEIR PROPERTIES

L.VEZİROVA

Azerbaijan State University of Oil and Industry,
RI Geotechnological Problems of Oil, Gas and Chemistry, Az1010 Baku, Azerbaijan, Azadlig av. 20.

In this work we report of functionalization of magnetite nanoparticles by hydroxyl containing diazacrown ether - macrocycle (MC) that is able to mimic the properties of natural siderophores. The structure of synthesized crown ether was investigated by NMR, mass-, FTIR spectroscopy methods. The morphology of prepared MC@Fe3O_4nano-ensembles was analysed by scanning electron microscopy SEM, X-ray diffraction XRD analysis methods. The quantitative analysis of nanostructures was determined by atom absorbance spectroscopy (AAS) as well as on the basis of Lambert-Beer law by UV spectroscopy method. It was found that the synthesized compounds were effective against gram-negative microorganisms Escherichia coli, Klebsiellaspp. and gram-positive Staphylococcus aureus, having multi drug resistance properties. Has been found that the nanostructures significantly increase the antimicrobial effect of cephalsporins and decrease their MIC.

PACS: 82.80.-d; 87.15.Fh
Keywords: crown ether, macrocycles, siderophores, nanoparticles.
E-mail: vazirova.leyla@gmail.com

1. INTRODUCTION

Crown ethers, with functional groups in a macrocyclic ring, open new directions for obtaining supramolecular nanostructures due to intermolecular interactions Conceptually supramolecular chemistry and nanotechnology have much in common, as the formation of nanostructures is based on the principle of self-assembly and self-organization and that is the essence of supramolecular ensembles. Supramolecular structures play a vital role in functioning of living organism. Their unique feature is that they arise spontaneously, via hydrophobic interactions, electrostatic effects that in turn arise from the interaction of functional groups of biomolecules with an aqueous environment and through non-covalent bonds that play important role in the formation of these structures [1]. All these naturally occurring supramolecular compounds, forming via self-assembling, are designed for realization of vital biological functions of living organisms [2].

So, synthetic analogues of such systems are very interesting, in term of its supramolecular properties, imitating the properties of naturally occurring systems. The crown ethers can demonstrate the properties of naturally occurring membrane active antibiotics, thanks to ionophore feature of macrocycle cavity to bind the cations trough ion-dipole, dipole-dipole non-covalent bonds [3]. After the binding, the ionophore antibiotics, such as valinomycin and nonactin, drag ions into the bacterial cell, change the permeability of the membrane and disrupt the oxidative phosphorylation [4]. Azacrown ethers, cryptands, thiacrown ethers and their derivatives, having nitrogen, sulfur atoms in macrocyclic ring, are able to selectively bind to metal ions. Azacrown ethers are able to bind the ions of transfer and rare earth metals. [5] Beside this, the synthesis of macroheterocycles, having various functional groups in their molecule, notably influences on the ability of these compounds to form supramolecular ensembles by means of non-covalent interactions [6].

Magnetite nanoparticles have already shown promising results in preclinical experiments for imaging contrast enhancement, tissue repair, magnetic hyperthermia and drug delivery [7,8,9,10].

Today's huge problem, faced to clinicians, is the problem of antibiotic resistance. Staphylococcus Aureus show the rise of the number of resistant strains to antibiotics, especially to B-lactames, particularly in developing countries. As a result, there is an urgent requirement of new modified drugs that are effective

against antibiotic-resistant bacteria. The one of the possible ways is nanostructuring of already used drugs that will enhance and improve their activity.

In accordance to above mentioned, it was interesting to synthesize the hydroxyl containing azacrown ether that is able to mimic the properties of natural siderophores and prepare the supramolecular ensembles of synthesized MC with magnetite nanoparticles MC with magnetite nanoparticles loaded by cephalosporin antibiotics. The investigation of their biological activity against gram-positive and gram-negative microorganisms is a matter of interest in terms of finding the synergistic effect of siderophore-mimic MC and magnetite NPs, loaded with cephalosporin antibiotics.

2. EXPERIMENTAL

Preparation of MC - general procedure - The ethylenediamine (0.003 mol), dissolved in 20 cm3 of methanol, was added dropwise to salysilaldehyde (1) (0.003 mol) in 150 cm3 of methanol. After the addition, the reaction mixture was stirred to room temperature, and 0.006 mol of sodium borohydride in 15 mL of dimethyl formamide was added in portions with stirring. The yellow colour of the reaction mixture disappears with addition of all portion of sodium borohydride, indicated to completion of hydrogenation. When the reduction was completed, mixture was poured in cold distilled water. Formed white precipitate was washed with water and diethyl ether, and then dried over anhydrous sodium sulphate. Removal of the solvent gave the product (4).The further purification was carried by recrystallization from mixture butanol-1.

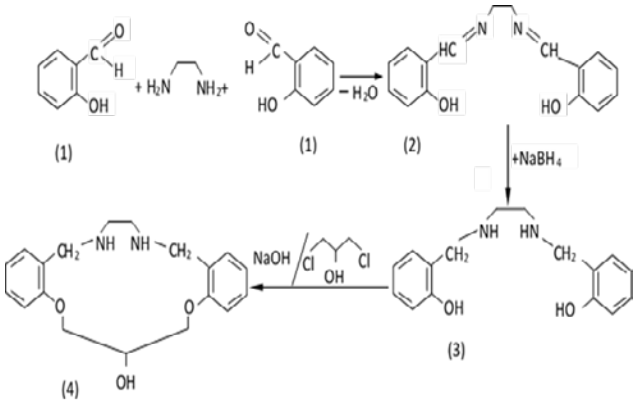

Scheme 1. The synthesis of MC 1,13-Diaza-5,9-dioxa-7-hydroxy-3,4:10,1-dibenzocyclopentadecan

Synthesis of nanostructures by functionalization of Fe3O4 with MC (MC@Fe3O4 NPs). Magnetic iron oxide nanoparticles are usually prepared by wet chemical precipitation from aqueous iron salt solutions in alkaline milieu, created by using NH4OH, in the atmosphere of gaseous nitrogen. [9] The formed Fe3O4 nanoparticles (NPs) were separated by strong NdFeB permanent magnet, repeatedly washed with distilled water and dispersed in ethanol

Characterization of structure- XRD X-ray diffraction analysis was performed on Rigaku Mini Flex 600 XRD diffractometer at ambient. FT-IR the functional groups, present in the powder samples of MC@Fe3O4 NPs, were identified by Fourier Transform Infrared (FTIR) spectroscopy. Scanning Electron Microscope (SEM) and Energy-Dispersive Spectrum (EDS) analysis. SEM and EDS analysis of prepared samples of MC@Fe3O4 nanoparticles were taken on Field EmissionScanning Electron Microscope JEOL JSM-7600F at an accelerating voltage of 15.0 kV, SEI regime.

Determination of antibacterial activity - Antibacterial activity of MC andMC@Fe3O4 was tested by diffusion method, performed on Petri dishes,on Staphylococcus aureus, Klebsiella spp. and Escherichia coli. [8] The synthesized substances were taken in amount equal to 30 μg. Escherichia coli were cultivated on Endo's medium, Klebsiellaspp. On Sabouraud medium and Staphylococcus aureus on Baird-Parker agar. Due to the fact that this method provides only quality data, microdilution method was also performed. By this method the MIC of prepared substances on Staphylococcus aureus, Klebsiella spp. and Escherichia coli was identified. To perform microdilution method the stock solutions of different concentrations of the substances were prepared in distilled sterile water and were distributed in 96 multi-well plates. Each well was inoculated with 0.1 mL of microbial suspensions of 0.5 McFarland turbidity, prepared from 24 h fresh culture. Sterility control wells and microbial growth controls were used. The plates were incubated for 24h at 37 °C [11] [12]. In order to measure antibacterial effect on biofilm development, the nutrient broth was deleted; wells were washed with PBS three times, dried 15 minutes in room temperature and stained by crystal violet 1% for 15 minutes. After the deletion of crystal violet 1%, wells again were washed 3 times with PBS 3 times and

dried at room temperature for 15 minutes. Further, the biofilm, formed onto the plastic wells, was re-suspended in 30% acetic acid and the intensity of the coloured suspension was assayed by measuring the absorbance at 590 nm [9, 11, 12].

The purity and crystalline properties of the MC@Fe3O4 were investigated by powder X-ray diffraction (XRD). The XRD patterns are shown in Figure 1. All the XRD peaks were well defined and corresponded to Fe3O4 nanoparticles with cubic structure.

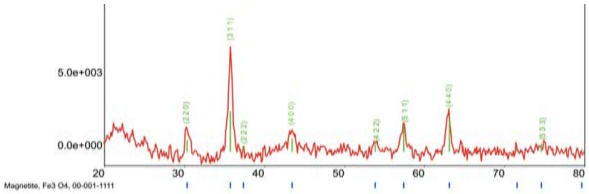

Figure 1. XRD pattern for the nanostructured MC@Fe3O4 NPs

The spectra of prepared nanostructures were compared with spectra of pristine MC and spectra of pristine Fe3O4, in order to determine the coordination sites of MC that may be involved in chelation with surface of magnetite nanoparticles.

As it seen from FTIR spectra, the absorption occurs through NH, OH and macrocycle's oxygen atoms by self-assembling via non-covalent interaction with surface of magnetic NPs

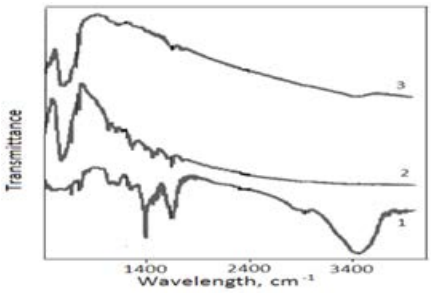

Figure 2. FTIR spectra (1) pristine MC, (2) MC@Fe3O4, (3) pristine Fe3O4

The prepared nanostructures were analysed by SEM and EDS, and the results are presented on Figure 3. As it seen from Figure 3(a), the obtained nanoparticles are homogenous and the size of nanostructures varies in the range from 8-15 nm and this very well correlates with the results, obtained from XRD analysis.

The points, identified in the EDS spectra Figure 3(b), demonstrate the presence of Fe and O as the main elements of the sample and support the data of magnetite nanoparticles formation.

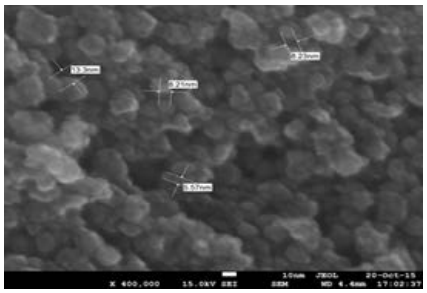

a)

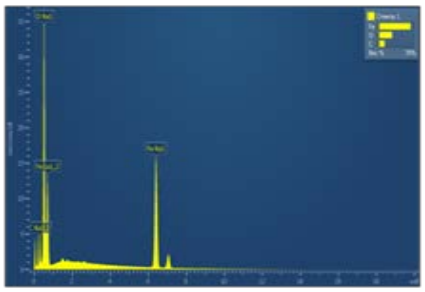

b)

Figure 3. a)SEM image of MC@ Fe3O4 NPs; b) EDS pattern of MC@Fe3O4 NPs

The synthesized MC has high absorption peak in the UV spectrum, observed at the 275 nm. This fact allows quantitatively to determine the amount of absorbed MC on Fe3O4 NPs. Quantitative analysis of absorbed MC onto surface of magnetite nanoparticles was determined by spectroscopic method on the basis of Lambert-Beer law.

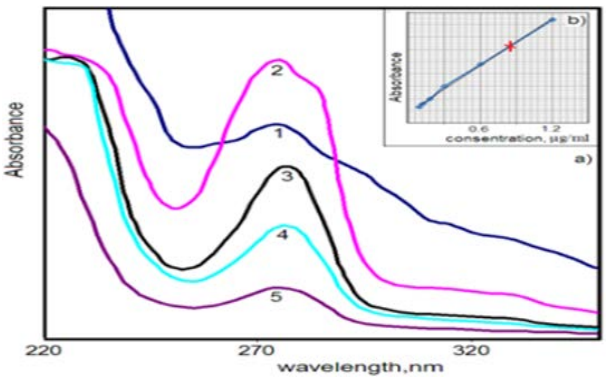

Figure 4. UV spectra of MC@Fe3O4 1) found 0.087 µg/ml; pure MC 2) 1.2 µg/ml 3) 0.6 µg/ml; 4) 0.3 µg/ml 5) 0.15 µg/ml;

3. RESULTS AND DISCUSSION

The obtained nanostructures were expected to reveal the biological activity against microorganisms, so they were tested toward gram-positive bacteria Staphylococcus aureus and gram-negative bacteria Escherichia coli and Klebsiella spp. We assumed that the synthesized MC would be able to reveal antimicrobial activity, due to ionoforic properties as well as MC@Fe3O4 nanostructures can mimic the properties of natural siderofores, especially in case of gram-negative microorganisms. The results of the microdiffusion method show that the inhibition zone, produced by MC on Staphylococcus aureus, was 14 mm in diameter, but there was no effect on Escherichia coli and Klebsiella spp. However, when it comes to MC@Fe3O4, the contrary results were observed. It has no effect on Staphylococcus aureus, but has produced an inhibition zone with the diameter 28 mm on Escherichia coli and 22 mm on Klebsiella spp. (Table 2). The antibacterial effect of MC on Staphylococcus aureus can be explained by the fact that it acts like ionophore, disrupting the membrane's potential of bacteria. [16] At the same time, in case of MC@Fe3O4, antibacterial effect is absent, probably, because Fe3O4 NPs blocked action sites of crown ethers, responsible for ionophore binding with membrane via OH, NH and MC' oxygen atoms by means of ion-dipole, dipole-dipole and etc. interactions. then it comes to Escherichia coli and Klebsiella spp., we can suppose that the mechanism is quite different. We can assume that hydroxyl substituted diazacrown ether is similar to siderophores in their ability to chelate iron. MC alone cannot penetrate through the thick membrane of gram-negative bacteria and produce antibacterial effect; however, laden with iron, it plays a role as a siderophore and more likely is more advantageous for bacterial cells than natural free-from-iron siderophore. In our opinion, the sum of all above-mentioned factors contributes to high antimicrobial effect of MC@Fe3O4 on gram-negative bacteria.

Further the broth microdilution method was assayed, and from its results was observed that the MIC of MC@Fe3O4 NPs on Klebsiella spp. was equal to 0.5 μg/mL. On Staphylococcus aureus the MIC of MC was equal to 1 μg/mL. In case of Escherichia coli, the MC@Fe3O4 NPs' MIC is 0.5 μg/mL (Figure 5).

	Escherichia coli	*Staphylococcus aureus*	*Klebsiella spp.*
MC	-	14 mm	-
MC@Fe_3O_4	28 mm	-	22 mm

Table 2. The diameter of inhibition zones, produced by MC and MC@Fe3O4, on Escherichia coli, Staphylococcus aureus and Klebsiella spp.

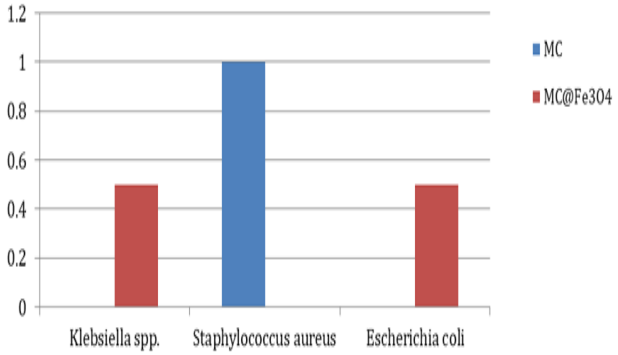

Figure 5. The graphic representation of the MIC (μg/mL) of MC@Fe3O4 and MC against Klebsiella spp., Staphylococcus aureus and Escherichia coli

Moreover, MC@Fe3O4 exhibited inhibitory effect on biofilm development of Klebsiella spp. almost in all concentrations from 20 to 0.5, demonstrating that the loading of crown ether into magnetic nanoparticles provides an improved delivery of the active compound to the bacterial target, even when it grows in biofilm (Figure 6).

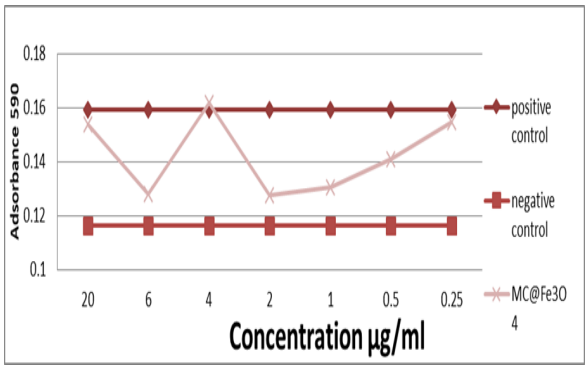

Figure 6. The graphic representation of Klebsiella spp.'s biofilm development in the presence of nano crown ether

According to the spectra, in case of Staphylococcus aureus, MC does not exhibit an inhibitory effect on

biofilm development.We can suppose that it is connected with the possible non-covalent interactions of MC with main constituents of biofilm such as DNA fraqments, polysaccharides' matrix and specific proteins. [18] So, it does not even reach to the bacterial cells, situated in biofilm.

We can assume that synthesizing new supramolecular compounds, creating new nanostructures of antibiotics, coupled by Fe3O4 NPs, and combining all these substances in nanoansembles can show significant results in the fighting against bacterial infections [12].

For expanding our research we diceided to Synthes nanostructures, based on Fe3O4, coated by MC and cephalosporin antibiotics (cefotaxime and ceftriaxone): MC@Fe3O4@cefotaxime (MC@Fe3O4@CTAX) and MC@Fe3O4@ceftriaxone (MC@Fe3O4 @CTRIX) NPs.

Antibacterial activity of pristine antibiotics and the prepared nanostructures were tested by diffusion method on Staphylococcus aureus and Escherichia coli, as described by Mayrhofer (2008). Cephalosporins were taken in amount 30 3g. The synthesized substances were also taken in amount equal to 30 3g. Escherichia coli was cultivated on Endo's medium and Staphylococcus aureus on Baird-Parker agar. Microbiological tests were performed on Petri dishes. Due to the fact that this method provides only quality data, mi crodilution method was also performed, as it is written by Jorgensen and Lee (1975). By this method the MICs of the prepared nanostructures and usual antibiotics were identified and further compared to each other.

The purity and crystalline properties of the MC@Fe3O4@CTAX and MC@Fe3O4@CTRIX were investigated by powder X-ray diffraction (XRD). The XRD patterns are shown in Figure 1 and 2 correspondingly. All the XRD peaks were well defined and corresponded to Fe3O4 nanoparticles with cubic structure. The spectra of prepared nanostructures were compared with spectra of pristine MC on the Figure 3 (b) and 4 (b); spectra of pristine cephalosporins Figure 3 (c) and 4 (c); and spectra of pristine Fe3O4 Figure 3 (d) and 4 (d); in order to determine the coordination sites that may be involved in chelation with surface of magnetite nanoparticles.

As it seen from FTIR spectra the absorption occurs through carboxylic, amine, CONH, hydroxyl groups of ceftriaxone and cefotaxime and NH, OH and cyclic oxygen atoms of MC by self-assembling via non-covalent interaction with surface of magnetic NPs. Thus, the IR spectra results provide strong evidences for the multiple chelation sites of MC and drugs molecules with surface of magnetite NPs.

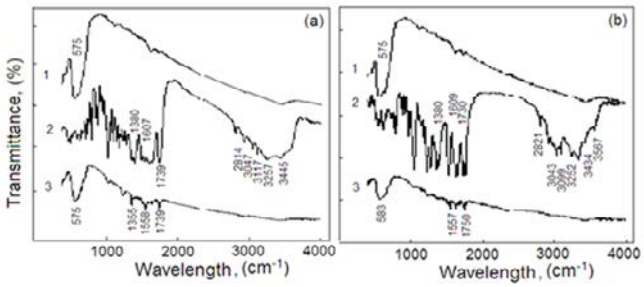

(a) (b)

Figure 7. (a) and 4 (a) present the FTIR spectra of MC@Fe3O4@CTAX and MC@Fe3O4@CTRIX correspondingly.

The surface morphology of the MC@Fe3O4@CTAX and MC@Fe3O4@CTRIX NPs, determined by SEM. As it shown the prepared nanostructures are monodisperse with almost uniform size approximately 6-13 nm. The average sizes of formed nanoparticles correlate well with data, obtained from XRD analysis.

Quantitative analysis of cephalosporins molecules, contained in MC@Fe3O4@CTAX and MC@Fe3O4@CTRIX NPs, was analyzed by UV spectroscopy methods on the basis of Lambert-Beer law and the iron content in NPs samples was determined by AAS method.

The microbiological assay was performed on two different strains of bacteria: Staphylococcus aureus and Escherichia coli. The choice was based on the results of our previous research, performed by Hasanova et al. (2015), showing that gram-negative and gram-positive bacteria react differently to nanostructures, containing magnetite nanoparticles. The Fe3O4@CTAX and Fe3O4@CTRIX have no antimicrobial effect on S. aureus. However, the results of agar diffusion test on Staphylococcus aureus show that the inhibition zones of pure cefotaxime and MC@Fe3O4@CTAX were almost the same, equal to 13 and 11 mm correspondingly. However, the effect of the MC@Fe3O4@CTAX on E.coli was significant. The diameter of inhibition zone of MC@Fe3O4@CTAX was 29 mm, whereas pristine cefotaxime produced 9 mm of inhibition zone's diameter. The

Fe3O4@CTAX NPs' inhibition zone diameter is 22 mm, that is also noticeably greater than that made by pure cefotaxime. MC@Fe3O4@CTRIX and Fe3O4@CTRIX produced the same inhibition zone with diameter 34 mm; however, pure ceftriaxone produced the zone with diameter equal only to 7 mm. According to obtained results, we can suggest that MC mimics the properties of natural siderophores, bound with iron, helps antibiotic to avoid the mechanism of the resistance, elaborated by bacteria. MICs of cefotaxime, ceftriaxone, MC@Fe3O4@CTAX and MC@Fe3O4@CTRIX on S.aureus were the same and equal to 6 μg/mL.MIC of Fe3O4@CTAX on E.coli was 6 times and MC@Fe3O4@CTAX 12 times lower than MIC of pristine cefotaxime. The results of ceftriaxone's nanostructures are even better. The MIC of Fe3O4@CTRIX was 12 times and MC@Fe3O4@CTRIX 24 times lower than MIC of pure ceftriaxone. The improvement of MIC on Escherichia coli correlates well with the increase of the antimicrobial effect, seen from diffusion method and also evidences that MC mimics siderophore and significantly improves the effectiveness of antibiotics.

4.CONCLUSİON

The synthesis of compounds, having biological activity, and modification of already exist drugs for application in targeting drug delivery are among the key solutions of such problems as the resistance of microorganisms, the toxicity and adverse side effects of usual antibacterial agents. Our research's results show that the combining of supramolecular and nanotechnological approaches can make a great impact on antibacterial therapy. Synthesized hydroxyl substituted diazacrown shows a significant antibacterial effect and low MIC on gram-positive S.aureus, whereas nanostructured hydroxyl substituted azacrown produces an impressive effect and low MIC on gram-negative microorganism K. spp. and E. coli, and even has ability to inhibit their growth in biofilm almost in all concentrations. The binding of MC to Fe3O4@CTAX and Fe3O4@CTRIX NPs overcomes the destroying of β-lactam ring of cephalosporins, due to their synergistic effect. It was shown that nanostructuring of cefotaxime and ceftriaxone significantly improves the antimicrobial effect of abovementioned drugs, even on the resistant strains of Escherichia coli. We can also conclude that the impressive synergistic effect of synthesized MC and cephalosporin antibiotics, united in magnetite based nanostructures, impressively decreases the MIC of antimicrobial agents. As consequence, the nanotechnological approach creates a possibility to reduce the dosage of taken medicines with keeping therapeutic effect high and side effects low.

5. REFERANCES

1. Steed E. et al. Supramolecular chemistry, 2nd edition, 2007, Chapter 1.7, pp.27-38.
2. Chris J. and John R. Medicinal Applications of Coordination Chemistry, The Royal Society of Chemistry, Chapter 4, 2007, p.203-205.
3. Tatsuya N. /Ag+ Selective Macrocycles Containing Soft Ligating Moieties and Regulation of Ag+ Binding, Journal of inclusion phenomena and molecular recognition in chemistry, 2007, Volume 32, Issue 2-3, p. 331-345.
4. VukUskoković V. et al. Nanostructured Platforms for the Sustained and Local Delivery of Antibiotics in the Treatment of Osteomyelitis, Critical ReviewsTM in Therapeutic Drug Carrier Systems,2005, 32(1), p.1–59,
5. Dena D., et al. Preparation and characterizationof 6-mercaptopurine-coated magnetite nanoparticles as a drug delivery system,Drug Design, Development and Therapy, 2013, p. 1015–1026,
6. Grumezescu A.M., et al /Biocompatible Fe3O4 Increases the Efficacy of Amoxicillin Delivery against Gram-Positive and Gram-Negative Bacteria. Molecules, 2014, p.19,
7. Magda L., Carlos R. /Applications of Magnetic Nanoparticles in Medicine: Magnetic Fluid Hyperthermia, PRHSJ ,2009, Vol. 28, No. 3, p.227-238.
8. Grumezescu, A.M., et al. /In Vitro Activity of the New Water-Dispersible Fe3O4@Usnic Acid Nanostructure against Planktonic and Sessile Bacterial Cells, Journal of Nanoparticle Research, 2013, vol.15, p.108-125
9. Marcel H. et al. /Comparative Analysis of Antimicrobial Activities of Valinomycin and Cereulide, the Bacillus cereus Emetic Toxin, Applied and environmental microbiology, 2011, vol. 77, p. 2755–2762
10. Kenneth N. Raymond (1994) Recognition and transport of natural andsynthetic siderophores by

microbes, Pure and Applied Chemistry, Vol. 66, No. 4, pp. 773-781, DOI:10.1351/pac199466040773

11. Saravanan P. et al. /How Staphylococcus aureus biofilms develop theircharacteristic structure,PNAS, 2012, vol. 109, no. 4, p.1281–1286.
12. Hasanova U.A. et al., /Nano-Coupling of Cephalosporin Antibiotic with Fe3O4 Nanoparticles: Trojan Horse Approach in Antimicrobial Chemotherapy of Infections Caused by Klebsiella spp. Journal of Biomaterials and Nanobiotechnology, 2015, 6, p. 225-235

BSU Publication | Journal of Low Dimensional Systems, v. 2 (1), 2018

ENVIRONMENTAL PROBLEMS OF ABSHERON PENINSULA AND CASPIAN SEA CAUSEDBY OIL AND GAS PRODUCTION

M.A.RAMAZANOV[1*], I.S.AHMADOV[1], U.A.HASANOVA[1],
LUCA DI PALMA[2], ANGELO CHIANESE[2]

[1]Baku State University, Z. Khalilov Street 23, Baku AZ1148, Azerbaijan
[2]Sapienza Università di Roma, via Eudossiana 18 - 00184 Roma, Italy

It is fact that as approximately 40% of the country's population and 70% of the industrial potential of the Azerbaijan is concentrated in the Absheron peninsula and most of the ecological problems in this region are caused by oil and gas production. The ecological sensitivity of this region requires an industrial system including oil and gas extraction that would have a minimum impact on the environment. In this review article, we attempted to elucidate the main ecological problems of Absheron peninsula and Caspian Sea region.Currently, in Absheron Peninsula transport, oil extraction, oil refineries, power plants, oil pipelines, radionuclides, solid waste are among the main contaminants. The major contaminants in the Caspian Sea are mainly the waste water, oil, hydrocarbons, nuclides, chlororganic compounds and heavy metals. The following factors must be taken into account while dealing with contamination of the region: firstly, irregular distribution of wastewater causes serious pollution of different coastal areas and the sea. Secondly, it carries littoral contamination from one zone to another one and pollutes that area too. Theattention should be paid to minimizing the accidents that occurred during the offshore oil drilling and transportation.

PACS numbers: 87.15.La; 87.10.+e
Keywords: ecological problems, oil and gas extraction, radionuclides, contamination, oil refineries, offshore oil industry
E-mail: mamed_r50@mail.ru

1. INTRODUCTION

The capital – Baku city and a number of densely populated surrounding areas of Azerbaijan Republic are located in the Absheron Peninsula and occupy more than 222 thousand hectares (ha). Approximately 40% of the country's population and 70% of the industrial potential of the Azerbaijan is concentrated in the Absheron peninsula and most of the ecological problems exist in this area are caused by this fact.Absheron Peninsula is rich with the oil and gas resources and since ancient times the minerals are extracted in these places. In 1901-1905, half of the total volume of oil in the world was extracted in Absheron. In 1940-1945, during the Second World War 70.1% of all oil in the former Soviet Union wasextracted in Azerbaijan. The long history of oil exploration has left the country with a massive legacy of oil and other chemical pollution, both land-based and offshore.

Environmental problems of the Absheron Peninsula. Main environmetal problems of the Absheron Peninsula is contamination of land by oil and layer waters during oil-gas extraction, formation of artificial lakes, accumulation of wastes, bad sewage systems. Absheron Peninsula and The Caspian Sea are under constant threat of pollution because the major industries and oil production, refining and transportation are located in these areas.The basic pollution sources of the Absheron Peninsula are the slops of the capital city Baku which has many different industrial objects, transport communication resources and urban transport, refineries and onshore and offshore exploitation of oil and gas wells. The increased density of anthropogenic load capacity in the Absheron industrial region based on energy consumption is more than 32–45 times higher than the normal level. The index of sustainable development is more than 33 times higher than the allowable value. Over 3 million tone of gum brine containing up to 25% of oil and 170000 tone of acid sludge have been disposed at the territory of the Baku Oil Processing Plant[1]. Currently, in Absheron Peninsula transport is considered to be the main source of air pollution, responsible for increase in NOx, organic chemical, and CO emissions. There is stationary sources of atmospheric pollution such as the release of associated gases by power plants, burning of untreated garbage; oil refineries, and factories in Sumgait. In Baku, emission of industrial pollutant

unrelated to oil industry is relatively small with exception of releases of chlorofluorides from air conditioners; refrigeration industries; and cement production [2].At present, oil production, chemical and mineral resources extraction and processing, power plants, and hospitals are the major generators of solid and hazardous wastes. Absheron Peninsula soil is known for having them most acute oil degradation with more that 10,000 hectares of land heavily contaminated. Copper, lead and zinc mines are the main sources of heavy-metal soil pollution. Steel plants produce dust containing 15-30% zinc, 3-5% lead, 0,1% cadmium. [3]. In some areas of Baku average concentrations of zinc in soils are up to 50-60 times the acceptable levels.

Much of Absheron Peninsula is contaminated by natural U-series and Th-series radionuclides, released in the production of oil and gas and, to a lesser extent, by anthropogenic radionuclides, including Sr-90 and Cs-137, from local industrial activities and trans-border transport. The region contains a large number of pipelines and artificial lagoons that have been used to retain excess groundwater and oil residues.

During the period of 2011-2013 years have been made 4097dosimetric measurement . Of these, 1366 or 34% exceeded a level of 5.4 μR/h., two standard deviations above the mean of the least contaminated route, a 79-km road between Baku and Guba. Along the routes Baku-Shemakha and Baku-Guba where no oil and gas activity had taken place, radiation levels of 5.1 ±1.5 and 4.2 ± 0.6 μR/h., respectively, were obtained. The readings for the route Baku-Guba were then used as representing negligible contamination to which the readings of the other sites was compared. In contrast, along the routes Baku-Lokbatan and Baku-Surakhani, that have seen oil- and gas-related activity, radiation levels were sometimes two or three orders of magnitude higher. The most highly contaminated sites were those of two abandoned iodine recovery facilities along the route Baku-Surakhani, the Ramani and Surakhanisites where readings up to 1450 μR/h were obtained. The contamination is due mainly to uranium and thorium in the formation water associated with the oil and gas. Radon measurements did not exceed 20 Bq/m3[4].

Now in the territories of Absheron Peninsula are located: thousands of running and abandoned oil wells; more than 3200 hectares of territories polluted by oil products and residual waters; the area of 3325 hectares including more than 200 small and big lakes the natural resources (salt, fishes etc.) of which are widely used by population.

Table 1. Summary of Dosimetry Measurements along nine selected Routes.

Route	Distance investigated in (km)	Number of measurements	Dose Rate μR/h			
			min	max.	mean	st. dev.
Baku-Lokbatan	101.0	694	1.7	187	5.7	2.5
Baku-GurdGapisi	24.6	136	2.2	7.8	3.8	1.3
Baku-Shemakha	36.9	249	2.5	14.5	5.1	1.3
Baku-Guba	79.2	377	2.7	5.8	4.2	0.6
Baku-Binagadi	35.3	308	2.5	15	3.7	1.1
Baku-Balakhani	41.5	430	2.5	8.8	3.8	0.7
Baku-Mashtaga	78.9	711	2.9	8.5	4.4	0.9
Baku-Azizbayov	75.0	574	2.4	37.5	7.5	4.9
Baku-Surakhani	70.0	570	31	825	74.8	85.5

Certainly, there is some degree radiation in these lakes, but they never were investigated from radio-ecological point of view. These lakes comprises: Jeyranbatan Reservoir, Masazir (Salty) lake, Mirzeledi lake, Gazan (Bloody) lake, Big shor lake, Emirjan lake, Gadji-Gasan lake, Girmizi lake, National Park Bulvar (Baku Bukhta) etc., which occupied considerable areas in Absheron Peninsula (Fig.1). The majority of these lakes were formed from layer and ground waters in the process of oil extraction. There is the similar situation in the marshy volcanic formations that exist in a great number in Absheron Peninsula (Fig.2)

Environmental problems of the Caspian Sea.An estimated human population of approximately 11 million is distributed around the Caspian shoreline. The main urban centers of population are concentrated on the western and southern shores. Coastal provinces in Iran and Azerbaijan, in particular, dominate the demography of the Caspian. The ecological status of the Caspian Sea is largely due to the growing potential of the offshore oil industry, oil transportation and offshore oil pipelines. The average

water level of the Caspian Sea is 27 m below the mean ocean level and it is one of the few reservoirs of the world with such a physical feature [5].

The water level of the Caspian Sea was dropping for decades prior to 1978, when it abruptly started to rise at that time. Long time interaction of lithosphere, atmosphere, hydrosphere, global and regional factors have rendered a unique geosystem in the Caspian basin [6].

Fig. 1. The map of Absheron Peninsula

Study of the unique geosystem in the Caspian basin and coastal regions is necessary for comprehension of various native factors affecting petroleum extraction operations. Understanding the changes in the basin's regime and the degree of anthropogenic impacts on different areas of the Caspian Sea is very important. According to the latest data, the 955-kilometer coast in the Caspian Sea, which belongs to Azerbaijan, controls the flowing waters of the Caspian Sea (310 industries, wastewater treatment plants, rivers) and 31 industrial installations (eg platforms) operating at sea with 341 control point [7].

In accordance to the report of BP for 2017 at present in Caspian Sea from Azeri-Chirag-deepwater Gunashli (ACG) complex is produce for the year was on average 588,000 barrels per day (b/d) (about 215 million barrels or 29 million tons in total) from the Chirag (51,000 b/d), Central Azeri (137,000 b/d), West Azeri (124,000 b/d), East Azeri (82,000 b/d), Deepwater Gunashli (117,000 b/d) and West Chirag (77,000 b/d) platforms. In 2017, ACG continued to safely and reliably deliver stable production. Total ACG production for the year was on average 588,000 barrels per day (b/d) (about 215 million barrels or 29 million tons in total) from the Chirag (51,000 b/d), Central Azeri (137,000 b/d), West Azeri (124,000 b/d), East Azeri (82,000 b/d), Deepwater Gunashli (117,000 b/d) and West Chirag (77,000 b/d) platforms.

At the end of the year, 115 oil wells were producing, while 54 wells were used for gas and water injection.

In 2017, ACG delivered an average of about 7.9 million cubic meters per day of ACG associated gas to SOCAR (2.9 billion cubic meters in total), primarily at the Sangachal Terminal but also to SOCAR's Oil Rocks facility. The remainder of the associated gas produced was re-injected for reservoir pressure maintenance.

The daily capacity of the Terminal's processing systems is currently 1.2 million barrels of crude oil and about 30 million standard cubic meters of Shah Deniz gas, while overall processing and export capacity for gas, including ACG associated gas is around 50 million standard cubic meters per day.

During 2017, the Sangachal terminal exported more than 283 million barrels of oil, of including third party volumes. More than 253 million barrels were exported through Baku-Tbilisi-Ceyhan (BTC), 28 million barrels through the Western Route Export Pipeline (WREP), and more than 2 million barrels via a separate condensate export line.

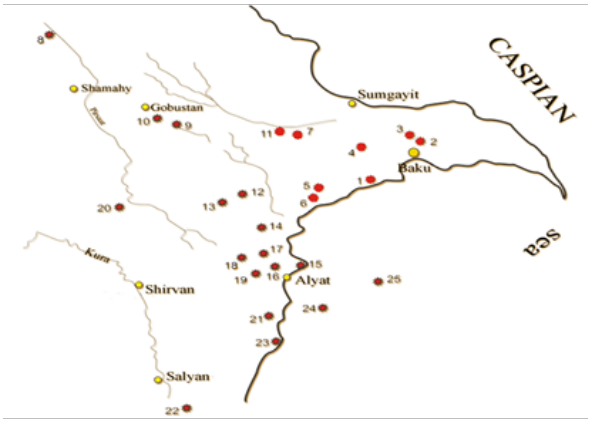

Fig.2 The map of mud volcanoes distribution in Absheron Peninsula

In 2017, the Shah Deniz field continued to provide deliveries of gas to markets in Azerbaijan (to SOCAR), Georgia (to GOGC), Turkey (to BOTAS) and to BTC Company in multiple locations.

During the year, the field produced about 10.2 billion standard cubic meters (bcm) of gas and 2.4 million tons (about 19 million barrels) of condensate. The existing Shah Deniz facilities' production capacity is currently 30.0 million standard cubic meters of gas per day or around 10.9bcma.

The greenhouse gas (GHG) emissions arise from the burning of fuels in internal combustion engines, heaters and flaring of unrecoverable gas. In 2014, BP emitted about 4,067,000 tons of gross GHG, which is almost 29% higher than in 2013. The main reason for this increase was higher volumes of flaring at the West and East Azeri platforms, as well as the start-up of the West Chirag.

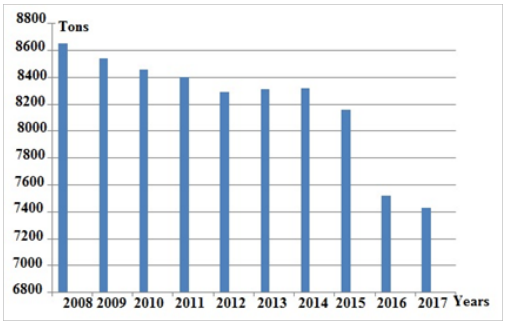

Fig.3. The dynamics of oil production in the SOCAR by years

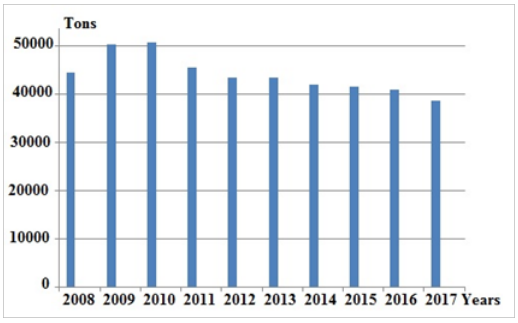

Fig.4. The dynamics of oil production in the Republic of Azerbaijan by years

The NOx emissions increased by 26% compared to 2013 reaching 11,179 tons. This correlates with 19% increase in fuel gas use. There was a similar increase in SOx emissions. This was influenced by a 26% increase in diesel usage due to increased drilling activities and the subsequent higher intensity of logistics operations. Other main contributors to SOx emissions include the Shah Deniz platform and the Sangachal terminal.

In 2014, BP in Azerbaijan recorded six oil spills, five of which were fully contained. BP continue formally reporting all material releases of hydrocarbons to the Ministry of Ecology and Natural Resources, as well as to the State Oil Company of the Republic of Azerbaijan.

BP operations in Azerbaijan generated a total of 368,839 tons of solid and liquid waste in 2014. The notable increase in the total volume of hazardous waste was caused by a significant amount of produced water sent for treatment and disposal as liquid waste. About 42% of the non-hazardous waste (5,690 tons) and20% of the hazardous waste (63,314 tons) was recycled or reused by our contractors. In 2014, BP continued to landfill treated hazardous drill cuttings accumulated at the Serenja facility from previous years by sending 69,193 tons to Sumgayit hazardous waste landfill. There were no shipments of nonhazardous drill cuttings from Serenja to the Sumgayit non-hazardous landfill cell.

BP continue to base our approach to drill cuttings management on three main disposal options: Discharge to sea is allowed for drill cuttings with synthetic-based mud (SBM) from the Chirag platform and with water-based mud (WBM) from other platforms and mobile drilling rigs. In 2014, BP intensified drilling program led to almost three-fold increase in the volume of drill cuttings discharged to sea (39,714 tones).

During the year, 9,745 tones of cuttings were injected into re-injection wells at the Azeri-Chirag-Deepwater Gunashli (ACG) field. The remaining 31,252 tones of cuttings (8% more than in 2013) were delivered to Serenja hazardous waste management facility. In 2014, there was a further reduction (from 21 to 12) of sewage treatment plant outages that result in untreated sewage releases offshore. However, the volume released increased by 5% from 195m3 to 204m3. At the Sangachal terminal, monitoring results of treated sewage showed compliance with all required parameters throughout the year. Along the export pipelines, an issue with elevated fecal coliforms parameter at the reed beds continued in 2014. A special monitoring was initiated to assess water quality across the reed beds area. Produced water volumes at the ACG field continue to rise. A total of 5,263,662 tones from ACG were separated at the Sangachal terminal in 2014. This represents an 18.5% annual increase. After treatment, 5,077,256 tones were exported back offshore for re-injection.

Produced water volumes from the Shah Deniz field are much smaller than volumes from the ACG. In

2014, about 30,906 tones were separated and placed into the dedicated storage ponds at the Sangachal terminal. The chemical composition of sediments has remained relatively stable and metal concentrations were within background levels. Hydrocarbon concentrations were not influenced by operational activities at the platform. There was no evidence that operations are having an impact on the macro benthic community, which is diverse and abundant throughout the survey area. Elevated barium concentrations may be related to discharged water-based mud (WBM) and/or drill cuttings.

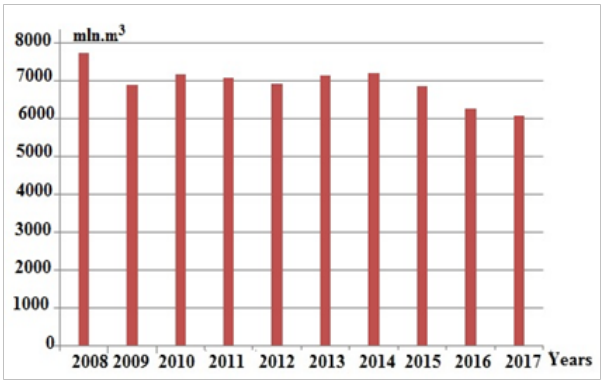

Fig.5. The dynamics of gas production in the SOCAR by years

The seabed environment around the platform has been fairly stable over a number of surveys. Hydrocarbon concentrations were higher in 2013. However, the composition was typical of the background and the results indicate that this increase was due to natural variability. The higher concentrations of barium indicate the presence of drilling wastes discharged in 2010. There was no evidence of any impact on the macro benthos from operations at the platform between 2011 and 2013 Sediment physical characteristics have changed very little in the north and south of the contract area, while in the central area changes have been recorded influenced by mud volcanoes.

The recorded hydrocarbon concentrations in 2013 were higher than those from 2007, and very similar to those from 2005. Physically, chemically and biologically the survey area remained relatively unchanged compared to previous surveys, indicating a stable environment.

The water quality had no evidence of hydrocarbon or heavy metal contamination. Phytoplankton species richness and community structure was similar to 2009 and 2011. The zooplankton community was similar to all previous surveys.

Hydrocarbon concentrations were higher than the previous surveys. The greatest increase between years has been identified at stations on the eastern side and southeast corner of the survey area. This may be due to the transportation of contaminated sediments by wave action from outside the bay. Sediments in the bay in 2013 were finer than those from surveys carried out in 2006-13. Phytoplankton was high in species richness. Although the community structure was similar, the zooplankton abundance was lower than during the two previous surveys.

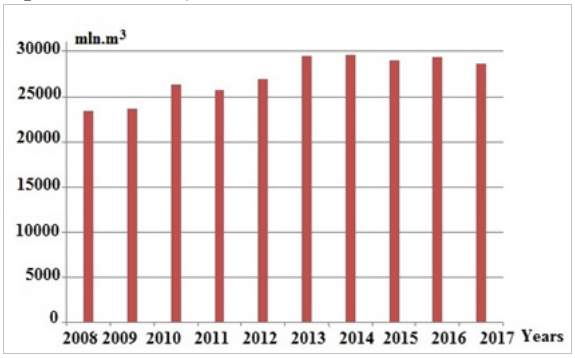

Fig.6.The dynamics of gas production in the Republic of Azerbaijan by years

Monitoring results for NO, NO2, SO2, PM10, benzene and total VOC around the facility were within air quality standards. Exceeding concentration of PM10 in a single station is considered to be due to natural wind-blown particulates from the surrounding land. The samples from several monitoring wells around the terminal showed evidence of the presence of some pollutants, not exceeding the human health commercial assessment criteria, but the concentrations of the same parameters from a majority of the monitoring wells were below the laboratory detection limits. The monitoring did not detect any pollutants above the acceptable standards. Higher concentrations of number of parameters in the upper wells indicates a potential contribution of these contaminants from offsite sources. There was a notable improvement in ecosystem condition, particularly in crust cover and bare patch indicators. An increase of grass cover since the previous surveys was observed. In three survey rounds 79 bird species were recorded within the area, of which 23 were resident species. There was no evidence of any reduction in bird biodiversity or

numbers, but there was an indication that human commensal species had increased. Evidence of species presence was observed on 86% of surveyed stations (total 73). In total, 21 species (10 reptiles, nine mammals and two amphibian) were recorded during the survey. The results show a relatively uniform distribution of animal presence across the area. Noise monitoring conducted at the three settlements adjacent to the terminal showed. Ambient air quality monitoring was carried out at five locations around PSA2 (NOx) and at two locations at IPA1 (NOx and SO2). All results were within the specified limits. Daytime environmental noise monitoring conducted in at several locations along the pipeline routes showed noise levels that were within the relevant requirements. Groundwater monitoring was carried out at the Garayazi aquifer and around PSA2. Surface water samples were collected at upstream and downstream locations at IPA1 and PSA2. All results were consistent with pre-construction baseline conditions and are compliant with relevant standards. Monitoring at each measure point indicated that restoration percentages now exceed 50% at sloped (59%) and flat (64%) sites along the pipelines than at the same sites (49% and 40% accordingly) in 2012Vegetation cover data indicates that 45% of the monitoring areas have vegetation cover equal to or greater than adjacent, undisturbed areas. At 88% of sites, the vegetation cover has shown an increasing trend over the seven years of monitoring. Four sites that in 2012 indicated a decreasing trend started to show an increasing trend. The basic contamination sources of the Caspian Sea are the followings: entering of pollutants from distance zones through atmosphere and water, unpurified industrial and agricultural wastewater, river shipping and seafaring, onshore and offshore exploitation of oil and gas wells, pollution within the works of sea bottom deepening. Currently 15 ml people live in Caspian coastal zones, whose life activity is directly connected with this sea. Each year 40-45 km 3 sewage flow into the Caspian Sea through rivers, of which Volga river shares 60 %. Unless these slops had distributed unevenly, then the thickness of that layer would have reached 10-11 cm. Kura and Ural rivers play a role in contamination of the Caspian Sea waters. Wastewater of Tbilisi, and Rustavi cities and industrial institutions, as well as various toxic substances used in agriculture enter the Caspian Sea via Kura river. Wastewater entering the Caspian from the littoral cities of the sea regarding Baku, Sumgayit, Makhachkala, Astrakhan, Turkmanbashi, Rasht, Anzali are deemed one of its main contaminants. Likewise exploitation of nautical oil wells and transportation of oil products, sea transport trigger pollution of the Caspian Sea as well.The most dangerous contamination for the Caspian Sea are oil hydrocarbons, hydrocarbons, carbonukleids, chloric organic compounds and heavy metals. In this regard, the sea oil industry and underwater oil pipelines which surround Absheron peninsula and half of Mangyshlag are the main points. Formerly the offshore oil industry and emergence of oil wells in the sea was considered achievement of science and technology. From that time, however some scholars warned about future after-effects of this technology. Nevertheless more than half a century has passed from those alert ideas, they prove to be correct to this day and we have already seen that the Caspian Sea has become worldwide problem. The environmental problem of the Caspian Sea now makes the whole world disquiet. As enclosed basins the Caspian Sea is one of the largest hydrocarbon raw centers for oil-gas reserve and potential. Enclosed basins have certain ecological problems. For instance: Depletion of natural resources quantitatively, degradation of anthropogenic, soil surface natural ecosystems and water ecosystems, contamination of sea milieu. The latter is considered the greatest problem. In terms of fish farm and sanitary-toxic features, the Caspian Sea condition was estimated as a beginning of crisis period in the end of Soviet Union. In this regard the Volga river basin and Caspian Sea littoral were proclaimed “environmental disaster zone” in 1992. Each year 40-45 km 3 sewage flow into the Caspian Sea through rivers, of which Volga river shares 60 %. Unless these slops had distributed unevenly, then the thickness of that layer would have reached 10-11 cm. Majority of apparent accidents in the sea and its littoral is certainly connected with oil industry located here. Thinking of facilities, leakage of oil products into the sea, fall of installations into disrepair and can be shown as an example. The Caspian Sea expose to hydrodynamic danger mostly in the southern and middle areas. Furthermore the Caspian Sea bottom is liable to mud volcanoes. Especially sulphur containing oil extracting areas are perilous. In case of strong earthquake, millions tons of sulphuric hydrocarbons may enter the air under 1000 atmospheric pressure, which is

considered global catastrophe. Transportation of oil in huge tankers causes pollution of the Caspian Sea as well. As the Caspian Sea is enclosed ecosystem, it is sufficient to become defunct through contamination by oil spills. The most polluted areas of the sea are at the same time environmental crisis areas regarding water areas of Baku, Sumgayit, Makhachkala, Turkmanbashi cities, sea oilfield regions under operation. The following factors must be taken into account while dealing with contamination of the lake: firstly, irregular distribution of wastewater causes serious pollution of different parts of the sea. Secondly, it carries littoral contamination from one zone to another one and pollutes that area too. Taking into consideration that wastes are collected on the water surface (upper layer) and create "water-atmosphere zone", it must be mentioned that mostly biologically essential areas of the sea are contaminated mainly due to those gathered sewage.

The environmental problems of the Caspian Sea are also related with its periodic level oscillation. The level of the sea which passed transgression period since 1978 rose gradually and caused serious threat. In this regard 2.5 m elevation of the sea water level caused 1-2 km area of the sea littoral to remain under the sea. For instance, 10-15 years ago a great deal of dwelling places and household areas located in the coastal strip of the southern region of the country (Lankaran-Astara) faced that calamity, the people and state were inflicted a considerable damage.

2. CONCLUSION

Absheron Peninsula and Azerbaijan sector of Caspian Sea is a unique habitat and an economically important environment for the countries. Oil extraction operations, transport, industry and oil transportation and offshore oil pipelines all are sources of contaminants of lands and water, atmosphere and environment. Intensification and modern approaches to oil production in these regions needs vitally important to put the environmental and ecological issues on top of all governmental contracts and foreign investment agenda. It is clear that all sources of pollutants, toxic pollutants must be identified and their maximum allowable concentrations in the seawater and sediments should be determined through establishment of regulatory levels. For this purpose, environmental standards for land, water and the atmosphere should be developed to the proper level. On the basis of modern technology, it is possible to minimize environmental risks of joint efforts of all participants who are involved in oil production and processing. It is fact that any investment towards preservation of the Caspian Sea's ecological condition would benefit all countries surrounding the Caspian basin and will act as a basis for prosperity and stability of the region.

3. REFERENCES

1. N. M. Ismaylov, S. I. Nadjafova, and A. Gasimova. Absheron Industrial Region—Environmental Stress Factors Arid Ecosystems, 2015, Vol. 5, No. 3, pp. 194–200.
2. Essays, UK. (November 2013). Baku In Azerbaijan: Pollution Levels. Retrieved from https://www.ukessays.com/essays/environmental-sciences/the-pollution-levels-of-baku-in-azerbaijan-environmental-sciences-essay.php?vref=1.
3. Tjalle T. Vandergraaf, Gudrat G. Mamedov, Mahammadali A. Ramazanov, Jalal A. Naghiyev, Afat A. Mehdiyeva, Nazim A. Huseynov. Determination of the radionuclide contamination on the absheron peninsula in Azerbaijan. Proceedings of the 14th International Conference on Environmental Remediation and Radioactive Waste Management, ICEM2011, September 25-29, Reims, France.
4. https://www.ukessays.com/essays/environmental-sciences/the-pollution-levels-of-baku-in-azerbaijan-environmental-sciences-essay.php#ftn1
5. Kosarev, A.N., Yablonskaya, E.A., 1994. The Caspian Sea. SPB Publishing House, The Hague, p. 259 .
6. Lilienberg, D.A., 1997. Tectono-klimaticheskiy mechanism klobanieyrovnia. Kaspia I zadachi geodinamicheskogo monitoringa. Investigation of the Caspian.
7. Environmental performance reviews Azerbaijan Second Review. Environmental Performance Reviews Series No. 31, New York and Geneva, 2010.

PHOTOCATALYTIC DEGRADATION OF ORGANIC PESTICIDES ON THE TITAN DIOXIDE NANOPARTICLES

G.SH.MAMMADOV, M.A.RAMAZANOV, U.A.HASANOVA , K.A.HUSEYNOV*

Baku State University, Z.Khalilov 23 Str., Baku, Azerbaijan

In this research work was studied photocatalytic properties of inorganic adsorbents on the basis of titanium dioxide (TiO2) of various allotropic structure. There is given comparative characteristic of efficiency of nanoparticles in the process of photo stimulated degradation of organic pesticides − such as chlordane on the surface of adsorbents. It is revealed that decomposition of a chlordane depends on phase structure of the photocatalyst. Has been found that the degradation occurs more actively, with application of TiO2 nanoparticles in the form of anatase.

PACS numbers: *91.62.Rt , 81.16.Hc
Keywords: Titanium dioxide, photocatalysis , degradation , pesticide , chlordane.
***E-mail**:kanan.huseynov@gmail.com

1. INTRODUCTION

It is known that the photocatalysts increase the rate of reaction under the influence of light [1]. This properties of photocatalysts are widely applied in cleaning and disinfecting air, where volatile organic compounds decay to safe molecules of water and carbon dioxide, artificial photosynthesis, splitting of water on oxygen and hydrogen, oxidation of organic pollutants with use of nanoparticles of metals oxides [2].

Today much attention is paid to questions of reduction of environmental pollution. There are different kinds of interactions: dynamic and steady between compounds in the biosphere. As a result of anthropogenic activities, these continuous links are often harmed in a continuous interaction, that is, an environment in which it is enough to break one link to cause serious damage since the entire chain - the biota consists of a lot of plant and animal organisms is disrupted [3]. Therefore under the influence of an anthropogenic factor, the surrounding environment constantly changes and unfortunately in the direction of environmental damage [4]. Pesticides are the pollutant which is consciously released in the environment and can be consider as the one of the major contaminant [5]. Pesticides strike various components of natural ecosystems: reduce biological efficiency of phytocenosis, a specific variety of fauna, reduce the number of useful insects and birds, and finally constitute to the pollution of ecosystem [6]. The pesticides containing chlorine (DDT, Chlordane, dioxine and etc.), differ not only in high toxicity, but also extreme biological activity and ability to cumulate in various links of a food chain [7]. Even in insignificant concentration pesticides suppress the immune system of an organism, increasing thus his sensitivity to infectious diseases [8]. In higher concentrations these impurity have mutagen and carcinogenic effect on a human body [9].

Discovery of pesticides - chemical means of protection of plants and animals from various wreckers and diseases - one of the most important achievements of modern science [10]. Today in the world for 1 ha area 300 kg chemicals are used. Unlimited use of pesticides (herbicides, insecticides, defoliants) has negative effect on quality of the soil. In this regard the fate of pesticides in soils and an opportunity to neutralize them in the chemical and biological ways is strenuously studied. The majority of pesticides have synthetic origin and are steady to biodegradation. Use of photocatalysts allows converting them to simple non-toxic compounds and protecting the environment.

Semiconductor photocatalysts are characterized by the big width of the forbidden zone, absorbing mainly in blue area and in the ultra-violet range of light. Now dioxide of titanium (TiO2) gain wide application. It is successfully applied in paint and varnish industry, by production of pigments, in synthesis of hydrogen by means of a photolysis of water, photocatalytic reduction of CO_2 to CH_4 and its homologies, in technological processes of water purification and air from organic impurity and others.

It is known that with decrease of the geometrical sizes to a nanolevel, many materials show new properties. In particular, nanodimensional particles of TiO_2 have the greatest photocatalytic activity (< 50 nm.). However even at such level there can be significant an influence of a crystal phase of material. Here is presented the comparative research of photocatalytic activity TiO_2 of rutile and anatase phase and also their mix, on the process of photodegradation of organic pesticides.

Chlordane - $C_{10}H_6Cl_8$ (belt, octachlorine, chlorindan) the technical product contains mix tsis- and a trance - isomers, related connections also are represents light yellow oil [11]. It is almost insoluble in water [12]. This pesticide is characterized by increased resistance and is intended to combat gnawing pests in crops as a contact intestinal insecticide [13]. It was also used to protect nonmetallic materials from termites.

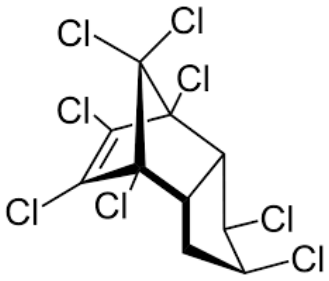

Figure 1.Molecular structure of Chlordane

2. EXPERIMENTAL

2.1 Materials

For a research have been taken commercial models (production of Sigma-Aldrich) of two polymorphic modifications of TiO_2 – rutile, anatase and their mix and also pesticide (Chlordane - $C_{10}H_6Cl_8$) .

2.2 Equipment

The distribution and morphology of the TiO_2 nanoparticles was studied by scanning electron microscope,energy dispersive spectrum (EDS) analysis and X-Ray Diffraction (XRD). Photocatalytic degradation of pesticides was carried out under the UV lamp (250W ultra-high pressure mercury lamp). The grade of photocatalytic degradation of pesticide (Chlordane) was monitored by gas chromatograph GC-2010 Plus.

Scanning electron microscope (SEM) analysis and energy dispersive spectrum (EDS) analysis of prepared samples of TiO_2nanoparticles were taken on Field Emission Scanning Electron Microscope JEOL JSM-7600F at an accelerating voltage of 15.0 kV, SEI regime.

XRD X-ray diffraction analysis was performed on Rigaku Mini Flex 600 XRD diffractometer at ambient. In all the cases, Cu K a radiation from a Cu X-ray tube (run at 15 mA and 30 kV) was used. The samples were scanned in the Bragg angle 2 h range of $20–90^0$.

2.3 Theprocessofphotocatalysis

Source solutions were prepared in amber-glass vessels by spiking ultra-pure water with organ chlorinated chemical reagents to approximate concentrations of 10 mg l1 of each compound [14, 15]. After the zero-time sample, the UV source lamp was initiated [16]. Sampling took place at predetermined intervals for total periods of 6 h. All sets were conducted in triplicates. Experiments start-up included flow, continuous magnetic stirring, and continuous water flow cooling [17].

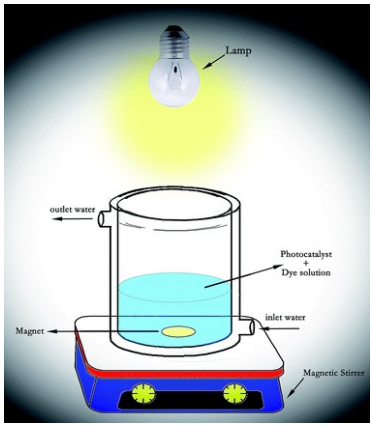

Figure 2.The schema of photocatalytic process wit application of TiO_2 nanoparticles

Have been prepared water solutions of pesticides with concentration: a= $12 \cdot 10^{-5}$mol, b=$6 \cdot 10^{-5}$mol, c= $3 \cdot 10^{-5}$mol and d = $1{,}5 \cdot 10^{-5}$. On the received optical spectra has been constructed the calibration curve by which change of concentration of pesticides which's defined on TiO_2 .

For a research of photodegradation of pesticides, the samples with different concentration of TiO_2 of different phase structure have been moistened and placed in a drying box for full drying.

Photocatalytic degradation of pesticides on TiO_2 was stimulated with radiation of samples an artificial light source. Its represented ventilated box. In the top part of a box the LED lamp 250W of ultra-high pressure Mercury is established (Viso Systems Wolta). Samples were placed under a lamp at distance of 10 cm and during 6 hours were lit and their optical spectra were measured.

3. RESULTS AND DISCUSSION

The morphology and size distribution of TiO_2 nanoparticles were studied by SEM, EDS and XRD methods. The results of analysis revealed that synthesized nanoparticles mostly consist of rutile structure forms. The prepared nanoparticles were analysed by SEM and EDS methods, and the results are presented on figure 3 (a,b). As it seen from Figure 3 (a) the obtained nanoparticles are homogenous and the size of nanoparticles varies in the range from 15 to 30 nm.

The points, identified in the EDS spectra in Fig.3(b),demonstrate the presence of Ti and O as the main elements of the sample and support the data of TiO2 nanoparticles formation (the other peaks are corresponding to Cu and C, being characteristic of the carbon-coated grid).This very well correlates with the results, obtained from XRD analysis.

The purity and crystalline properties of the TiO_2 nanoparticles were investigated by powder X-ray diffraction (XRD) method. The XRD patterns are shown in Fig.4.All the XRD peaks were well defined and corresponded to TiO_2at rutile phase. In the pattern all lines can be indexed, using the ICDD (PDF-2/ Release 2011 RDB) DB card number 00-001-1292.

The purity and crystalline properties of the TiO2 nanoparticles were investigated by powder X-ray diffraction (XRD) method. The XRD patterns are shown in Fig.4.

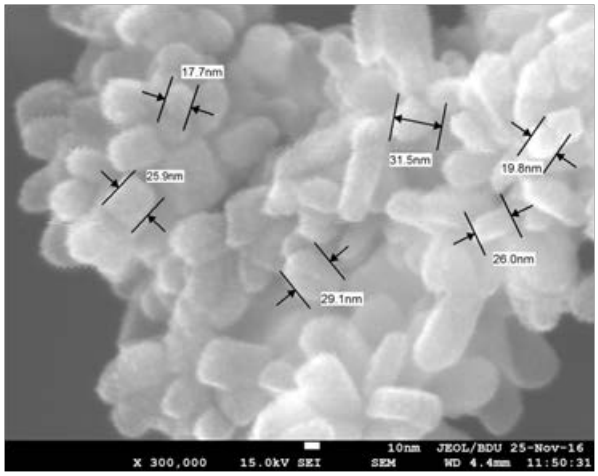

a)

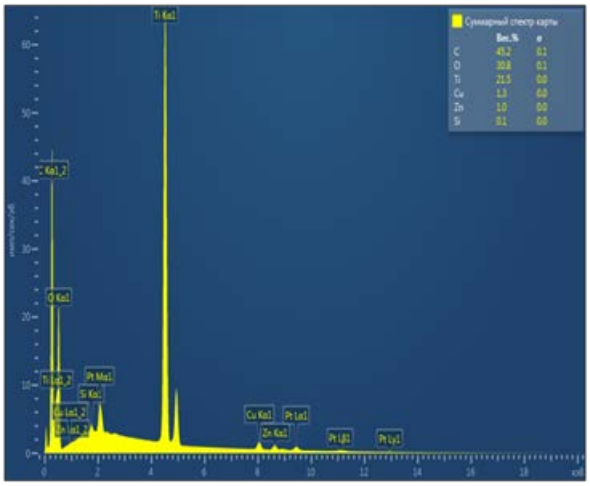

b)

Figure 3. a)SEM image of the TiO_2 NPs; b) EDS spectra of TiO_2NPs

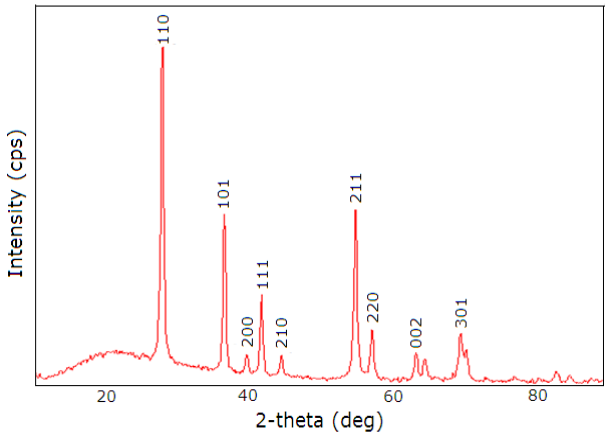

Figure 4 . XRD pattern for the TiO_2 NPs

It is statistically justifiable to deduce that a significant reduction in the concentration of organicsin solution is due to photolysis, though as indicated previously that this does not take place in isolation under semiconductor photo catalytic

applications. It stands to reason that purely photolytic induced reaction pathways may form part of the overall oxidation reaction mechanisms. The photolytic process itself may be inclusive of solution-derived advanced oxidation process phenomena such as coupled UV/chloride, though the contributions of these processes are expected to be minimal. The relevance of the photolysis chlorine coupling oxidation potential is based on the resultant free charged chloride ions in solution delivered by dehalogenation mechanistic reactions that are plausible in the photo catalyst concept. The peroxide molecule results from conduction band reductive reactions with the electron accepting oxygen molecule.

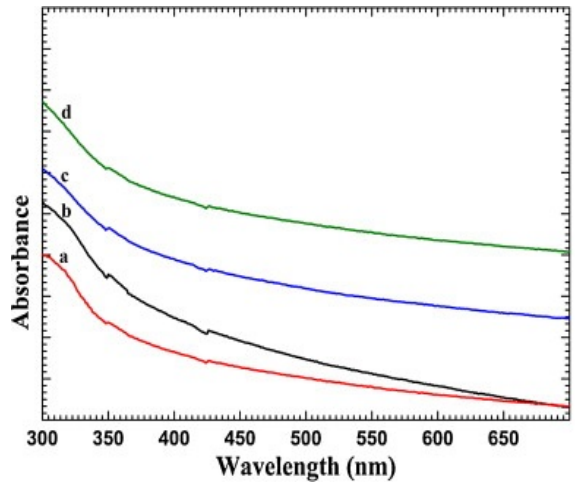

Figure5. UV spectra of photo degradation on TiO2 samples

Follows from Fig. 5 and 6 that at 6 h radiation chlordane degradation reached of 90%. The analysis of the anatase and rutile effect on the degradation of chlordane revealed that the depending on the phase structure of TiO2 the efficiency of the photocatalytic properties of TiO_2 can considerably change.The experiments results show that at low concentrations of pesticide the anatase is more effective than rutile, and the rutile alone demonstrates the medium activity, whereas the blend of rutile and anatase has got the lowest efficiency Fig.6 (b). In case of increasing concentration of photocatalyst there is shown that the anatase is less effective than rutile as well as its blend with anatase, and the rutile alone demonstrates the medium activity, whereas the blend of rutile and anatase has got the higher efficiency Fig.6 (a).

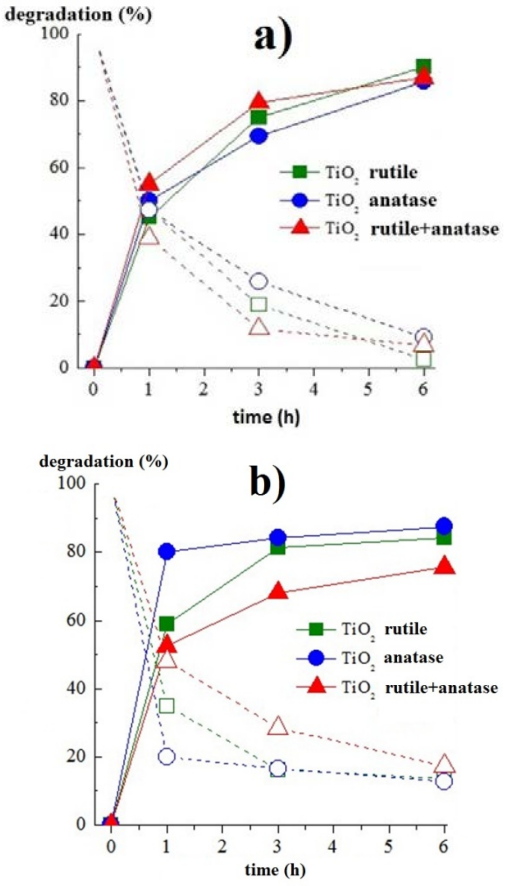

Figure 6. Process of photodegradation on TiO2 samples with different phase structure
a) $12 \cdot 10^{-5}$mol, b) $6 \cdot 10^{-5}$ mol.

4. CONCLUSION

The comparative research of process of photocatalytic degradation of organic pesticide on TiO2 surface with different phase structure is conducted: rutile, anatase and their blend. Optical spectra of samples have allowed to find out that 6 h radiation have sufficient 90% efficiency of degradation of initial amount of pesticides. The photodegradations of chlordane were conducted in the presence of direct UV irradiation and in combination with titanium dioxide semiconductor catalyst. The primary study objective was to determine the oxidation mechanism selectivity between the three structurally dissimilar organ chlorinated compounds by catalyst load manipulation and tracking of the oxidation process.

5. REFERENCES

1. Carp O. et al. /Progress in Solid State Chemistry, 2004. №32. p. 33-177
2. Tang W. et al. / Chemosphere, 1995, 31, №9. p. 4157-4170
3. Kostedt W.L. et al./ Environmental Science & Technology, 2005. 39. p. 8052-8056.
4. Hua Sheng Qin Li. et al. Applied Catalysis B: EnvironmentalVolumes 138–139, 17 July 2013, Pages 212-218 https://doi.org/10.1016/j.apcatb. 2013.03.001
5. Primet M. et al. The Journal of Physical Chemistry, 1971, 75(9), p. 1216-1220
6. Dorian A. H. et al. Journal of Material Scienses,2011, 46, p.855–874 , DOI: 10.1007/s 10853-010-5113-0
7. Lu G., et al. Journal of Chemical Physics, 1995102, p. 3005-3008
8. Ulrike Diebold . et al., Surface science Reports 48, 2003, p. 53-229
9. Pelaez M. et al. / Applied Catalysis B: Environmental, v. 125, p. 331– 349. doi:10.1016/j.apcatb.2012.05.036
10. Khuzwayo Z. et al. Southafrican journal of chemical engineering, 23 2017, p. 25.
11. Brudnowska B. et al. Arch Environ Contam Toxicol., 2001, 40, p. 173-178.
12. Chang S. et al. Chemosphere 2006, v.63,p.58-63.
13. Pandit G. G. et al. Environ Int., 2006, 32, p.240-243.
14. Kaneko M. et al. Journal of Surface Engineered Materials and Advanced Technology, 4, p.369-378. doi:10.4236/jsemat.2014.46041
15. Kansal.S. et al. Engineering, 2012, v. 4, № 8, p. 416-420. doi:10.4236/eng.,2012, 48055
16. Andreozzi R. et al. Chemical Engineering Transactions, 2011, 24, p. 1261-1266, DOI: 10.3303/CET1124211
17. Khan M. N. et al. Journal of Modern Physics, 2011, v.2,№9, p. 962-965. doi:10.4236/ jmp.2011.29115

Journal of LDS

Address:
Az1148, Z.Khalilov str. 23,
Baku State University, BSU publication, Baku,
Azerbaijan

E-mail: journal_lds@bsu.edu.az; mhhuseyng@bsu.edu.az

Published by the Baku State University and devoted to original papers in experimental and theoretical physics, chemistry and biology

ISSN 2308-068X